THERMOELECTRIC SYSTEM MODELING AND DESIGN

by

Buddhima Pasindu Gamarachchi

A thesis

submitted in partial fulfillment

of the requirements for the degree of

Master of Science in Mechanical Engineering

Boise State University

August 2017

BOISE STATE UNIVERSITY GRADUATE COLLEGE

DEFENSE COMMITTEE AND FINAL READING APPROVALS

of the thesis submitted by

Buddhima Pasindu Gamarachchi

Thesis Title: Thermoelectric System Modeling and Design

Date of Final Oral Examination: 20 June 2017

The following individuals read and discussed the thesis submitted by student Buddhima Pasindu Gamarachchi, and they evaluated his presentation and response to questions during the final oral examination. They found that the student passed the final oral examination.

Yanliang Zhang, Ph.D.   Chair, Supervisory Committee

John F. Gardner, Ph.D.   Member, Supervisory Committee

Inanc Senocak, Ph.D.   Member, Supervisory Committee

The final reading approval of the thesis was granted by Yanliang Zhang, Ph.D., Chair of the Supervisory Committee. The thesis was approved by the Graduate College.

DEDICATION

To my family, parents Asoka and Bandula, and brother Isuru

ACKNOWLEDGEMENTS

ABSTRACT

Thermoelectric generators (TEGs) convert heat to electricity by way of the Seebeck effect. TEGs have no moving parts and are environmentally friendly and can be implemented with systems to recover waste heat. This work examines complete thermoelectric systems, which include the (TEG) and heat exchangers or heat sinks attached to the hot and cold sides of the TEG to maintain the required temperature difference across the TEG. A 1-D steady state model is developed to predict the performance of a TEG given the required temperatures and device dimensions. The model is first validated using a 3-D model and then is used to examine methods to improve the TEG performance. A numerical model is developed to predict the thermal performance of heat exchangers to be used in combination with the TEG model. The combined thermoelectric generator – heat exchanger model, is compared with a 3-D model and then used to predict the performance of a TEG – heat exchanger system used to recover waste heat from a diesel engine. Next natural convection heat sinks are modeled and studied to be implemented with the TEG. A model is developed to predict the performance of a system applied for power harvesting in a nuclear power plant. The model is also used to design a system to recover waste heat from the human body. Finally, a novel natural convection heat sink is suggested, where microwires act as the extended surface for the heat sink. The microwire heat sink is modeled accounting for the relevant thermal physics. The microwire heat sink is used in combination with the TEG model to predict the performance of a system used to recover waste body heat.

TABLE OF CONTENTS

LIST OF TABLES

xiii

LIST OF ABBREVIATIONS

TE   Thermoelectric

TEG   Thermoelectric Generator

TEM   Thermoelectric Module

HX   Heat Exchanger

HS   Heat Sink

INTRODUCTION

Thermoelectric Effect

The thermoelectric effect is the conversion of a temperature gradient into a voltage difference or the process of using electricity to obtain a temperature gradient between two different materials that conduct electricity. The thermoelectric effect is widely used in a conventional thermocouple used for temperature measurement. With the advancement of modern semiconductor materials, the thermoelectric effect can be utilized for thermoelectric power generation or thermoelectric cooling. The thermoelectric effect consists of three effects, the Seebeck effect, Peltier effect and the Thomson effect.

Seebeck Effect

The Seebeck effect named after Thomas Johann Seebeck is the phenomenon in which a temperature gradient between two different electrical (semi)conductors produces a voltage difference. When the semi-conductors are connected to an electric circuit in series, heat can be converted into electricity [1]. The Seebeck coefficient, α is defined by the following equation:

$$\alpha = -\frac{\Delta V}{\Delta T} \tag{1-1}$$

where V is the voltage and T is the temperature. The Seebeck effect results from the diffusion of charge carriers from the hot side to the cold side in the thermoelectric material due to the charge carriers having higher thermal energy on the hot side compared to the cold side as illustrated in Figure 1. Charge carriers in the n-type material are

electrons, and electron holes constitute charge carriers in p-type materials. The gradient of charge carrier distribution forms an electric field, which restricts the diffusion caused by the temperature difference. Equilibrium is reached when the two opposing forces balance each other, and an electrochemical potential known as the Seebeck voltage is created resulting from the temperature gradient.

Peltier Effect

The Peltier effect is the reverse process of the Seebeck effect. When an electrical current is passed through two different electrical (semi) conductors, heating at a rate of q occurs at one end of the junction and cooling at the other end. The Peltier coefficient, π is defined as the ratio of the current to the rate of cooling as defined by the following equation:

$$\pi = \frac{I}{q} \qquad (1\text{-}2)$$

where I is the electric current and q is the rate of cooling. The Peltier effect is important in solid-state cooling in thermoelectric coolers.
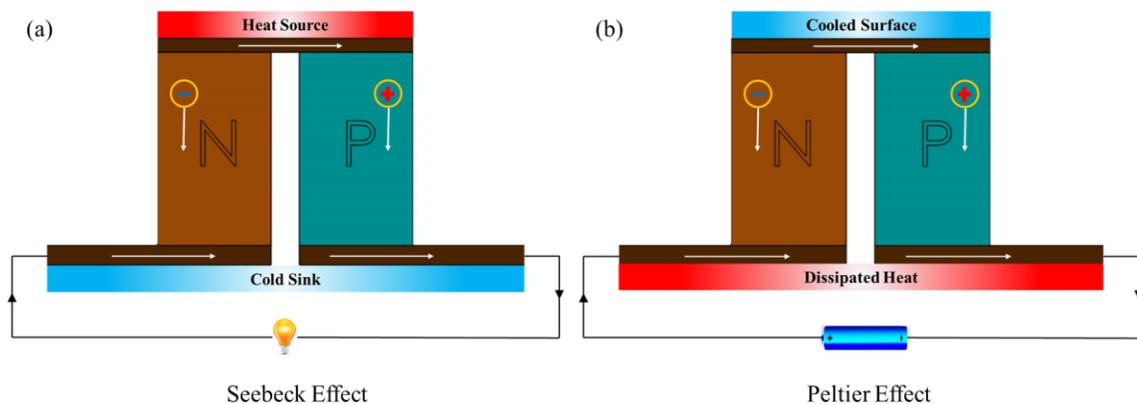
Figure 1: **(a) The Seebeck effect is observed when a temperature difference causes a voltage difference across the hot and cold side. (b) The Peltier effect is observed when an electric current causes cooling at one junction and heating at the other of two dissimilar semiconductors.**

Thomson Effect

The Thomson effect relates to the rate of heat generation caused by the temperature dependent nature of the Seebeck coefficient. The Thomson coefficient β, which is dependent upon the rate of change of the Seebeck coefficient with temperature, is defined by the following equation[1]:

$$\beta = T\frac{d\alpha}{dT} \tag{1-3}$$

where T is the temperature and α is the Seebeck coefficient.

Thermoelectric Figure of Merit

The thermoelectric figure of merit is widely used in the thermoelectric field to estimate the performance of a thermoelectric material. The thermoelectric figure of merit Z is defined as follows:

$$Z = \frac{\sigma\alpha^2}{\kappa} \tag{1-4}$$

where α, σ and κ are the Seebeck coefficient, electrical conductivity and thermal conductivity of the thermoelectric materials respectively. The numerator of the thermoelectric figure of merit is defined as the thermoelectric power factor. The non-dimensional thermoelectric figure of merit, ZT, is given as follows:

$$ZT = \frac{\sigma\alpha^2 T}{\kappa} \tag{1-5}$$

where T is the absolute temperature. A thermoelectric generator can operate under two conditions, operate with the goal of obtaining maximum power or function with the goal of operating at peak efficiency. The TEG efficiency can be related to the figure of merit

depending on the operating condition. For the peak efficiency operating condition the heat-to-power conversion efficiency is obtained by the following equation:

$$\eta_{max(E)} = \frac{\Delta T}{T_h} \frac{\sqrt{1 + Z \cdot T_{avg}} - 1}{\sqrt{1 + Z \cdot T_{avg}} + \frac{T_c}{T_h}} \qquad (1\text{-}6)$$

where ΔT is the temperature difference between the hot and cold sides, T_h is the hot side temperature measured in Kelvin. It is important to note the thermoelectric figure of merit is a function of the Carnot efficiency $\Delta T/T_h$. Z is the thermoelectric figure of merit of the materials, T_c is the cold side temperature measured in Kelvin and $T_{avg} = (T_h + T_c)/2$. The heat-to-power conversion efficiency is related to the thermoelectric figure of merit for the maximum power operating condition, which is primarily used in waste heat recovery applications by the following equation:

$$\eta_{max(P)} = \frac{\Delta T}{T_h} \frac{ZT_h}{ZT_m + ZT_h + 4} \qquad (1\text{-}7)$$

The relationship between device efficiency and average ZT are plotted for both the maximum efficiency and maximum power operating conditions in Figure 2. The figure shows that with increasing ZT the device efficiency approaches the Carnot efficiency for a given temperature difference between the hot and cold sides of the TEG.
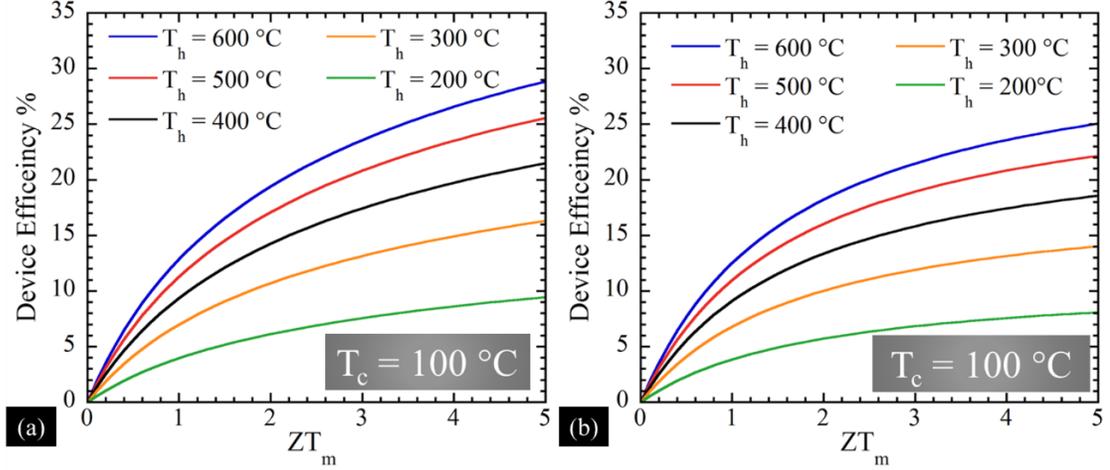
Figure 2: **(a) Thermoelectric device efficiency vs. average ZT for a TE device operating at the maximum efficiency condition. (b) Thermoelectric device efficiency vs. average ZT for a TE device operating at the maximum power condition**

The equation relating device efficiency to the thermoelectric figure of merit fails to take into account any temperature dependent variations in the thermoelectric properties, as well as any contribution from the Thomson effect, which is dependent upon the change in the Seebeck coefficient with temperature as explained in the previous section. Kim et al. have suggested a relationship with better accuracy [2]. The proposed relationship accounts for the temperature dependent nature of the thermoelectric properties and any influence from the Thomson effect. The conversion efficiency can be related to the thermoelectric figure of merit using the following relationship [2]:

$$\eta_{max(E)} = \eta_c \frac{\sqrt{1 + (ZT)_{eng}(a/\eta_c - 1/2)} - 1}{a(\sqrt{1 + (ZT)_{eng}(a/\eta_c - \frac{1}{2}} + 1) + \eta_c} \tag{1-8}$$

$$(ZT)_{eng} = \Delta T \frac{(\int_{T_c}^{T_h} S(T)dT)^2}{\int_{T_c}^{T_h} \rho(T)dT \int_{T_c}^{T_h} \kappa(T)dT} \tag{1-9}$$

$$a = \frac{S(T_h)\Delta T}{\int_{T_c}^{T_h} S(T)dT} \tag{1-10}$$

where η_c is the Carnot efficiency, $(ZT)_{eng}$ is the engineering figure of merit, and a is the intensity of the Thomson effect. S, ρ, and κ are the temperature dependent Seebeck coefficient, electrical resistivity and thermal conductivity of the material. T, T_h, T_c, and ΔT are the temperature, hot side temperature, cold side temperature and the temperature difference between the hot and cold sides measured in Kelvin.

Thermoelectric Generators and Their Applications

Thermoelectric generators consist of numerous thermoelectric unicouples arranged electrically in series and thermally in parallel as illustrated in Figure 3. The different components of a thermoelectric unicouple are also shown in Figure 3. The purpose of the copper headers connected to the thermoelectric legs is to complete the electric circuit, while the top and bottom copper headers serve the purpose of reducing thermal stress. The ceramic layers in the unicouple act as an electrical insulator, and prevents the electric circuit from shorting.
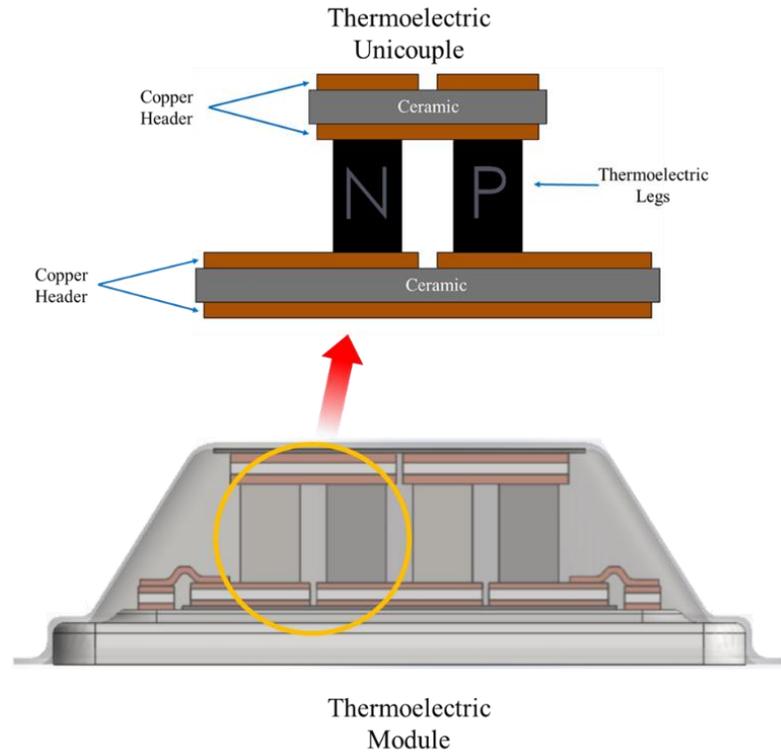
Figure 3:   A thermoelectric module and a thermoelectric unicouple are shown, with the different components of the unicouple identified.

Thermoelectric applications can be divided into energy conversion and cooling

applications. The Seebeck effect is implemented to convert heat energy into electricity,

and the Peltier effect is used for thermoelectric cooling. Thermoelectric devices require

no moving parts and are environmentally friendly, which makes it easy to be

implemented with other systems. Thermoelectric generators are a viable option for waste

heat recovery applications, and some of the applications are illustrated in Figure 4.

Thermoelectric generators have been implemented to recover waste heat from a diesel

engine [3]. Furthermore, around 70% of fuel used in automobiles is discharged as waste

heat [4], which can be employed as a heat source for thermoelectric generators, in order

to improve the fuel efficiency of the automobile. Similarly, waste heat from aircraft

engines has been utilized as a heat source for thermoelectric generators to improve the

overall efficiency of rotorcraft engines which can lose up to 70% of the potential chemical energy [5]. Thermoelectric energy generation can be implemented wherever a heat source is available and ideally, a waste heat source due to the low heat-to-electricity conversion efficiency. The human body exudes a considerable amount of heat energy, and thermoelectric generators have been implemented to utilize the waste heat from the body. Thermoelectric generators that recover waste heat from the body are used to power such devices as wireless sensor nodes, electrocardiograms, and pulse oximeters. [6-8]. Furthermore, TEGs can be integrated into residential heating systems, which require both fuel and electricity for heat production and electricity for operating its electric components. These heating systems are more reliable in providing heat during extreme weather conditions than conventional systems connected to the power grid. Thermoelectric modules can be implemented to make such systems truly self-powered [9]. TEGs have also been incorporated with residential gas-fired boilers with a 4% heat-to-electricity conversion efficiency [10].
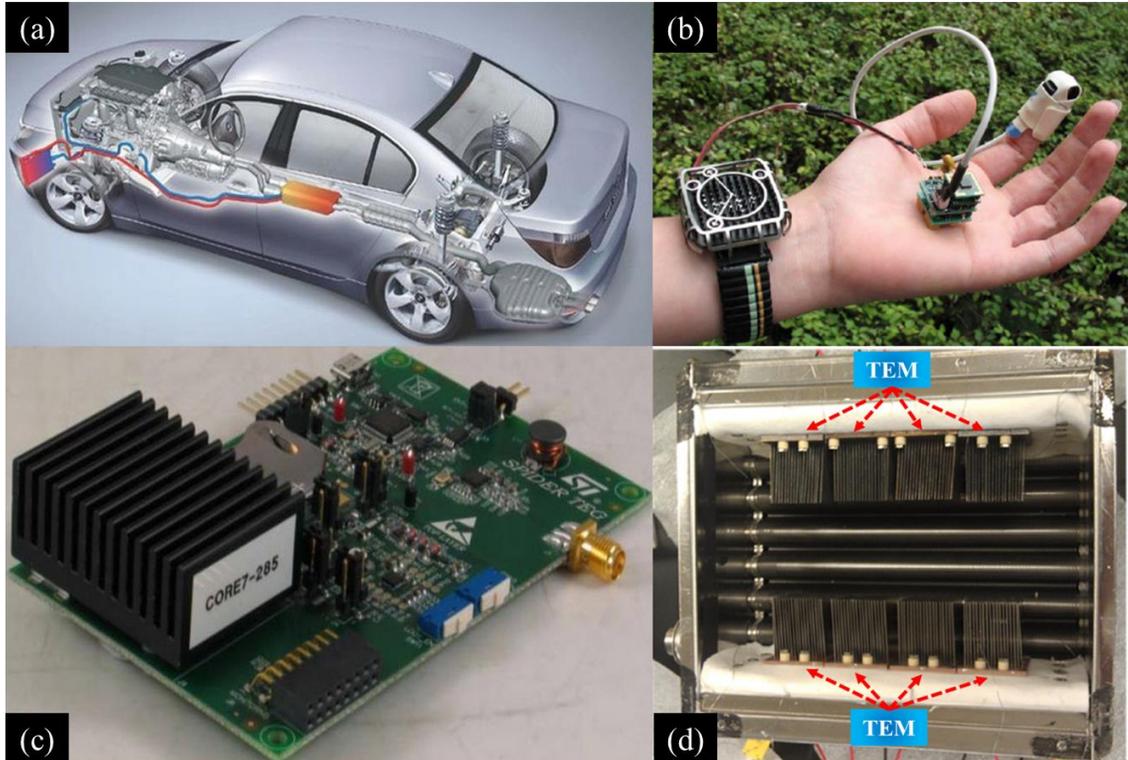
Figure 4: **(a) A TEG applied to a car to recover waste heat from the exhaust [11] (b) A pulse oximeter powered by a TEM [7] (c) An autonomous wireless sensor node powered by a TEM (d) TEMs integrated into a gas-fired boiler [10]**

Thermoelectric Materials

As suggested by the thermoelectric figure of merit, the three critical properties for

a thermoelectric material are its Seebeck coefficient, electrical conductivity, and thermal

conductivity. Thermoelectric effects are predominantly observable in semiconductor

materials. The Seebeck coefficient, which is critical to the thermoelectric effect, is

inversely proportional to charge carrier concentration, whereas the electrical conductivity

is proportional to the charge carrier concentration. The thermal conductivity in

semiconductors is dominated by phonons, which are atomic vibrations [12].

Thermoelectric materials are classified into three categories based on the operation

temperature. Bismuth based alloys combined with Antimony, Tellurium, and Selenium

have high ZT as illustrated in Figure 5 are used for low-temperature applications up to

around 450K. The intermediate temperature range used for heat recovery applications up to around 850 K consist primarily of lead Chalcogenides, Skutterudites, and Half-Heuslers. While thermoelements employed in high-temperature applications up to 1300 K consist of silicon Germanium alloys [1]. Lead based thermoelectric materials are highly toxic and have weak mechanical strength. Skutterudites, which are rare earth metal-based minerals, suffer from having poor thermal stability as well as being of limited supply in nature. On the other hand, Half-Heusler alloys are environmentally friendly, mechanically and thermally robust and the cost is dependent upon the Hafnium material. Half-Heuslers alloys consist of a XYZ chemical composition, where X can be a transition metal, a noble metal, or a rare-earth element, where Y is a transition metal or a noble metal, and Z is a main group element [13].
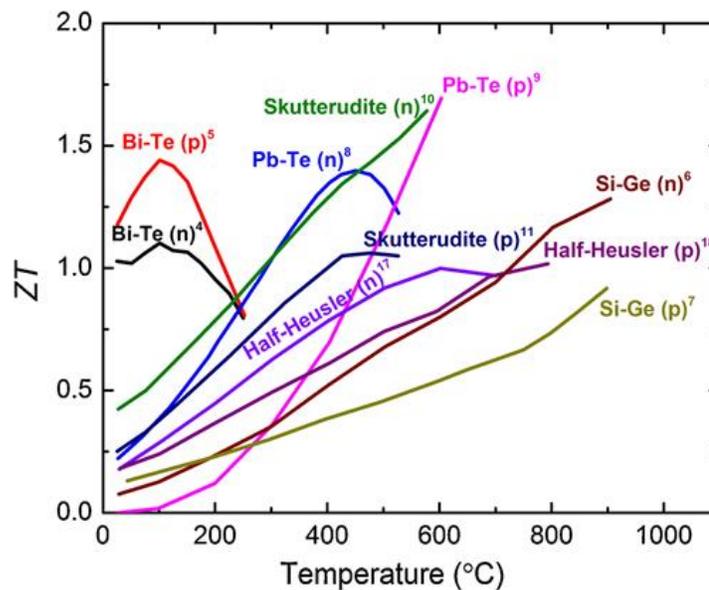
Figure 5:   **An overview of ZT vs. Temperature for various materials [13].**

Objective and Organization of this Thesis

The purpose of this thesis research is to examine and model thermoelectric systems. Thermoelectric systems are composed of a thermoelectric generator, which is accompanied by heat exchangers or heat sinks on the hot and cold side of the TEG. The first task that was accomplished was the development of a finite element model to predict the performance of a thermoelectric unicouple, which is then extended to a thermoelectric module. The work done in developing the finite element model for a thermoelectric unicouple is detailed in Chapter 2, along with suggestions for improving the unicouple performance. Chapter 3 describes the development of a TEG – Heat exchanger model. The heat exchanger model developed in Chapter 3 utilizes forced convection. The TEG – Heat exchanger model builds on the TEG model developed in Chapter 2. Natural convection heat sinks and their application with TEGs are examined in Chapter 4, with the development of a TEG-Heat Sink model. The work culminates in the development of a microwire heat sink model, which is developed to be used in collaboration with the TEG model to recover waste heat from the human body. As each chapter focuses on somewhat varied topics, the literature review is done on a per chapter basis. Additionally, the equation variables for each chapter are independent of each other, stemming from the fact that heat flow and heat transfer coefficients are used throughout this work in different context.

TEMPERATURE DEPENDENT FINITE ELEMENT MODEL FOR A

THERMOELECTRIC MODULE

Introduction

Thermoelectric material properties are temperature dependent, and in practical

use, there is a significantly large temperature gradient along a thermoelectric unicouple.

As indicated in Figure 6, the P-type Half-Heusler material is particularly sensitive to

temperature. With a temperature change from 100 °C to 600 °C, a 100%, 174% and 32 %

changes are observed in the Seebeck coefficient, electrical resistivity, and thermal

conductivity respectively.
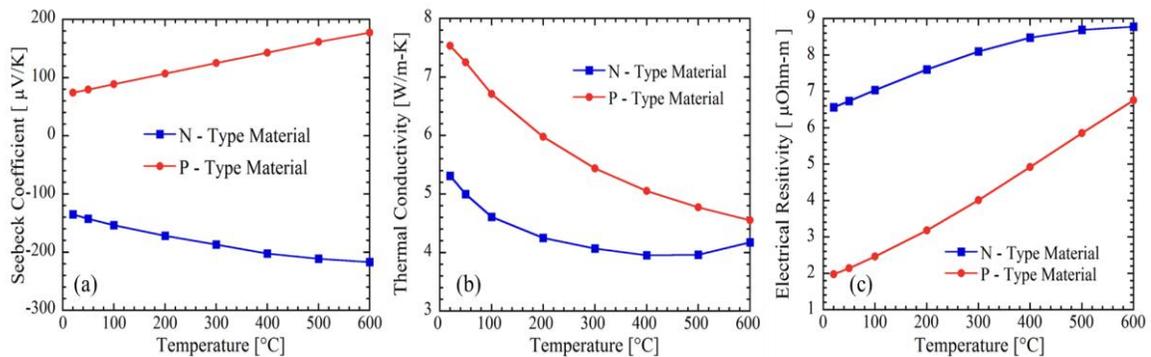
Figure 6:   **Temperature dependent properties of the Half-Heusler alloy.**

Much of the work done on modeling thermoelectric unicouples has been done in

an ANSYS environment [14] or COMSOL environment [15]. Similar thermoelectric

models do not take into account the temperature dependence of the material properties

[16] or the influence of the headers attached to the unicouple [17 -20]. With the goal of

accurately predicting, the thermoelectric power generation and heat-to-power conversion

efficiency of a thermoelectric module a steady-state finite element model was developed in a MATLAB environment.

Temperature Dependent Model

<u>Model Assumptions and Boundary Conditions</u>

The following assumptions were made to simplify the model.

1) The temperature variation was assumed one-dimensional through the unicouple. The reasoning for this assumption was that the temperatures at the hot and cold side of a unicouple are fixed and assumed constant. Furthermore, there are no significant heat losses from the lateral sides of the unicouple.

2) The energy generation or absorption was assumed constant throughout the finite element, and material properties are assumed to be constant within a given finite element.

3) Convection and radiation heat transfer from the external surfaces of the unicouple were ignored in the model.

4) The whole of the top surface of the unicouple is assumed to be at the constant hot-side temperature, and the bottom surface is assumed that of the cold-side temperature. This assumption is utilized as the boundary condition for the model.

5) The module power output and voltage were obtained by the product of the number of unicouples and the power output and voltage of a single unicouple respectively.

<u>Thermoelectric Power Generation</u>

The energy generation terms are significant for the finite element solution. The two primary energy generation/absorption are the Peltier heat generation/absorption at the

boundaries and joule heat generation in the unicouple. Joule heat generation occurs in the resistive elements of the electrical circuit, and net Peltier heat absorption occurs in the thermoelectric legs, as explained by Figure 7. The purpose of the ceramic layer is to act as an electrical insulator, while the copper headers connecting the legs aid in completing the electrical circuit and top and bottom copper headers are integrated with a heat exchanger or heat sink.
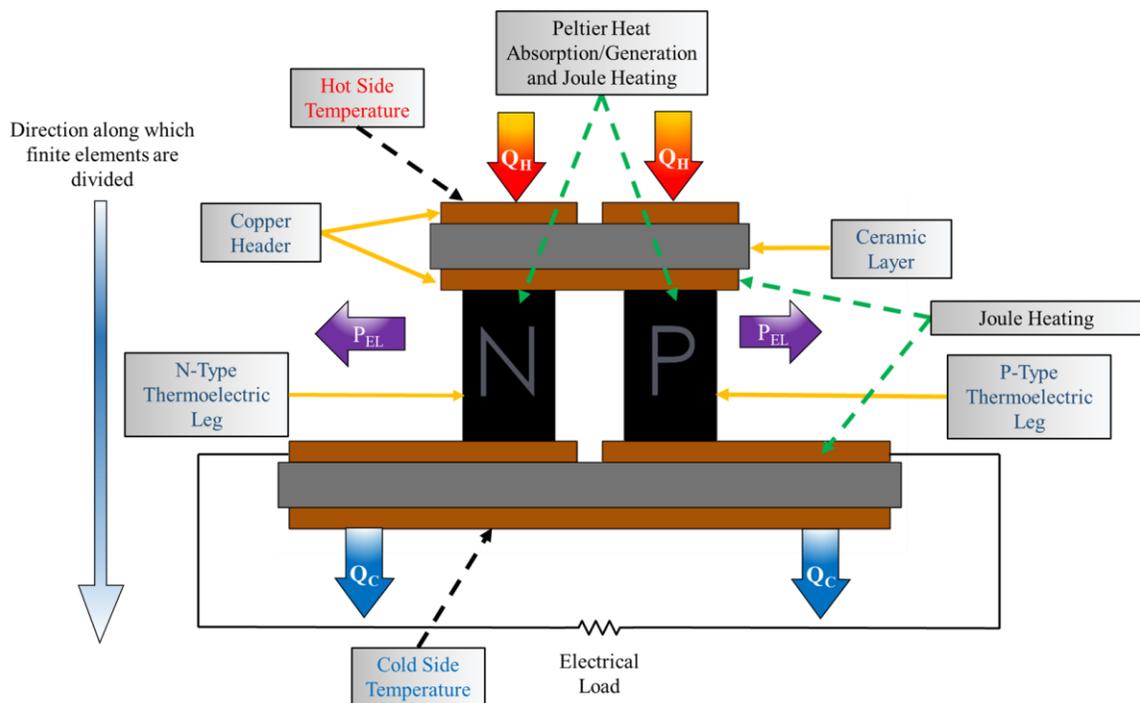
Figure 7: The unicouple components labelled. Q_H is the heat flow into the unicouple when the hot side temperature is maintained at a given value. Q_c is the heat leaving the cold side of the unicouple when the cold side temperature is maintained at a fixed value. P_{EL} is the thermoelectric power generated by the unicouple.

The thermoelectric power generation calculations are done on both the n and p legs separately. The primary principal used to obtain the power generation is the first law of thermodynamics. The thermoelectric unicouple is divided vertically into 100 finite elements as illustrated in Figure 8(a). One hundered elements were chosen as the results do not vary significantly by increasing the number of elements over 100. The

thermoelectric power generated by the unicouple is equal to the sum of the difference between the heat input and heat leaving each segment in the thermo-electric leg. It is important to note that for the thermoelectric power generation calculation, only segments covering the thermoelectric legs are considered, although the complete unicouple is segmented in the model.

The heat transferred into a finite element containing a thermoelectric leg is given by the following equation:

$$Q_{h,p,n} = abs(\alpha_{p,n}(T)) \cdot (T_{no,p,n}) \cdot I + K_{p,n}(T_{no,p,n} - T_{no+2,p,n}) - \frac{1}{2}I^2 \cdot R_{el,p,n} \qquad (2\text{-}1)$$

The heat leaving a finite element containing a thermoelectric leg is given by the following equation:

$$Q_{c,p,n} = abs(\alpha_{p,n}(T)) \cdot (T_{no+2,p,n}) \cdot I + K_{p,n}(T_{no,p,n} - T_{no+2,p,n}) + \frac{1}{2}I^2 \cdot R_{el,p,n} \qquad (2\text{-}2)$$

where $Q_{h,p,n}$ is the heat transferred in to the p-leg and n-leg segments, and $Q_{c,p,n}$ is the heat transferred from the cold side of the p-leg and n-leg segments. The first terms on the right hand side of equations 2-1 and 2-2 account for the Peltier heat at the boundaries of the segment, where $\alpha_{p,n}(T)$ is the temperature dependent Seebeck coefficient of each segment. $T_{no,p,n}$ is the temperature of each element at the upper node of the element and $T_{no+2,p,n}$ is the temperature of the bottommost node of each element, the nodes, and elements of the model are shown in Figure 8(a). I is the current through the two legs, which are connected in series. The second term on the right side of equations 2-1 and 2-2 account for the thermal conduction through the thermoelectric legs, where $T_{no,\,p,n}$ and $T_{no+2,p,n}$ are defined as above. $K_{p,n}$ is the thermal conductance of each element which is given by the following equation:

$$K_{p,n} = \frac{\kappa_{p,n}(T) \cdot A_{p,n}}{l_{p,n}} \qquad (2\text{-}3)$$

where $\kappa_{p,n}(T)$ is the temperature dependent thermal conductivity in each segment, $A_{p,n}$ is the area of each segment and $l_{p,n}$ is the height of each segment. The third term on the right hand side of equations 2-1 and 2-2 account for any Joule heat produced in the elements. The model assumes that half the Joule heat is transferred to the top of the element and the other half is transferred to the bottom of the element. $R_{el,p,n}$ is the electrical resistance of each segment defined as follows:

$$R_{el,p,n} = \frac{\rho_{p,n}(T) \cdot l_{p,n}}{A_{p,n}} \qquad (2\text{-}4)$$

where $\rho_{p,n}(T)$ is the temperature dependent electrical resistivity of each segment. The thermoelectric power generated in each segment is obtained by the difference between $Q_{h,p,n}$ and $Q_{c,p,n}$ in each segment described the following equation:

$$P_{p,n} = Q_{h,p,n} - Q_{c,p,n} \qquad (2\text{-}5)$$

The open circuit voltage is critical in obtaining the current through the circuit and is obtained by summing the individual voltage drops across each segment. The electric current through the unicouple is obtained using the open circuit voltage across the unicouple by the following equations:

$$V_{oc} = \sum_{i=1}^{N} \left(\alpha_p(T) - \alpha_n(T) \right) \left(T_{no} - T_{no+2} \right) \qquad (2\text{-}6)$$

$$I = \frac{V_{oc}}{R_{el,TEC} + R_{el,L}} \qquad (2\text{-}7)$$

where $R_{el,TEC}$ is the electrical resistance of the unicouple and $R_{el,L}$ is the external load resistance, and N is the number of elements. When the goal is to obtain maximum power from a thermoelectric device, the external load resistance is set equal to the electrical resistance of the unicouple. On the other hand, if efficiency is of more importance, $R_{el,L} =$

$R_{el,TEC}(1 + ZT)^{1/2}$, where ZT is the thermoelectric figure of merit of the material at the average temperature of the unicouple. The model is also setup to simulate a current swipe, where the load resistance is varied from 0 to a value greater than $R_{el,TEC}$. As indicated by the equations above, it is necessary to obtain the temperature profile along the thermoelectric unicouple; this process is explained in the following section.
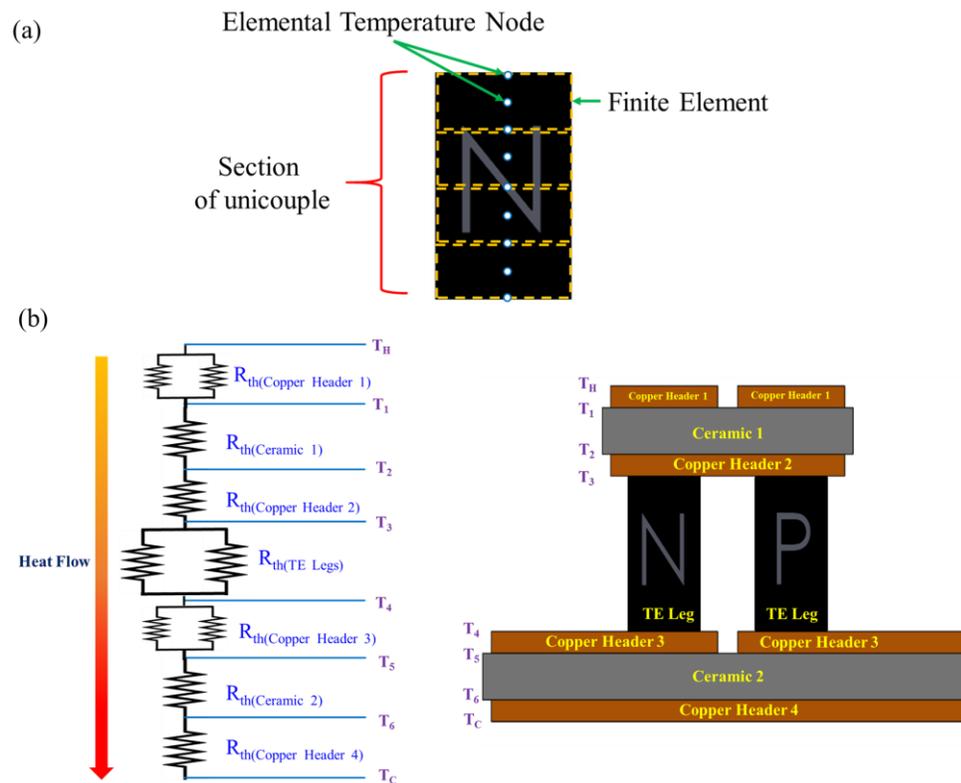
Figure 8: **(a) The division of the unicouple along its vertical length into finite elements and the corresponding nodes, each element shares a node with its neighboring element (b) The simplified thermal circuit for the unicouple and the components of the unicouple**

Temperature Profile

  The temperature profile of the thermoelectric unicouple was obtained by solving a one-dimensional finite element model of the unicouple, which requires the assembly of a

global stiffness matrix and a forcing vector. The temperature profile can be obtained by the matrix solution as follow:

$$T = K^{-1}F \qquad (2\text{-}8)$$

where T is the temperature vector, K^{-1} is the inverse global stiffness matrix, and F is the forcing vector. The assembly of the global stiffness matrix requires elemental stiffness matrix, which is obtained as follows [21]:

$$K_e = \int_l [B]^T[D][B]A_e dx \qquad (2\text{-}9)$$

where B is a term borrowed from structural mechanics called the strain displacement matrix, the D matrix contains the elemental thermal conductivity terms, and A_e is the area of the element. The model uses one-dimensional quadratic elements, which allows an accurate solution to be obtained with a smaller number of elements in comparison to linear elements. The elemental stiffness matrix for this model simplifies to the following equation:

$$K_e = \frac{A_e k_e}{l_e}\begin{bmatrix} 14 & -16 & 2 \\ -16 & 32 & -16 \\ 2 & -16 & 14 \end{bmatrix} \qquad (2\text{-}10)$$

where l_e is the element thickness. It is important to note that each element will have its own, temperature dependent thermal conductivity term, κ_e. The elemental area would change according to the geometry of the headers and the thermoelectric legs. The global stiffness matrix is assembled using the individual stiffness matrix while taking into consideration that each element has three temperature nodes illustrated in Figure 8(a). The elemental loading vector was developed taking into consideration energy generation

or absorption in the element, which is the Peltier heat absorption/generation and Joule

heat produced in each element:

$$F_e = \int_l G[N]^T A dx \tag{2-11}$$

where G is the volumetric energy generation/absorption, N is the shape function, and A is

the elemental area. For a one-dimensional quadratic element, the forcing vector reduces

to the following vector:

$$F_e = \frac{G_e A_e l_e}{6} \begin{bmatrix} 1 \\ 4 \\ 1 \end{bmatrix} \tag{2-12}$$

where G_e is the elemental volumetric energy generation/absorption, A_e and l_e are defined

as above. Once again, the global loading vector was assembled using each of the

elemental loading vectors while considering that each element has three temperature

nodes.

It must be noted that an initial temperature profile (initial guess) is needed to

obtain the required terms for the elemental stiffness matrix (temperature dependent

thermal conductivity) and forcing vector (thermoelectric power generation in an

element). The thermal circuit illustrated in Figure 8(b) is used to obtain the temperatures

at critical boundaries along the unicouple, and a linear profile is assumed between those

boundaries to obtain the initial temperature profile (intial guess). The temperature

dependent properties and energy generation terms are evaluated using the initial

temperature profile. Once the temperature profile is obtained using equation 2-8, it is

used to obtain the temperature dependent global stiffness matrix and forcing vector. This

process is repeated until the difference between the temperature profiles is less than the

convergence criteria as explained by the following equation:

$$\sum_{i=1}^{elems} abs(T_{old(i)} - T_{new(i)}) < CC \qquad (2\text{-}13)$$

where T_{old} is the temperature profile obtained from the previous iteration, T_{new} is the new temperature profile, *elems* is the number of elements and *CC* is the convergence criteria set equal to 1°C. Once the final temperature profile is obtained, it is used in equations 2-1 through 2-7 to obtain the thermoelectric power generated by a unicouple.

Contact Resistance

The brazing process between the thermoelectric legs and headers can induce an electrical resistance. The electrical contact resistance is captured into the overall circuit, by adding it as an additional resistor, using an electrical resistivity of $1*10^{-9}\Omega\text{-m}^2$ [22]. The electrical contact resistivity was obtained from experimental data and numerical simulations. The electrical contact resistance is obtained using the following equation:

$$R_{cont} = \frac{\rho_{cont}}{A_c} \qquad (2\text{-}14)$$

where ρ_{cont} is the electrical contact resistivity value of $1*10^{-9}\Omega\text{-m}^2$, and A_c is the area of contact between the legs and the copper headers.

Model Validation

The one-dimensional model was compared with a 3-D model developed in an ANSYS environment for three different material types. The ANSYS model was developed for a unicouple with the dimensions in Table 1. The ANSYS model used a fine mesh with 19359 elements and 98186 nodes and further details regarding the ANSYS model can be found in Appendix I. The finite element model results were also compared with available experimental data for the Half-Heusler alloy. The experimental data compared is expected to be published in 2017 and was obtained using a similar

experimental setup that is described by Zhang et al.[10]. Table 1 illustrates the

dimensions of the unicouple components, which are the dimensions used for the

experimental data obtained. The unicouple that was experimentally tested is illustrated in

Figure 9, as well as the temperature profile of the unicouple obtained from the 3-D

ANSYS model.

Table 1   Dimensions of the unicouple elements

Component	Thickness/Height [mm]	Area [mm x mm]
Copper Header 1	0.203	[1.93 * 1.96]*2
Ceramic 1	0.635	2.26 * 4.51
Copper Header 2	0.203	1.96 * 4.21
P-Leg	2.400	1.50 * 1.50
N-Leg	2.400	1.50 * 1.50
Copper Header 3	0.203	[1.96 * 4.07]*2
Ceramic 2	0.635	2.26 * 8.81
Copper Header 4	0.203	[1.96 * 8.50]*2
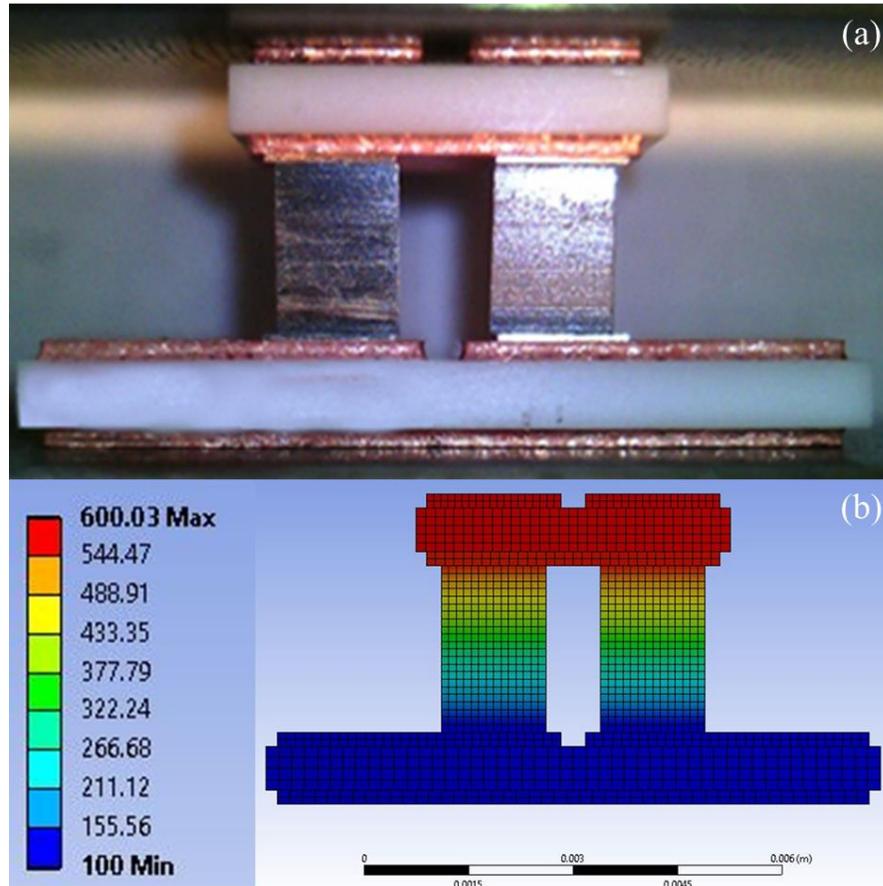
Figure 9: **(a) Thermoelectric unicouple that was experimentally tested with results in Figure 11. (b) Temperature profile along unicouple for the 3-D ANSYS model for a hot side temperature of 600°C and cold side temperature of 100 °C, the results from the ANSYS model are available in Figure 11, Figure 14, and Figure 16**

The ANSYS model developed was used to compare results from the finite element model for two additional materials, Bi_2Te_3 and PbTe with the temperature dependent materials shown in Figure 10.
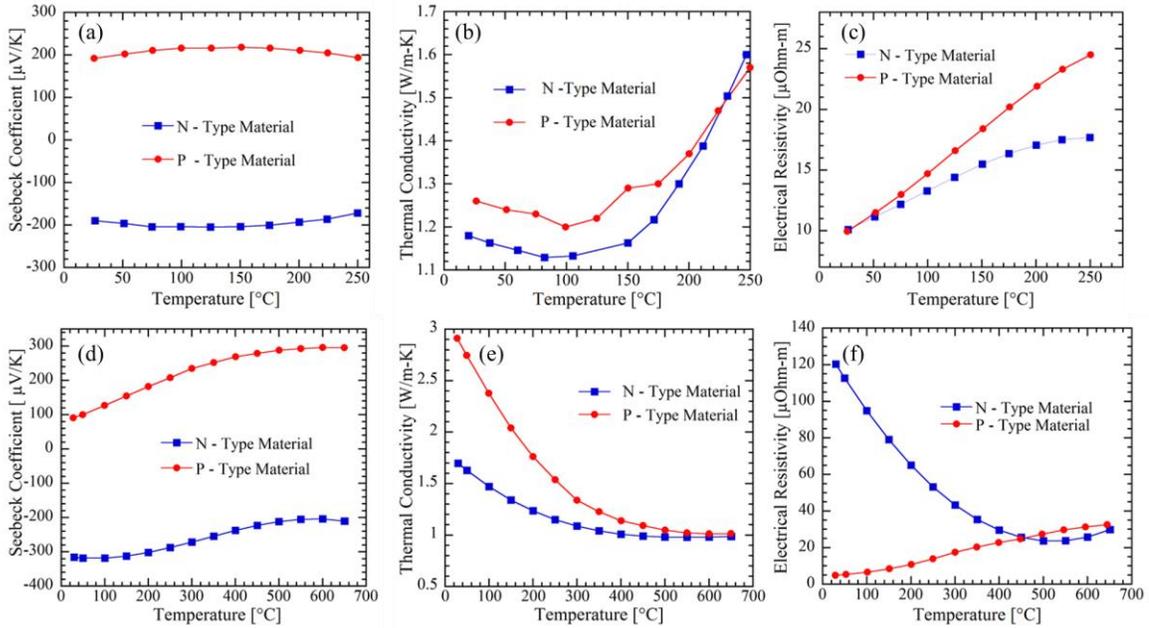
Figure 10: **Temperature dependent properties of the Bi$_2$Te$_3$ material (a) Seebeck Coefficient (b) Thermal Conductivity (c) Electrical Resistivity. Temperature dependent properties of the PbTe material (d) Seebeck Coefficient (e) Thermal Conductivity (f) Electrical Conductivity.**

The results for the Half-Heusler alloy unicouple was compared for hot side temperatures of 200 °C, 300 °C, 400 °C, 500 °C and 600 °C while maintaining the cold side temperature at 100 °C as illustrated in Figure 11. The power results for the Half-Heusler material compare fairly well with the ANSYS model with an average percent error of 11.93%. The discrepancies in the power values are due to differing values of the leg hot and cold side temperatures. The temperature difference between the leg hot and cold sides influence the open circuit voltage of the unicouple, which in turn affects the power produced by the unicouple. The leg hot side temperature (T$_3$ from Figure 8) is lower in the 3-D model compared to the 1-D model. Similarly, the leg cold side temperature (T$_4$ from Figure 8) is smaller in the 1-D model. Therefore, a larger temperature difference is observed across the legs for the 1-D model, which results in larger power being produced. The discrepancies in the temperatures of the legs are due to heat spreading effects in the 3-

D model as shown by the lateral temperature variations in Figure 12. The 1-D model assumes temperature variation along the vertical direction only, and lateral heat spreading is not accounted for. The average percent difference for the efficiency is 2.57%, the errors in the power calculations are carried over to the efficiency calculations, however, they are offset to a certain degree by the overestimation of the heat flowing into the unicouple.
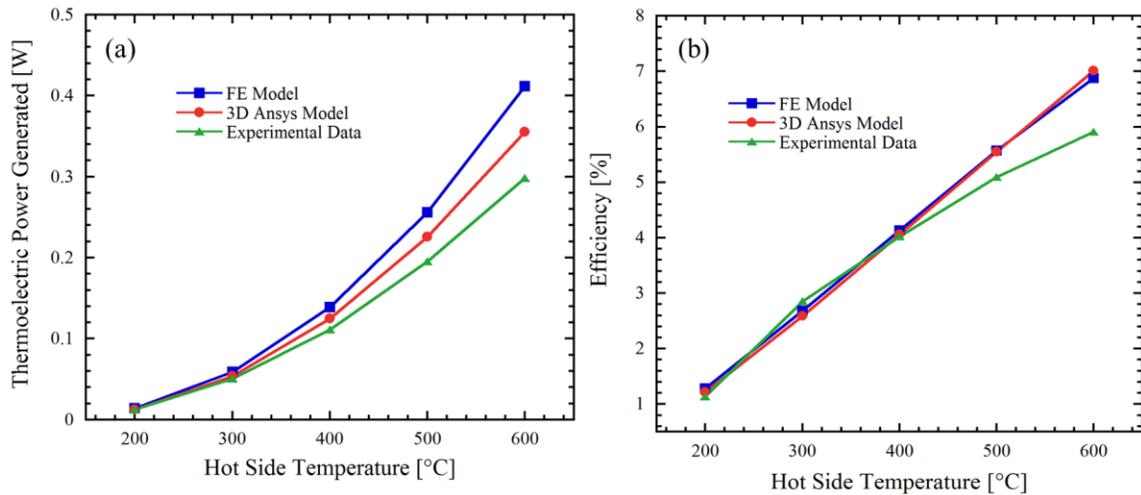
Figure 11: **(a) Peak thermoelectric power generation of a unicouple composed of the Half-Heusler alloy compared to a 3D ANSYS Model and experimental data. (b) Unicouple efficiency compared with a 3D ANSYS Model and experimental data.**

The discrepancies of the finite element model with the experimental results are explained by an underestimation of the electrical contact resistivity included in the finite element model. Furthermore, the finite element model fails to account for any thermal contact resistances between contacting surfaces, which are experienced by the experimental unicouple. The finite element model ignores any natural convection or radiation effects from the external surfaces of the unicouple, which could explain the larger discrepancies with the experimental data at larger hot side temperatures.
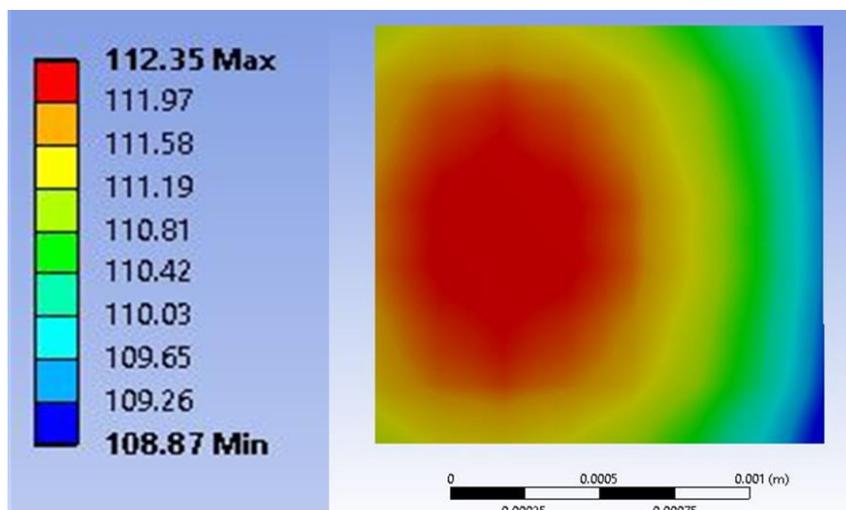
Figure 12: **A cross-sectional view of the bottom surface of the n-type leg. Lateral temperature variations are observed in the ANSYS model, which is not accounted for in the 1-D finite element model.**

The power and efficiency curves obtained by varying the load resistance are displayed in Figure 13 (a) and (b) for the five different hot side temperatures. The device voltage decreases from the open circuit voltage to zero as the current is increased by varying the load resistance as shown in Figure 13(c). The maximum power is obtained at a device voltage that is equal to half the open circuit voltage.
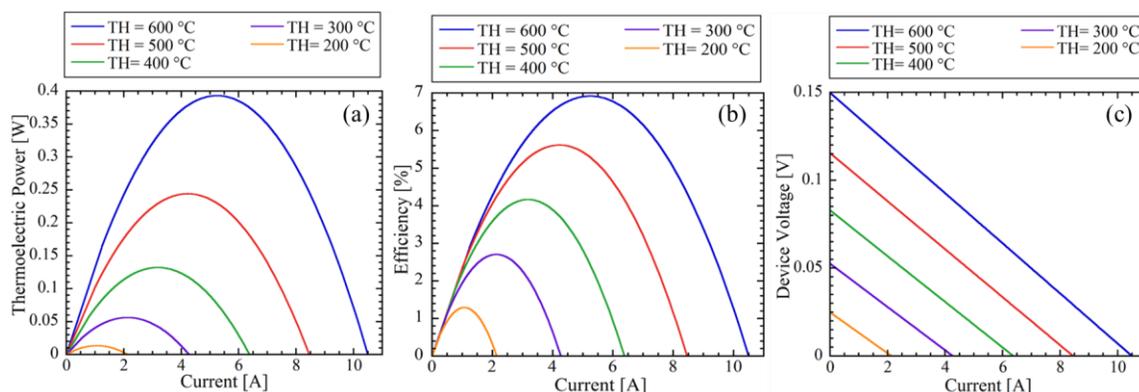
Figure 13: **(a) Thermoelectric power generated for varying current for a unicouple composed of the Half-Heusler alloy. (b) The TEG efficiency for varying current for a unicouple composed of Half-Heusler alloy (c) Device voltage vs. electric current for a unicouple composed of the Half-Heusler alloy.**

Similarly, the power generated and efficiency was compared for a unicouple composed of Bi_2Te_3. The hot side temperature was increased from 50°C, 100°C, 150 °C, 200°C and 250°C, which is its operating limit while maintaining the cold side temperature at 20 °C. The power and efficiency results are compared in Figure 14. The average percent error in the power calculations is 2.73% for the Bi_2Te_3 material, whereas the average percent error for the efficiency calculation is 14.2%. The better accuracy in the power calculations are accounted for by smaller discrepancies in the leg hot (T_3 from Figure 8) and cold side temperatures(T_4 from Figure 8) when compared with the 3-D ANSYS model. The discrepancies in the heat flow are attributed to the model underestimating the heat flow into the model, considering 3-D heat spreading effects are not accounted for in the model.
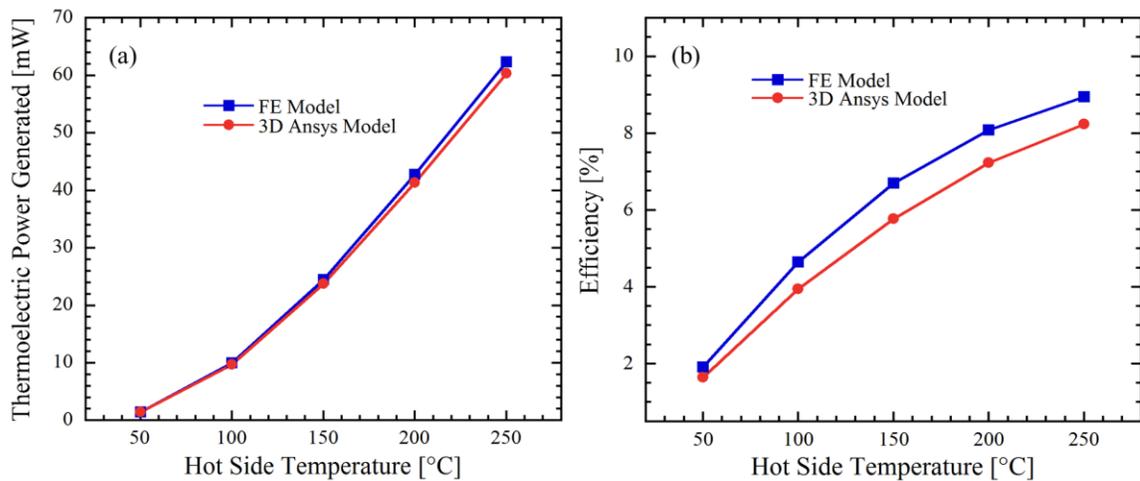
Figure 14:   (a) Peak thermoelectric power generation of a unicouple made of the Bi_2Te_3 material compared to a 3D ANSYS Model (b) Unicouple efficiency compared with a 3D ANSYS Model.

The power and efficiency curves obtained by varying the load resistance is displayed in Figure 15. The electrical current values are restricted by the open circuit voltage values, which are smaller for the unicouple composed of the Bi_2Te_3 material compared to the unicouple composed of the Half-Heusler material.
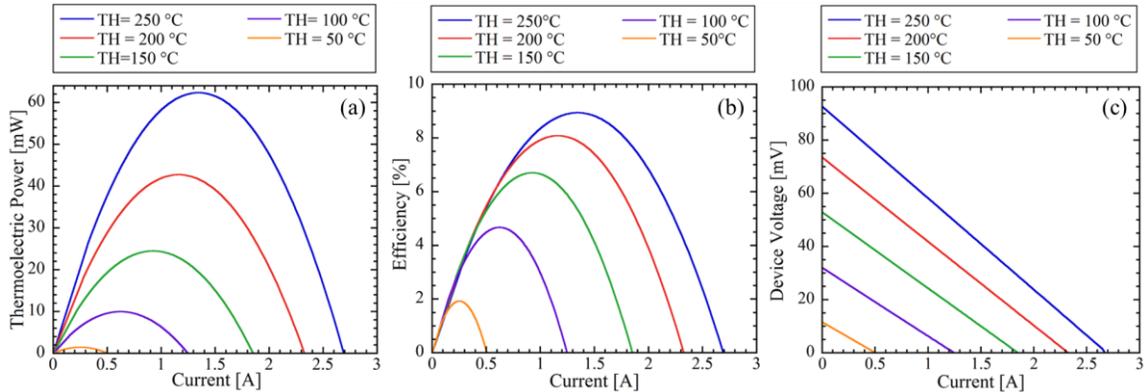
Figure 15: **(a) Thermoelectric Power Generated for varying current for a unicouple composed of the Bi$_2$Te$_3$ material (b) The TEG efficiency for varying current for a unicouple composed of the Bi$_2$Te$_3$ material (c) Device voltage vs. electric current for a unicouple composed of the Bi$_2$Te$_3$ material.**

Finally, the thermoelectric power and efficiency of a unicouple composed of PbTe was compared for hot side temperatures of 200 °C, 300 °C, 400°C, 500°C and 600°C, while the cold side temperature was held at 100 °C as shown in Figure 16. The average percent error in the power calculations for the PbTe material are 4.85% and 7.85% for the efficiency calculations. The better accuracy in the PbTe unicouple model is possibly explained by the smaller variations in thermal conductivity of PbTe in the operating temperature of the material.
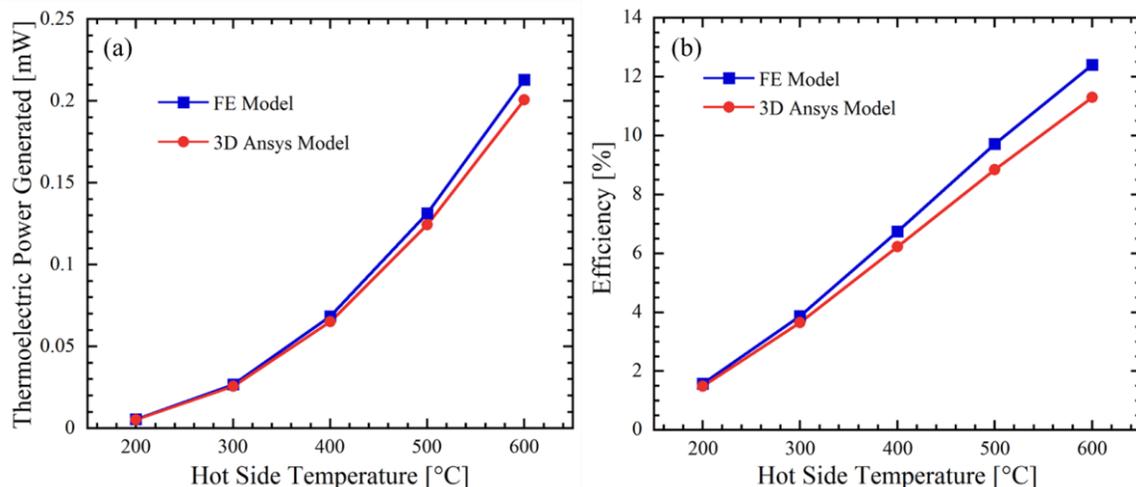
Figure 16: **(a) Peak thermoelectric power generation of a unicouple composed of the PbTe material compared to a 3D Ansys Model (b) Unicouple efficiency compared with a 3D Ansys Model**

Similar to the Half-Heusler alloy unicouple and Bi_2Te_3 unicouple, the power and efficiency curves were obtained by varying the load resistance, which resulted in the power and efficiency curves in Figure 17 (a) and (b). The accompanying voltage vs. current curves are displayed in Figure 17(c).
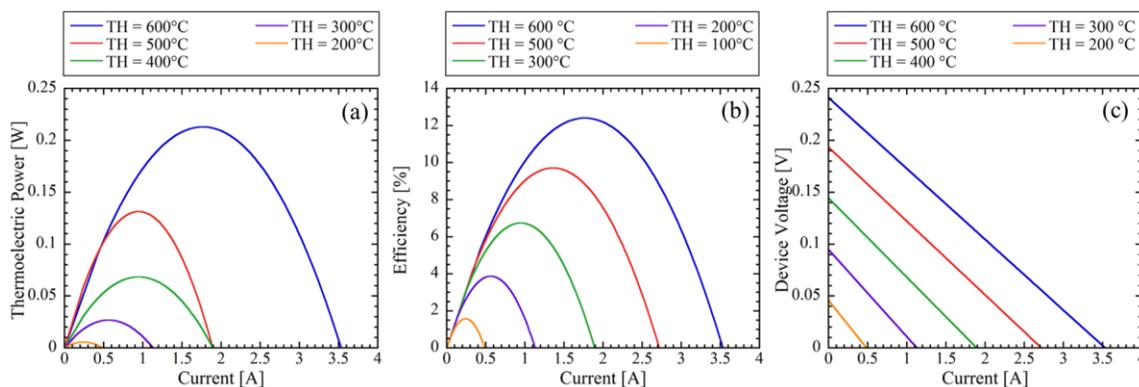
Figure 17: **(a) Thermoelectric Power Generated for varying current for a unicouple composed of the PbTe material (b) The TEG efficiency for varying current for a unicouple composed of the PbTe material (c) Device voltage vs. electric current for a unicouple composed of the PbTe material.**

Thermoelectric Thin Films

Bulk thermoelectric modules are difficult to implement with or in small-scale devices. Furthermore, it is challenging to design flexible bulk thermoelectric modules. Thin film thermoelectrics uses semiconductor processing to create nano-structured thin films used as the thermoelectric legs. These films have a thickness of around $10\,\mu$m, compared to the leg heights of 1-2 mm discussed previously. The miniature scale of the thin film devices results in flexible thermoelectric devices, which can be beneficial when the heat source has a contoured surface, such as the human body. Flexible thermoelectric devices are an attractive option for powering power sensors, biomedical devices and wearable electronics [23]. The thermoelectric model was used to predict the performance of a thin film thermoelectric device with an area of 2mm by 0.01mm and height of 10.5 mm, consisting of five thin films for a cold side temperature of 20 °C with the material properties detailed in [23]. The power density is the ratio of the total thermoelectric power generated to the surface area occupied by the TEG. The experimental power density and open circuit voltage results in [23] are compared with the finite element model results in Figure 18. An average percent difference of 11.5% is observed for the power density, and an average percent difference of 5.4% is observed for the open circuit voltage.
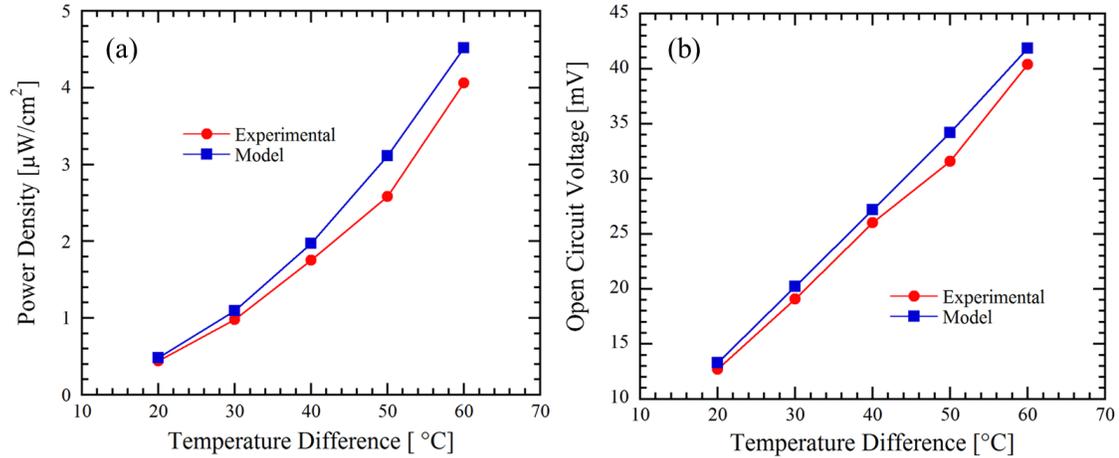
Figure 18: **(a) Power density vs. temperature difference compared with experimental results. (b) Open circuit voltage vs. temperature difference compared with experimental results [23].**

Ceramic Material

The thermoelectric power generated by a unicouple can be increased by having the largest possible temperature difference between the thermoelectric legs (temperatures T_3 and T_4 from Figure 8). For the Half-Heusler material model described in the previous section, the temperature difference across the legs is 463.05°C, when the temperature difference across the unicouple is 500°C. The temperature drop across the copper and ceramic components of the unicouple accounts for the 36.95°C difference. As copper is an effective thermal conductor, the temperature drop across the copper header is negligible. However, there is a 30.968°C temperature drop across ceramic 1 and a 4.99°C temperature drop across ceramic 2. If a larger ratio of the 500°C temperature difference can be had over the thermoelectric legs, the unicouple performance could be improved by having a larger open-circuit voltage resulting in more thermoelectric power generated. The performance of the unicouple can be improved by eliminating the ceramic component of the unicouple; however, the ceramic element serves to act as an electrical insulator, which is essential for the unicouple. A larger temperature difference could be obtained across the thermoelectric

legs by reducing the thermal resistance of the ceramic component, which could be accomplished by:

a) Using a thinner ceramic component

b) Using an electrical insulator with a larger thermal conductivity

In this thesis, the latter option was examined. The thermal conductivity of the ceramic currently used Alumina (Al_2O_3) varies from 24.7 W/m-K at room temperature to 6.59 W/m-K at 600°C as illustrated in Figure 19. Three other electrical insulators with better thermal conductivities are considered in this section. The three materials of interest are Aluminum Nitride, Silicon nitride, and Beryllium oxide. Alumina is the industry standard for electronic substrates [24] and is the ceramic chosen in the model in the previous section. It offers the advantages of having relatively high strength, a high service temperature, being chemically inert and having a lower cost when compared to the other materials. Beryllia (BeO) has the highest thermal conductivity values of 259.4 W/m-K at room temperature and 46.79 W/m-K at 600°C among the materials considered. However, it is extremely expensive due to high powder costs. Furthermore, it is also considered a toxic substance, which limits its application. Aluminum nitride (AlN) has a thermal conductivity of 200 W/m-K at room temperature and 40.46 W/m-K at 600°C, which is comparable to the thermal conductivity of Beryllia. It offers a non-toxic alternative to Beryllia and has good oxidation resistance, which is significant at high temperatures. However, similar to Beryllia it is expensive and is only feasible in limited applications. Silicon nitride (Si_3N_4) has thermal conductivity values of 63.5 W/m-K at room temperature and 38.31 W/m-K at 600 °C; additionally, it offers high-temperature strength and thermal

shock resistance, which makes it an attractive material for high-temperature applications

[25].
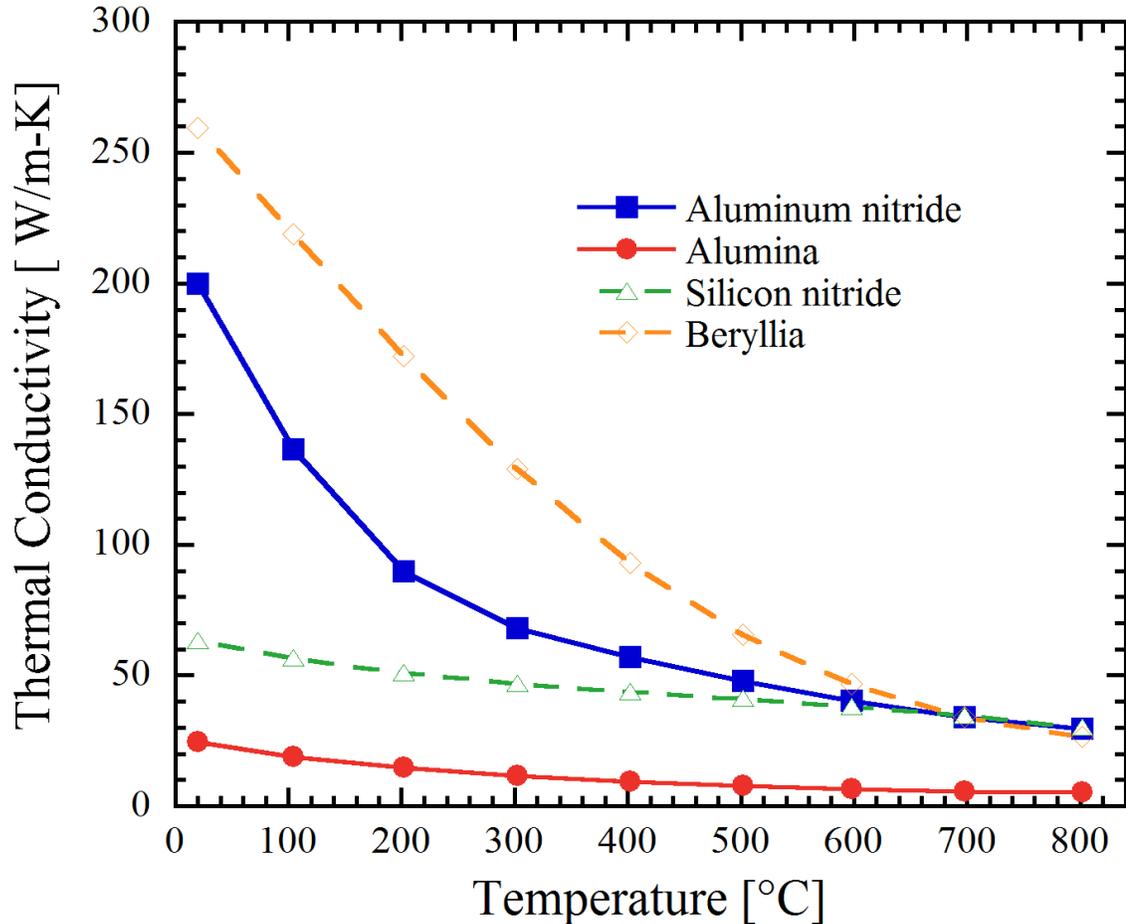
Figure 19: **Thermal Conductivity vs. Temperature comparison of ceramics that can be used as an electrical insulator for a unicouple [25]**

As the goal of this section is to show the significance of the ceramic layer, thermoelectric legs with lower thermal resistance are chosen compared to the values in Table 1. The updated values leg heights are 1.7mm and leg area of 2mm by 2mm, while the copper and ceramic header dimensions are as in Table 1. For the comparison between the ceramics, the unicouple dimensions were kept the same, and the Half-Heusler material was chosen for the unicouple legs. As illustrated in Figure 20 there is a temperature

difference of 479.6 °C across the legs when Beryllia is used as the electrical insulator when compared to a temperature difference of 417.3°C when Alumina is used. It should be noted that unicouples with Aluminum Nitride and Silicon Nitride as the ceramic exhibit relatively similar temperature profiles to that of the unicouple with Beryllia as the ceramic, and were not included in the figure to improve clarity.
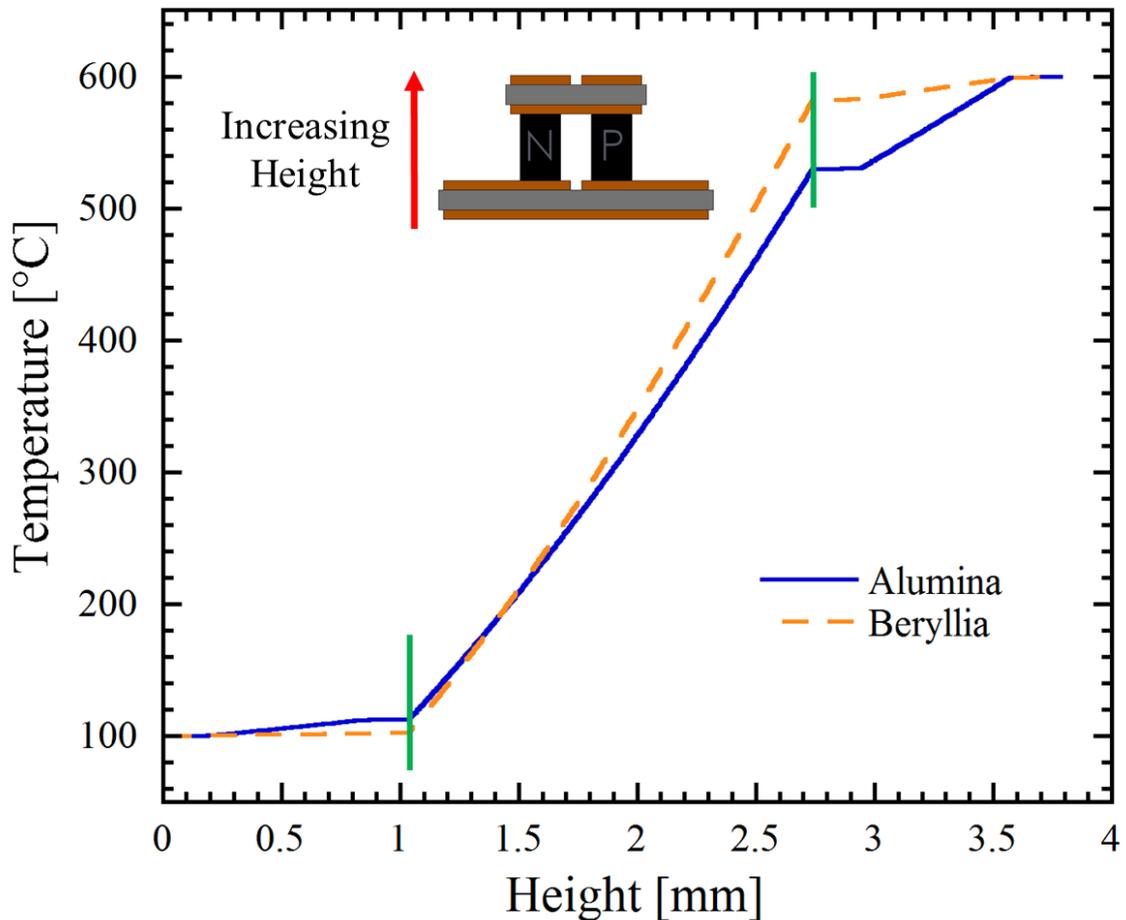
Figure 20: **Temperature profile of the unicouple for a unicouple that has Alumina as the ceramic and Beryllia as the ceramic; the green lines are used to indicate the temperature along the thermoelectric legs.**

The larger temperature differences across the thermoelectric legs for the unicouples with Beryllia, Aluminum Nitride and Silicon Nitride illustrated in Figure 21(a) induce a larger open circuit voltage across the unicouple shown in Figure 21 (b).

The improvements in the open circuit voltages are 1.16 for Aluminum Nitride, 1.15 for

Silicon Nitride and 1.17 for Beryllia when compared with the open circuit voltage of the

unicouple with Alumina as the ceramic. The enhancements in the power results are 1.33

for Aluminum Nitride, 1.30 for Silicon Nitride and 1.34 for Beryllia when compared with

the power output of the unicouple with Alumina as the ceramic as shown in Figure 21(c).

It is interesting to note that although the Beryllia material has a higher overall thermal

conductivity compared to Aluminum Nitride and Silicon Nitride, the improvements in the

thermoelectric power are comparable to the unicouples with AlN and Si_3N_4 as the

ceramic. This observation is explained by the fact that the temperature the top ceramic

experiences is in the 500°C -600°C range. The average thermal conductivities of Beryllia,

Aluminum Nitride, and Silicon Nitride is 56.13 W/m-K, 44.28 W/m-K, and 39.78 W/m-k

respectively in the 500°C to 600 °C temperature range.
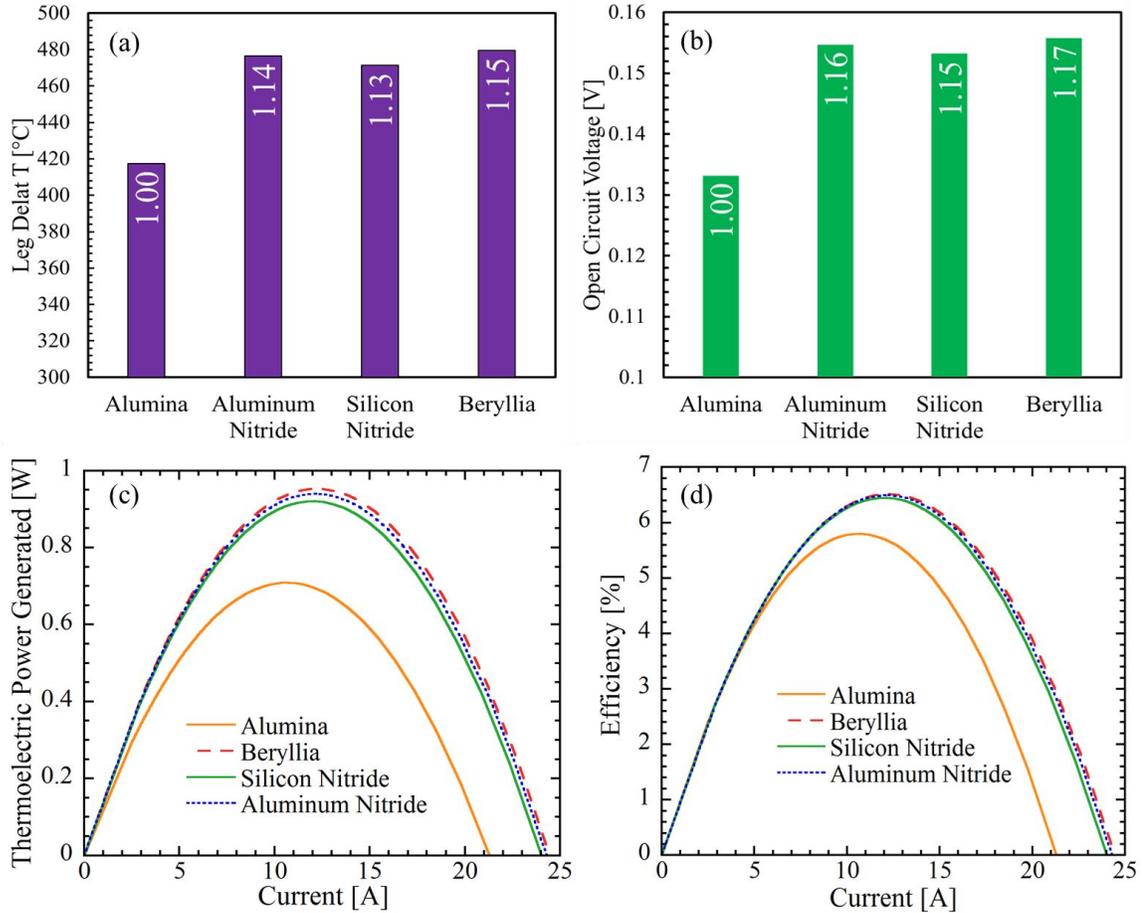
Figure 21: **(a) The temperature drop across the legs for the four different unicouples. (b) A comparison of the open circuit voltage for the four different unicouples (c) Power generated vs. electric current comparison for unicouples composed of the four different ceramic material (d) Efficiency vs. electric current for unicouples made of the different ceramic**

The enhancements in the power results are approximately a square of the improvements in the open circuit voltage, which are validated by the fact that the thermoelectric power for the maximum power condition from a unicouple can be approximated by the following equation:

$$P_{TEC} = \frac{V_{oc}^2}{4 \cdot R_L}$$

(2-15)

where V_{oc} is the open circuit voltage and R_L is the load resistance, which is set to be equal to the resistance of the unicouple. The improvements in efficiency are 1.12 for the

unicouple with a ceramic composed of Aluminum Nitride, 1.11 for one with Silicon Nitride, and 1.12 for one with Beryllia, which corresponds to the increase in the temperature difference across the legs.

Segmented Leg Unicouples

One of the major limitations of thermoelectric generators holding it back from large-scale production is their low heat-to-power conversion efficiencies. The conversion efficiency is itself capped by the Carnot efficiency $\eta = (T_h - T_c)/T_h$ as demonstrated by equations 1-6 and 1-7. The conversion efficiency is dependent upon the thermoelectric figure of merit, which is temperature dependent as illustrated in Figure 22, suggesting that certain thermoelectric materials perform better at specific temperatures.
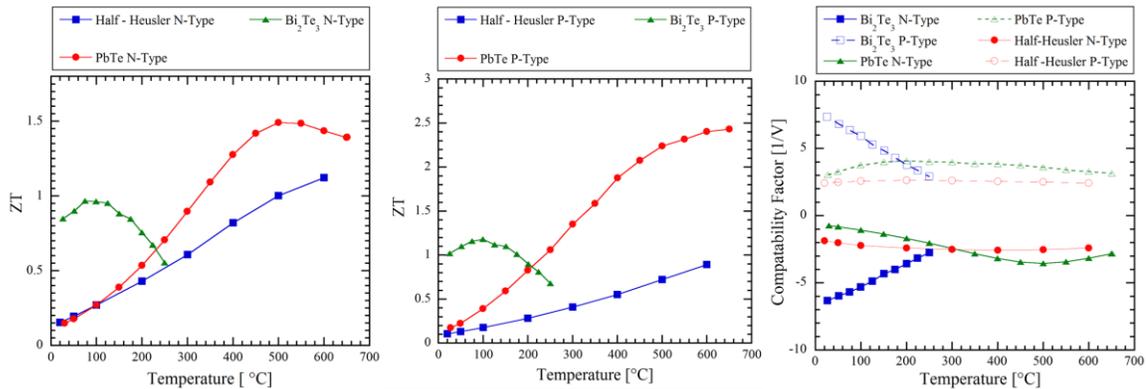
Figure 22: **(a) ZT of the N-Type for the respective materials. (b) ZT of the P-Type for the respective materials (c) Compatibility factor for the Half-Heusler alloy, PbTe material, and Bi₂Te₃ material.**

This observation begs the question, whether a thermoelectric unicouple can be designed by placing a combination of thermoelectric materials along the unicouple leg, i.e. using a high-temperature thermoelectric material in the high-temperature region of the unicouple and using a low-temperature material in the low-temperature region of the unicouple. Segmented generators and cascaded thermoelectric generators illustrated in

Figure 23 are utilized to achieve this goal. The primary difference between a segmented

and cascaded thermoelectric generator is that a cascaded generator uses an independent

electrical circuit for each stage (material), whereas a segmented generator uses one

electrical circuit.

Segmented TEG   Cascaded TEG
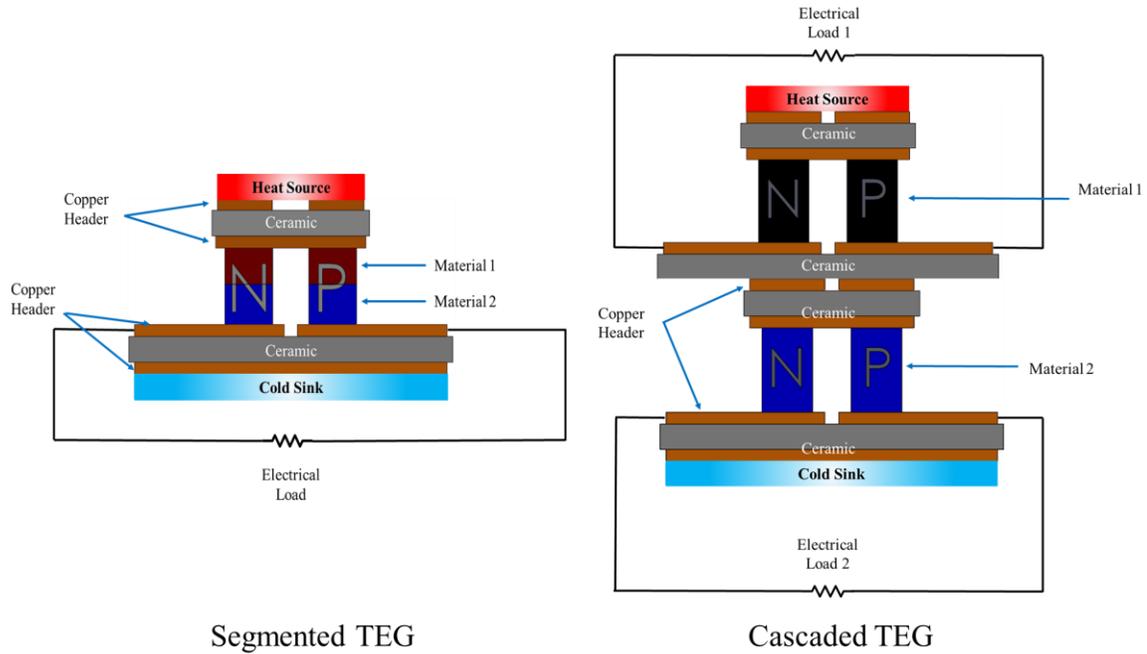
Figure 23:   A segmented TEG and cascaded TEG are illustrated using a single unicouple. The primary difference is the use of two different electrical loads connected to the different stages in the cascaded TEG and the use of a single circuit in the segmented TEG.

Thermoelectric Compatibility

      Utilizing segmented thermoelectric legs puts forward the problem of

thermoelectric compatibility. From equation 2-7, it is shown that peak power of a

thermoelectric unicouple is dependent upon the electric current through it, for the peak

power condition this is obtained by setting the load resistance equal to the electrical

resistance of the unicouple. When two materials are segmented the same current flows

through both materials, however, the optimum electric current will be different for both

materials as they would have different electrical resistivites. Furthermore, each material has its own optimum relative current density defined by the following equation [26]:

$$u = \frac{J}{\kappa \nabla T} \tag{2-16}$$

where J is the electric current density, κ is the thermal conductivity and ∇T is the temperature gradient. If the relative current density of the two-segmented materials differs significantly, the thermoelectric efficiency may decrease when compared to using a single material [26]. The thermoelectric compatibility equation may be utilized to select materials, which can be used for segmentation:

$$s = \frac{\sqrt{1 + zT} - 1}{\alpha T} \tag{2-17}$$

where ZT is the thermoelectric figure of merit, α is the Seebeck coefficient, and T is the absolute temperature. Initially, it was suggested that two materials with compatibility factors differing by a factor of 2 would decrease efficiency when segmented [27, 28]. However, Ouyang and Li suggest that it is the smooth transition of the compatibility factors at the temperature boundaries that is significant [29]. A smooth transition is observed in the compatibility factor for the p-type at 200°C for Bi_2Te_3 and PbTe, and a similar transition can be witnessed for Bi_2Te_3 and Half-Heusler at 250 °C in Figure 22(c). For the n-type material, the transition is observed at the limit of the Bi_2Te_3 operating temperature of 250 °C. Additionally, it is also observed that the thermoelectric figure of merit of Bi_2Te_3 is larger than that of the Half-Heusler and PbTe materials from 20°C to approximately 225 °C for the n-type material and 200°C for the p-type material.

Design of Segmented Leg Unicouples

The thermoelectric unicouple model was modified to predict the performance of a unicouple containing a Half-Heusler segment and a Bi_2Te_3 segment (unicouple A).

Additionally, a unicouple containing a PbTe segment and a Bi$_2$Te$_3$ segment (unicouple B) was designed. The two newly designed unicouples were then compared with conventional unicouples containing only a single material of PbTe and Half-Heusler alloy for a hot side temperature of 600°C and cold side temperature of 20°C.

Taking into consideration the transition of the compatibility factor between Bi$_2$Te$_3$ and the Half-Heusler material and the thermoelectric figure of merit of both materials, 250°C appears to be a suitable interface temperature. This observation means that the segmented unicouple would be designed such that the Bi$_2$Te$_3$ segment of the unicouple will experience a temperature from 250 °C to 20 °C. Similarly, the Half-Heusler alloy segment will have a hot side temperature of 600°C, and a cold side temperature of 250°C. The total height of the unicouple was kept similar to that in Table 1. In order to obtain the required interface temperature, the thermal resistances of the segments have to be adjusted according to the required interface temperature. While keeping the leg areas constant, the following equation can be utilized to obtain the ratio of the two segment heights [30]:

$$\frac{l_{p1}}{l_{p2}} = \frac{\int_{T_{int}}^{T_h} \lambda_{p,1}(T)dT}{\int_{T_c}^{T_{int}} \lambda_{p,2}(T)dT} \tag{2-18}$$

$$\frac{l_{n1}}{l_{n2}} = \frac{\int_{T_{int}}^{T_h} \lambda_{n,1}(T)dT}{\int_{T_c}^{T_{int}} \lambda_{n,2}(T)dT} \tag{2-19}$$

$$l = l_{p1} + l_{p2} = l_{n1} + l_{n2} \tag{2-20}$$

where $l_{p,n,1}$ is the length of the p and n type top segment, $l_{p,n,2}$ is the height of the p and n type bottom segment. T_h is the temperature at the interface between the top copper header and the top segment; T_{int} is the temperature at the segment interface, T_c is the temperature

at the interface between the bottom copper segment and the bottom segment, and l is the total height of the combined leg. The leg heights of each segment obtained by equations 2-18 through 2-20 and are shown in Table 2.

Table 2   Height of the material segments in unicouple A and B

Segment	Unicouple A	Unicouple B
Half-Heusler alloy segment	2.106 mm	-
PbTe segment	-	1.618 mm
Bi_2Te_3 segment	0.294 mm	0.782 mm
Total Height	2.4 mm	2.4 mm

The power and efficiency curves are compared in Figure 24 for both the Half-Heusler-Bi_2Te_3 segmented unicouple (unicouple A) and the PbTe-Bi_2Te_3 segmented unicouple (unicouple B) compared with only using a single material. The models were run for a hot side temperature of 600°C and cold side temperature of 20°C and compared using similar geometric properties with the difference being leg heights defined in Table 2. For the segmented Half-Heusler unicouple there was a 16 % increase in the power output, while there was 61 % increase in the peak efficiency. The higher increase in the efficiency is explained by the fact that the compatibility factor is utilized to find matching materials, which can be used to improve efficiency. While improvements in power generation are expected with improved efficiency, the primary improvement is in the heat to power conversion efficiency. Similarly, for the PbTe-Bi_2Te_3, segmented unicouple a 49.5% improvement was observed for power, and an increase of 65.5% was observed for the efficiency.
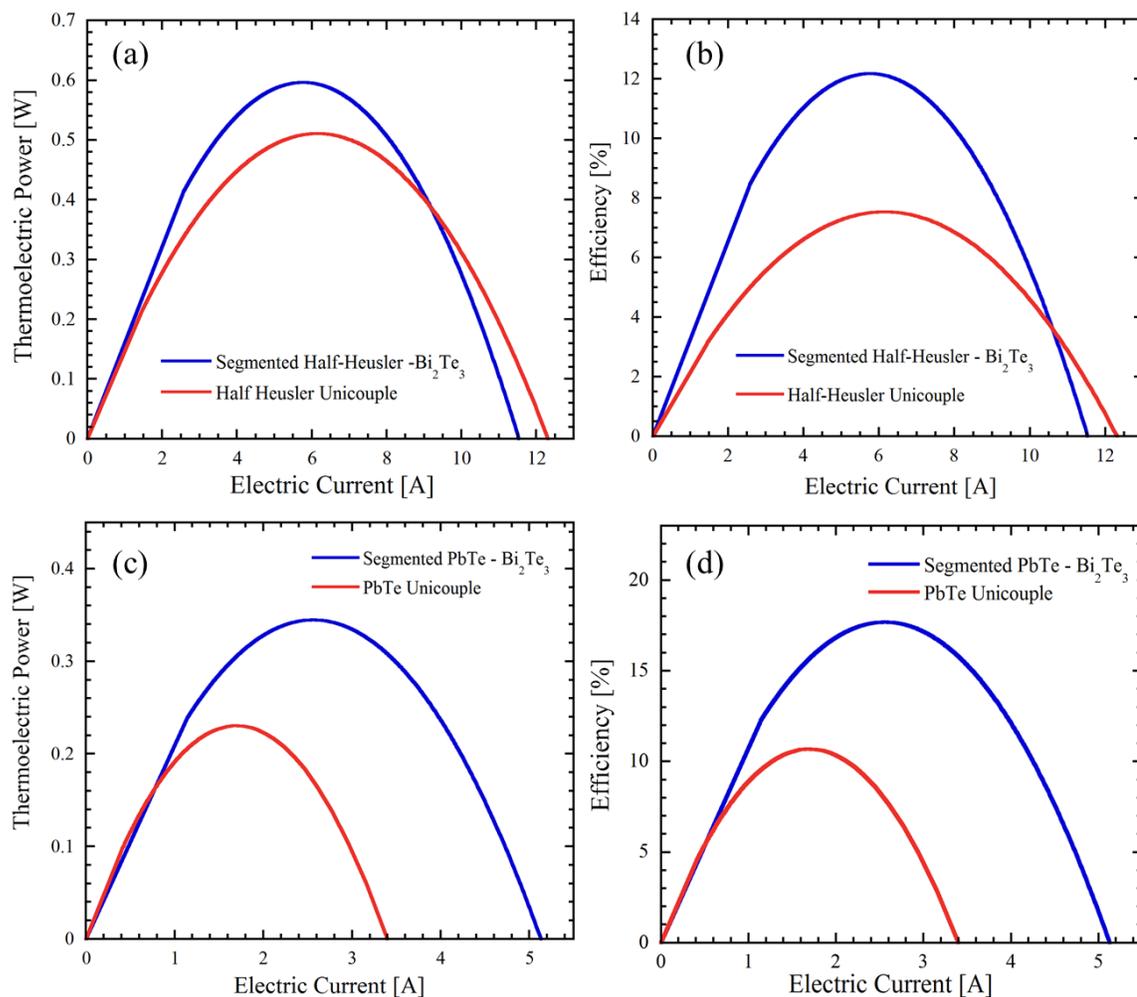
Figure 24: **(a) Thermoelectric power and (b) efficiency comparison for the Half-Heusler-Bi₂Te₃ unicouple compared to a unicouple composed only of the Half-Heusler alloy. (c) Thermoelectric power and (d) efficiency comparison for the PbTe-Bi₂Te₃ unicouple compared to a unicouple composed only of the PbTe material.**

THERMOELECTRIC GENERATOR – HEAT EXCHANGER MODEL

Introduction

Thermoelectric generators are often accompanied by heat exchangers with the goal of maintaining the required temperature difference across a thermoelectric module. Compact heat exchangers are used in waste heat recovery when there is a restriction on the available space, for instance in automotive waste heat recovery applications [3]. Further, applications of compact heat exchangers include high-temperature polymer electrolyte membrane fuel cell exhaust heat recovery [19] and waste heat reclamation from jet engines[5]. Heat exchangers, which utilize forced convection, are often used, as the waste heat is often available as a flowing hot fluid.

Heat exchanger models have been developed to be used in combination with thermoelectric generator models. A plate-fin heat exchanger model has been developed in combination with a TEG model to predict the electrical power output and overall heat transferred to be implemented for automotive waste heat recovery [16]. The model uses the hot exhaust gas as the hot side fluid and the liquid coolant for the cold side fluid. A similar numerical model has been developed for a TEG to be used with a parallel-plate heat exchanger [17]. Cylindrical shell and straight fin heat exchangers offer an alternative to parallel plate heat exchangers to recover waste heat from an automotive. A numerical heat transfer model has been developed along with a TEG model to predict the heat transfer and electrical power performance of a combined system [20].

A heat exchanger model is developed to complement the thermoelectric module model for steady state operation. The model developed in a MATLAB environment is solved by considering the first law of thermodynamics in every finite control volume illustrated in Figure 25. The inputs to the heat exchanger-TEG model are the geometry of the heat exchanger and the inlet temperatures of the working fluids as well as the temperature dependent fluid and thermoelectric properties.

Model Assumptions

The following assumptions were made to simplify the heat exchanger model.

1) The model divides each spacing in the heat exchanger as an individual channel, which leads to the following assumptions

    a. The mass flowrate in each channel is identical and is obtained by dividing the total flowrate by the number of channels.

    b. The heat transfer coefficient and friction factor in each section of the channel is constant for the control volume.

2) Lateral variations in temperature are ignored.

3) The model assumes the flow is fully developed when entering each channel. The heat exchangers are usually accompanied by a diffuser, which is not included in the model.

4) Constant fluid temperatures are assumed in each control volume and a constant fin base temperature is assumed for each control volume.

5) The lateral sides of the heat exchanger are assumed to be perfectly insulated.

Control Volume – Energy Balance

The model is solved by portioning each segment of the TEG-heat exchanger system into finite control volumes as illustrated in Figure 22. The fundamental principal used to solve the model is the first law of thermodynamics, by equating the heat flow through the fins to be equal to the heat flow through the thermoelectric modules. The TEG-Heat exchanger model is split into two symmetric components as shown in Figure 25 and calculations are performed on one section to minimize computational expense. The length of one control volume needs to be the length of the thermoelectric module.
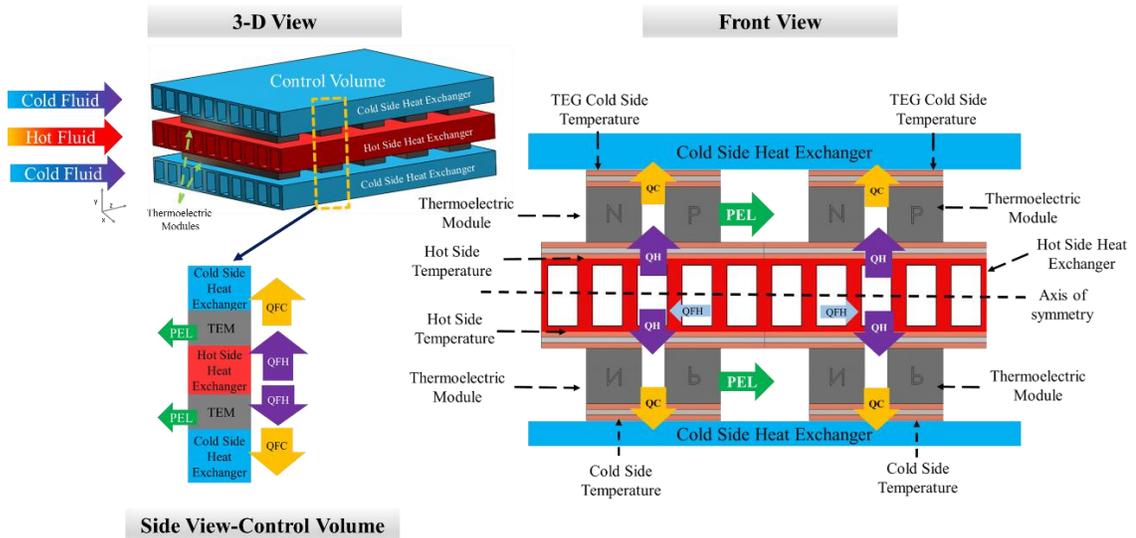
Figure 25: **TEG – Heat Exchanger model illustrated with a 3-D view, front view and a side view explaining the energy balance concept used in the model. QH is the heat flow into the hot side of the TEG within the control volume and QC is the heat flow from the cold side of the TEG to the cold-side heat exchanger. QFH is the heat flow from the hot side heat exchanger within the control volume and QFC is the heat flow from the cold-side heat exchanger in the control volume. PEL is the thermoelectric power generated by the TEG.**

The heat flow through the heat exchanger in the control volume is given by the following equation by using the adiabatic fin tip condition [31]:

$$Q_f = M \cdot tanh\left(m \cdot \frac{fh}{2}\right) \cdot (N_f - 1) + A_{uf} \cdot h \cdot (T_b - T_f) \tag{3-1}$$

$$M = \sqrt{h \cdot P \cdot k \cdot A_c} \cdot (T_b - T_f) \qquad \text{(3-2)}$$

$$m = \sqrt{\frac{h \cdot P}{k \cdot A_c}} \qquad \text{(3-3)}$$

where fh is the fin height, N_f is the number of fins, A_{uf} is the un-finned area, T_b is the fin base temperature of the control volume, T_f is the fluid temperature within the control volume and h is the channel convection coefficient which will be discussed in detail in the next section. P is the fin perimeter, k is the thermal conductivity of the fin material, and A_c is the cross-sectional area of the fin. The heat flow into the module, Q_h is equal to the heat transferred through the fins in the control volume, while the heat flow leaving the cold side of the module, Q_c is equal to the heat transferred through the cold side heat exchanger, QFC. The difference between the heat entering and leaving the module is equal to the thermoelectric power generated by the module as explained in the previous chapter. An iterative process solves the TEG-Heat Exchanger model, and the energy balance criteria have to be met for each control volume. The difference between the heat flow through the hot side of the heat exchanger (QFH) and the heat flow into the module (QH) has to be less than the required convergence criteria of 10^{-4}W. Similarly, the difference between the heat flow leaving the cold side of the module (TC) and the heat flow through the cold side heat exchanger (QFC) has to be smaller than the convergence criteria. The iterative process requires solving the base temperature of both the hot and cold side heat exchangers for the control volume. The exit temperature of the fluid in the control volume will be the inlet temperature of the next one and is obtained by the following equation:

$$T_{f,out} = T_{f,in} - \frac{Q_f}{\dot{m} \cdot c_p} \qquad (3\text{-}4)$$

where $T_{f,out}$ is the exit temperature of the fluid in the control volume, Q_f is the heat

transferred by the heat exchanger within the control volume, $\dot{m}$ is the mass flowrate and

c_p is the specific heat of the fluid.

Channel Convection Coefficient

The channel convection coefficient utilized in the model are obtained from

available empirical correlations. Similar numerical models [16, 17] have used Reynolds

number dependent empirical correlations for the convection coefficients for channel flow.

The current model uses convection coefficients for smooth rectangular ducts, which are

dependent upon the channel width to height ratio. The hydraulic diameter, d_h dependent

Reynolds number for the channel flow is obtained by the following equations:

$$Re = \frac{v_{ch} \cdot d_h}{v_f} \qquad (3\text{-}5)$$

$$d_h = \frac{4 \cdot A}{P} \qquad (3\text{-}6)$$

where v_{ch} is the channel velocity, v_f is the kinematic viscosity, P is the wetted perimeter,

and A is the channel cross-sectional area. The critical Reynolds number for a rectangular

inlet geometry varies from 2000 to 3100 with the upper limit at 10000 [32]. For this

model, laminar and turbulent flow is analyzed with the critical Reynolds number being

2500 based on the empirical correlation used. The convection coefficient evaluated using

the Nusselt number relationships for the laminar and turbulent regions are obtained using

the following equations [32]:

$$Nu = 7.541 \cdot (1 - 2.61\alpha + 4.970\alpha^2 - 5.199\alpha^3 + 2.702\alpha^4 - 0.548\alpha^5) \qquad (3\text{-}7)$$

$$Re \leq 2500$$

$$Nu = 0.024 \cdot Re_{dh}^{0.8} Pr^{0.4} \qquad\qquad Re \geq 2500 \ (T_s > T_f) \qquad (3\text{-}8)$$

$$Nu = 0.026 \cdot Re_{dh}^{0.8} Pr^{0.3} \qquad\qquad Re \geq 2500 \ (T_f > T_s) \qquad (3\text{-}9)$$

$$h = \frac{Nu \cdot k_f}{d_h} \qquad\qquad\qquad (3\text{-}10)$$

where α is the height to spacing ratio, Re is the hydraulic diameter dependent Reynolds number, Pr is the Prandtl number, k_f is the fluid thermal conductivity, d_h is the hydraulic diameter defined above, T_s is the surface temperature, and T_f is the fluid temperature.

Compact heat exchangers defined as having a surface area of 650 m^2 per cubic meter [33] are widely used in applications such as automotive waste heat recovery due to spatial constraints. The following equations developed by Weiting [34] for compact rectangular offset plate fin heat exchangers are considered in the model as well:

$$j = 0.483 \cdot \left(\frac{hxl}{d_h}\right)^{-0.162} \cdot \alpha^{-0.184} \cdot Re^{-0.536} \qquad Re \leq 1000 \qquad (3\text{-}11)$$

$$j = 0.242 \cdot \left(\frac{hxl}{d_h}\right)^{-0.322} \cdot \left(\frac{t_f}{d_h}\right)^{-0.089} \cdot Re^{-0.368} \qquad Re > 1000 \qquad (3\text{-}12)$$

$$h = j \cdot Re \cdot Pr^{1/3} \cdot \frac{k_f}{d_h} \qquad\qquad (3\text{-}13)$$

where j is the Colburn factor, hxl is the heat exchanger length, t_f is the fin thickness, and the other variables are similar to that defined above. The Colburn factor is a modified version of the Stanton number taking into consideration variations in the fluid Prandtl number [32]. There are certain limitations in extending these empirical correlations to compact channel flow. The empirical correlations are obtained for offset plate fin heat exchangers, which means that there is a boundary layer developing on the thickness of the plate. In addition, there is turbulence generated by the plate thickness at the leading edge and wake flow developed at the trailing edge. However, the influence of the fin

thickness is not included in the correlation for the laminar region, suggesting the influence of the fin thickness is limited in laminar flow [34].

Model Validation

The TEG heat exchanger model was compared with an available computational fluid dynamics and ANSYS model, which was developed for a TEG-Heat Exchanger system for automotive waste heat recovery from a diesel engine [3]. The model was compared using the convection coefficients for duct flow using equations 3-10 and the convection coefficients for compact offset fin heat exchangers using equation 3-13. The model was compared for fin packing fractions of 10%, 15%, 20%, 25%, and 30 % and fin thicknesses of 0.1mm, 0.2mm, 0.3mm and 0.4 mm encompassing in 20 different designs. The exhaust of a car resemble the properties of air, and the temperature dependent properties of air were used in the model. The hot-side heat exchanger is composed of Nickel as it has a high thermal conductivity, high service temperature and corrosion resistance [3]. The cold side temperature of the TEG was assumed constant at 94°C, which can be accomplished by using water as the cold side fluid. The following figure illustrates the input into the model and Table 3 lists the parameters.
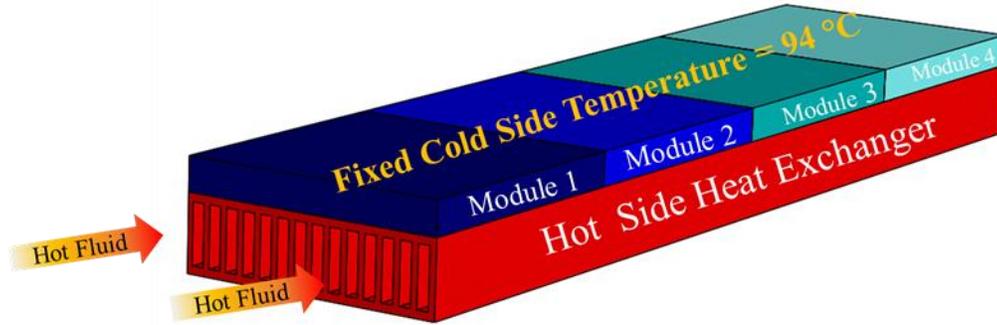
Figure 26:   Input parameters for the TEG – Heat exchanger model. Four modules with a fixed cold side temperature are combined with the hot side heat exchanger.

Table 3   Input to the TEG – Heat Exchanger Model

Input	Value
Exhaust Inlet Temperature	558 °C
Hot Side Fluid	Exhaust gas (Air)
Number of Modules	4
Module Size	40mm x 40 mm x 4.9 mm
TEM Cold Side Temperature	94 °C
Heat Exchanger Width	40 mm
Heat Exchanger Length	160 mm
Heat Exchanger Height	20 mm
Heat Exchanger Material	Nickel

The average heat flow through each TEG is compared in Figure 27 for a TEG – Heat exchanger model that uses convection coefficient of (a) duct and (b) compact heat exchanger with a 3-D model developed in ANSYS Icepak. The 3-D model results are available in [3]. The heat exchangers with a fin thickness of 0.1mm provide more

channels and a larger fin surface area, resulting in better heat flow compared to the other heat exchanger designs. However, the better thermal performance comes at the cost of a larger pressure drop across the heat exchanger. The model using the compact heat exchanger convection coefficient appears to show more consistent results when compared with the model using the duct convection coefficient. The discrepancies between the two models developed can be attributed to the limitations of the empirical convection coefficients used and the lateral heat spreading that is captured in the 3-D model. The mismatch in convection coefficients between the models results in a mismatch in the heat transferred through the heat exchanger, which can be used to explain the discrepancies observed in Figure 27. Furthermore, the model accuracy could be improved by accounting for the heat spreading within the heat exchanger. The model assumes that the base temperature in each control volume is maintained at the same temperature, this is not the case in the 3-D ANSYS model.
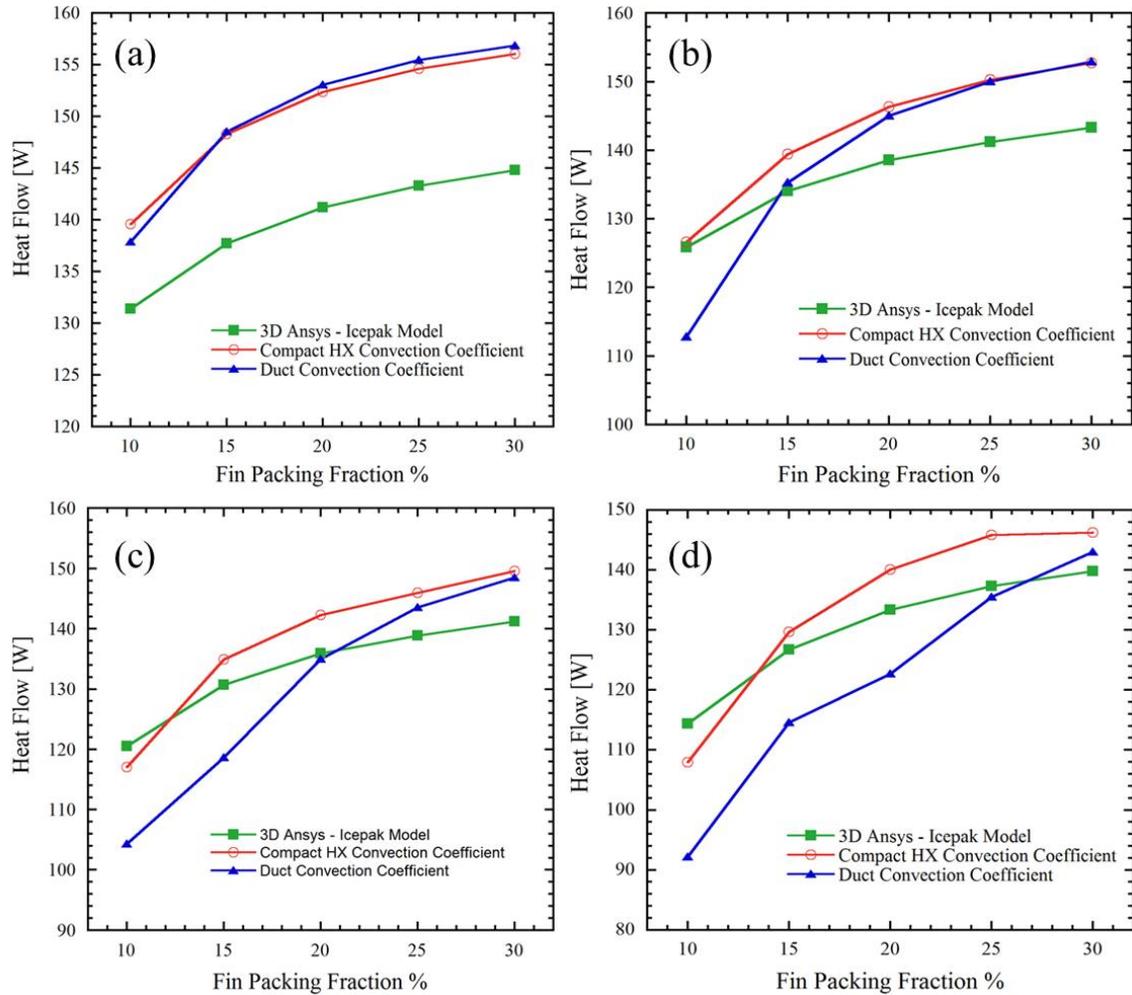
Figure 27: **The average heat flow through each module compared with a 3D Model using the TEG – Heat Exchanger Model that uses compact heat exchanger convection coefficients and duct convection coefficients for (a) fin thickness = 0.1 mm (b) fin thickness = 0.2 mm (c) fin thickness = 0.3 mm (d) fin thickness = 0.4 mm[3].**

The average percent difference between the models using the two different types of convection coefficients are compared in Table 4. The compact heat exchanger convection coefficient model has marginally smaller percent errors compared to the duct convection coefficient model.

Table 4   Average percent error comparison between the two models. The percent error values are obtained assuming the 3-D model values as the exact or theoretical value.

Fin Thickness	Duct Convection Coefficient model	Compact Heat-Exchanger Convection Coefficient model
0.1 mm	7.60 %	7.50 %
0.2 mm	5.79 %	4.63 %
0.3 mm	6.37 %	4.36 %
0.4 mm	8.13 %	4.76 %

The temperature difference between the TEG hot and cold side is critical to the thermoelectric performance of the TEG. The average temperature difference between the TEGs are compared for the different heat exchanger designs evaluated. The results follow similar trends to the average heat flow results shown in Figure 27.
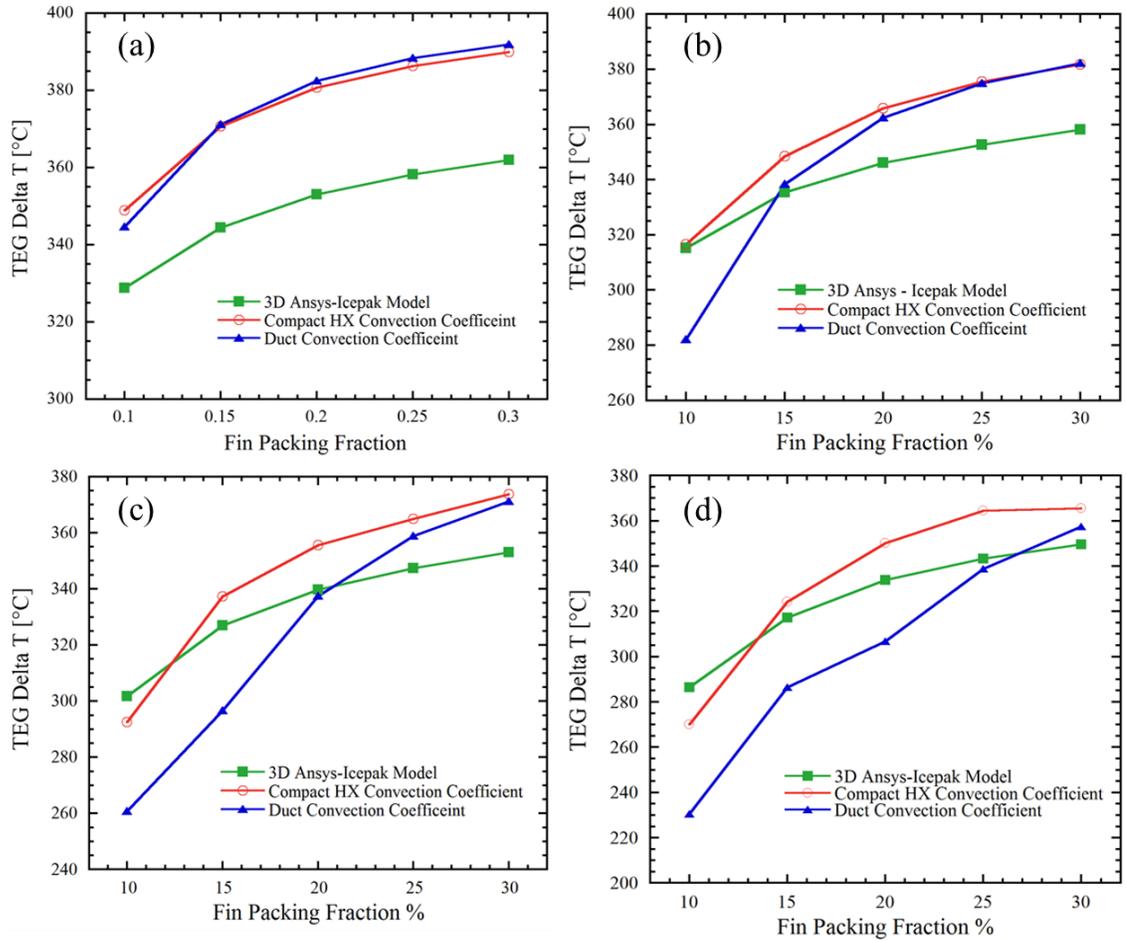
Figure 28: **The average temperature difference across each module compared with a 3D Model using the TEG – Heat Exchanger Model that uses compact heat exchanger convection coefficients and duct convection coefficients for (a) fin thickness = 0.1 mm (b) fin thickness = 0.2 mm (c) fin thickness = 0.3 mm (d) fin thickness = 0.4 mm[3].**

The average module power generation and efficiency are shown in Figure 29 for the different heat exchanger designs. The largest TEG power generation of 7.75 W is obtained for the heat exchanger design with a fin thickness of 0.1mm and packing fraction of 30%. This design has the largest heat flow through it resulting in more power generated. Additionally, this design resulted in the largest temperature difference between the TEG, corresponding to the largest TEG efficiency of 4.96 %. It should be noted that the 0.1mm – 30% packing fraction heat exchanger has a significantly larger pressured

drop compared to the other designs. When the heat exchanger design is considered both

pressure drop and heat transfer capabilities of the heat exchanger should be evaluated.
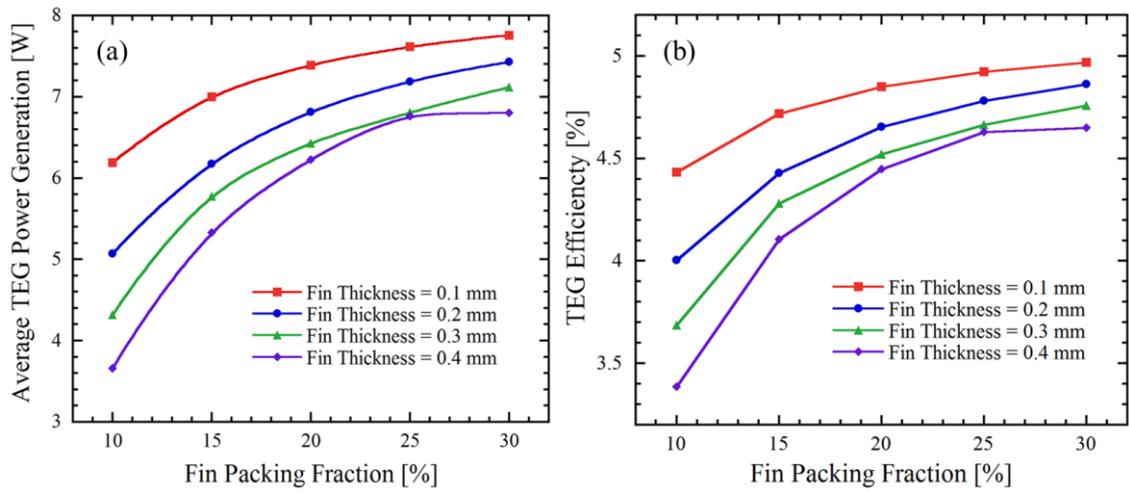
Figure 29: **(a) The average thermoelectric power generated by a module for heat exchanger fin thicknesses of 0.1 mm, 0.2 mm, 0.3 mm and 0.4 mm (b) Average module efficiency for heat exchanger fin thickness of 0.1mm, 0.2mm, 0.3 mm and 0.4 mm.**

THERMOELECTRIC GENERATORS COMBINED WITH NATURAL

CONVECTION HEAT SINKS

Introduction

Natural convection heat sinks can be incorporated with TEGs to maintain the cold

side temperature of the TEG. There are many instances when it is not possible to

integrate a forced convection heat sink with a TEG, for instance when a TEG is used to

recover waste heat from the body. Furthermore, natural convection heat sinks are much

more reliable than forced convection heat exchangers. Natural convection heat sinks

require almost no maintenance, which makes them ideal to be implemented with TEG

devices that are used to self-power electric devices. Additionally, natural convection heat

sinks require no pumping power, as compared to forced convection heat sinks, which

means that all the power generated by a TEG can be used to power devices, and none of

the energy is expended on pumping power. However, heat transfer coefficients for natural

convection heat sinks are much smaller than forced convection heat exchangers.

Buoyancy effects drive natural convection, which is dependent upon density variations of

the fluid, which in turn require a significant temperature difference between the surface in

consideration and the ambient fluid. Natural convection heat sinks are classified into

plate fin heat sinks and pin fin heat sinks, whose performance is influenced by the heat

sink orientation with regard to the gravitational field. This section looks at vertical plate

and pin fin heat sinks, as well as horizontal base pin fin heat sinks, where the primary

difference in the models are the convection coefficients of the heat sinks. The three

different types of heat sinks are illustrated in Figure 30 with their orientation with respect to the gravitational field shown. The heat sinks are then optimized to be used with a TEG to power a wireless sensor using waste heat from a pipe in a nuclear power plant. Finally, optimized heat sinks are combined with TEGs to harvest waste body heat which can be used to power wearable electronics.
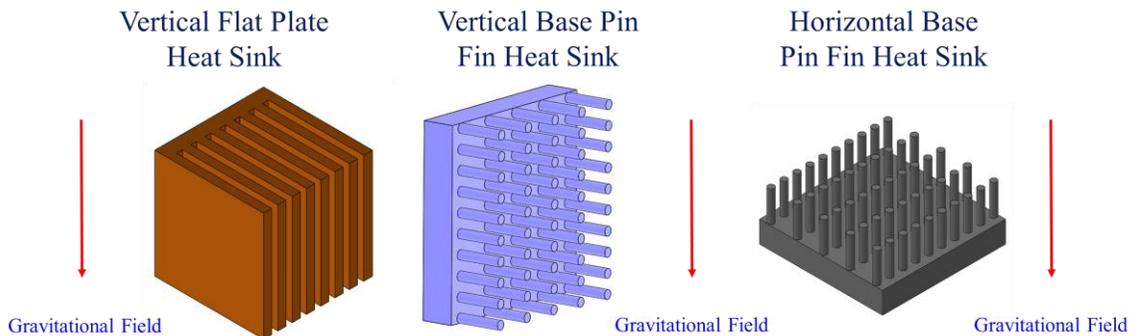
Figure 30: **The three different types of heat sinks considered in this section.**

Vertical Flat Plate Heat Sink Model

As stated in the introduction section, the primary difference between the heat sink models are the convection coefficients of the heat sinks. Natural convection coefficients for parallel plate heat sinks are obtained from work done by Bar-Cohen et al. [35]. The convection coefficient builds on work initially done by Bar-Cohen [36]. It is important to note the convection coefficient apply to finned geometries, which takes into consideration asymmetric heat flow. A 1-D analytical steady state model is developed to predict the thermal performance of vertically oriented natural convection plate fin heat sinks. The primary direction of heat transfer is from the base of the heat sink to the ambient. Consequently, the model assumes that there are no lateral variations in temperature along the heat sink base. The key parameter used to evaluate the performance of a heat sink is the thermal resistance of the heat sink defined as follows:

$$R_{th} = \frac{T_b - T_{amb}}{Q_{HS}} \tag{4-1}$$

where T_b is the temperature of the heat sink base. T_{amb} is the ambient temperature, and Q_{HS} is the heat flow through the heat sink. The heat flow through the heat sink by heat convection was obtained as follows:

$$Q_{HS} = n_{fin} \cdot q_{fin} + h_{base} \cdot A_b \cdot (T_b - T_{amb}) \tag{4-2}$$

where n_{fin} is the number of fins, A_b is the unfinned base area, T_b is the heat sink base temperature, and h_{base} and q_{fin} are defined by the following equations. The unfinned base area is treated as a vertical flat plate, and the convection heat transfer coefficient is obtained as follows:

$$h_{base} = 0.59 \cdot Ra_L^{1/4} \cdot k_f / L \tag{4-3}$$

where k_f is the thermal conductivity of air, and L is the vertical length of the heat sink, and the Rayleigh number, Ra_L is obtained as follows:

$$Ra_L = g \cdot \beta \cdot \theta_b \cdot Pr \cdot L^3 / v^2 \tag{4-4}$$

where g is gravity, β is the coefficient of thermal expansion, θ_b is the temperature difference between the heat sink base and the ambient, Pr is the Prandtl number, and v is the kinematic viscosity of the fluid. The heat transfer from each of the individual plate-fins, q_{fin}, is obtained as follows[31]:

$$q_{fin} = M \cdot tanh(m \cdot H) \tag{4-5}$$

where H is the height of the plate fins extruding in the horizontal direction, M and m are fin parameters defined as follows:

$$M = \sqrt{h \cdot P \cdot k \cdot A_c} \cdot (T_b - T_{amb}) \tag{4-6}$$

$$m = \sqrt{(h \cdot P)/(k \cdot A_c)} \qquad (4\text{-}7)$$

where k is the thermal conductivity of the fin material, P is the fin perimeter, and A_c is the cross-sectional area. The convection heat transfer coefficient, h from non-isothermal asymmetric plates, take into account the two limiting spacing conditions for flat plate heat sinks, small fin spacing, and large fin spacing. The convection coefficient considering the spacing limits above is obtained as follows [35]:

$$h_{fin} = \frac{k_a}{s} \cdot \left(\frac{576}{(\eta_{fin} \cdot El)^2} + \frac{2.873}{(\eta_{fin} \cdot El)^{\frac{1}{2}}} \right)^{1/2} \qquad (4\text{-}8)$$

where s is the spacing between the plate fins, η_{fin} is the fin efficiency, and El, the Elenbaas number, which is a modified version of the Rayleigh number, is obtained as follows:

$$El = (g \cdot \beta \cdot \theta_b \cdot Pr \cdot s^4)/Lv^2 \qquad (4\text{-}9)$$

The first term in parentheses in equation 4-8 accounts for the small fin spacing condition, while the second term represents the large spacing condition. When the heat sink is used for applications with large temperature differences, radiation effects become significant and are considered in the heat sink model. Radiation heat transfer from the outer surfaces of the heat sink was considered in the model, as these surfaces have a view factor of 1 with the ambient. The heat transfer by radiation is given by the following equation:

$$Q_r = A_r \cdot \sigma \cdot \varepsilon \cdot \left(T_{HS}^4 - T_{amb}^4 \right) \qquad (4\text{-}10)$$

where A_r is the heat sink area transferring heat by radiation to the ambient, σ is the Boltzmann constant, ε is the emissivity of the heat sink material, and T_{HS} is the average heat sink temperature. It is important to note that the model uses absolute temperature values for the radiation analysis.

Vertical Base Pin Fin Heat Sink Model

Vertical base pin fin heat sinks are another viable option to be used along with TEGs to harvest waste thermal energy. Pin fin heat sinks have better thermal performance compared to flat plate heat sinks when the mass of the heat sink is considered [37]. A one-dimensional heat transfer model is developed similar to the vertical flat plate heat sink model. The primary differences between the two models are the fin geometry, the fin cross-sectional area, and the fin perimeter. In addition to the fin geometry, the convection coefficient for pin fin heat sinks is different to that of the vertical plate heat sinks. The convection coefficient for pin fin heat sinks are influenced by four limiting conditions, which are listed below:

1) Small vertical spacing with small horizontal spacing

2) Small vertical spacing with large horizontal spacing.

3) Large vertical spacing with small horizontal spacing.

4) Large vertical spacing with large horizontal spacing.

The work done by Joo et al. [37] consider convection coefficients for each limiting case and combine them to match empirical data. The convection coefficient for limiting case 1 looks at densely packed heat sink with a large number of pins in both the horizontal and vertical directions. The convection coefficient for the densely packed condition is obtained by modeling the fin array as a porous medium:

$$h_{fin,1} = \frac{S_h S_v}{\pi d L} \cdot \frac{4 S_h S_v - \pi d^2}{48} \cdot \frac{\rho_f c_p g \beta \eta_{fin}(T_b - T_\infty)}{v_f} \tag{4-11}$$

where S_h and S_v are the horizontal and vertical spacing, d is the fin diameter, L is the heat

sink length, ρ_f is the fluid density, c_p is the specific heat of the fluid, g is the acceleration

of gravity, β is the thermal coefficient of expansion, η_{fin} is the fin efficiency, v_f is the

kinematic viscosity of the fluid, T_b is the base temperature and T_∞ is the ambient

temperature. For the second limiting case, the pins are arranged in a vertical direction

with large horizontal spacing and can be modelled as an isolated vertical array of

cylinders by the following equation:

$$h_{fin,2} = \frac{k_f}{L} \cdot \left[0.3669 \frac{S_v}{d} - 0.0494 \right] Gr_L^{1/4} \tag{4-12}$$

$$Gr_L = \frac{g \beta \eta_{fin}(T_b - T_\infty)L^3}{v_f^2} \tag{4-13}$$

where Gr_L is the length dependent Grashof number and the other variables as defined

above. For the third limiting case, pins are arranged in a single horizontal direction with

large vertical spacing, and the convection coefficient is obtained by the following

equation:

$$h_{fin,3} = \frac{k_f}{d} \cdot [2.132 S_h^* - 0,4064] \left(\frac{g \beta (T_b - T_\infty)}{\alpha_f v_f d} \right)^{0.188} \tag{4-14}$$

$$S_h^* = \frac{S_h^*}{d^{3/4} L^{1/4}} \tag{4-15}$$

where S_h^* is the non-dimensional horizontal spacing and α_f is the thermal diffusivity of the

fluid, and the other variables are defined as above. The final limiting condition accounts

for a pin fin with large horizontal and vertical spacing, which is an isolated horizontal

cylinder with the convection coefficient given by the following equation:

$$h_{fin,4} = \frac{k_f}{d} \cdot 0.85 Ra_d^{0.188} \tag{4-16}$$

$$Ra_d = \frac{g\beta\eta_{fin}(T_b - T_\infty)d^3}{\alpha_f \nu_f} \tag{4-17}$$

where Ra_d is the fin diameter dependent Rayleigh number and the other variables as defined above. The four convection coefficients are combined to match experimental data and reduces to the following equation:

$$h_{fin} = [(h_{fin,1}^{-1.3} + h_{fin,2}^{-1.3} h_{fin,3}^{-1.3})^{\frac{8}{1.3}} + h_{fin,4}^{-8}]^{\frac{1}{-8}} \tag{4-18}$$

Horizontal Base Vertical Pin Fin Heat Sink Model

Initial work on pin fin heat sinks was done by Sparrow and Vemuri [38]. They performed experiments in air to measure the combined convection and radiation heat transfer from (1) horizontal fins with a vertical base plate, (2) vertical fins with a downward facing base plate and (3) vertical fins for an upward facing base plate. Horizontal base plate vertical pin fin heat sinks have been numerically and experimentally been studied by Sahray et al. [39]. A mean convection coefficient for a heat sink is obtained taking into consideration fin height, fin packing fraction (which considers fin spacing) and heat sink base area. The convection relation is obtained for vertical square pin fins on a horizontal base. The Nusselt number correlation and convection coefficient are given by the following equations:

$$h_c = \frac{k_f \cdot Nu_s}{S} \tag{4-19}$$

$$Nu_s = 0.0285 \left\{ 1 - exp\left(-\frac{H}{W}\right) \right\} \dots \tag{4-20}$$
$$\dots \left\{ 1 + 1.50 exp\left(-0.07\frac{L}{H}\right) \right\} Ra_s^{1/2} \left\{ 1 - exp[-\frac{7000}{Ra_s}] \right\}^{1/3}$$

$$Ra_s = \frac{g\beta\Delta T S^3 Pr}{v^2} \tag{4-21}$$

$$S = P - W \tag{4-22}$$

where k_f is the fluid thermal conductivity, Nu_s is the spacing dependent Nusselt number, S is fin spacing defined by equation 4-22. L is the heat sink base width, H is the pin height, Ra_s is the spacing dependent Rayleigh number, P is fin pitch, W is the pin width and the variables in equation 4-21 are similar to that defined in the previous sections.

TEG for Power Harvesting in a Nuclear Power Plant

Introduction

Constant monitoring of temperature, pressure, and radiation levels are critical to the safe operation of a nuclear power plant. Wireless sensor nodes are used to monitor the temperature pressure and radiation levels in a nuclear power plant. When natural disasters such as the Fukushima Daiichi nuclear incident in March 2011 occur, where power supply from both the on-site and off-site power depletes, monitoring systems lose function and cannot collect critical information regarding the nuclear plant status. The loss of off-site power in nuclear plants is a frequent occurrence where 42 power outages have been recorded from 1997 to 2004 [40]. Thermoelectric generators can be utilized to self-power wireless sensor nodes making nuclear power plants safer. Furthermore, cost savings can be observed by eliminating cable installation and maintenance. The lack of required maintenance and reliability of natural convection heat sinks make them an ideal candidate to be used with a thermoelectric generator to power wireless sensor nodes.

TEG – Heat Sink System Model for Powering a Wireless Sensor Node

A one-dimensional model was developed in a MATLAB environment combining the thermoelectric model from chapter two and the corresponding heat sink model. The

primary direction of heat transfer is from the pipe (Heat Source) to the ambient.

Therefore 1-D heat flow through the TEG and heat sink is considered as illustrated in

Figure 31. The inputs into the heat transfer model are the TEG hot side temperature (T_H),

and the ambient temperature (T_{amb}). The combined model is solved by an iterative

process, which requires that the heat leaving the cold side of the TEG (Q_c) match the heat

flow through the heat sink (Q_{HS}) as explained by the following equation:

$$\text{abs}(Q_c - Q_{HS}) < CC \qquad \text{(4-23)}$$

where CC is the convergence criteria equal to 10^{-6} W. When the convergence criterion is

met, the model will solve for the cold side temperature. Eventually, the model will output

the heat flow through the TEG, while obtaining the cold side temperature of the TEG, the

power output of the TEG, as well as the operational current and voltage. The external

temperature of a nuclear power plant piping system can vary from 200°C – 350°C, the

lower limit of 200 °C was used in the model.
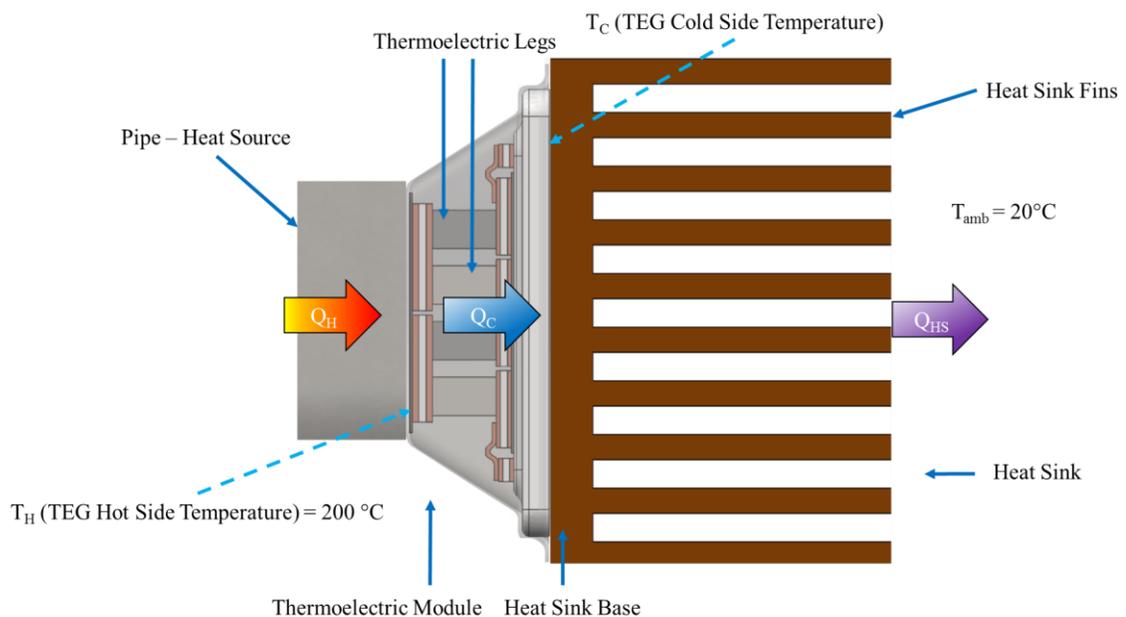
Figure 31: **Heat Transfer model accounting for the heat flow through TEG and the heat sink, where Q_H is the heat flow into the hot side of the TEG, Q_C is the heat**

leaving the cold side of the TEG, and Q_{HS} is the heat flow from the heat sink to the ambient. The heat sink plates are vertically oriented, and the figure illustrates a top view.

<u>Heat Sink Design</u>

A vertical flat plate heat sink was chosen to be placed on the cold side of the TEG. Vertical flat plate heat sinks have better thermal performance compared to a vertical base –horizontal pin fin heat sink when the overall mass of the heat sink is insignificant [37]. The design of the vertical flat plate heat sink was optimized with the goal of obtaining the smallest thermal resistance. Table 5 lists the conditions that were held constant for each optimization.

Table 5   Constant input parameters

Parameter	Value
Base Thickness	1 cm
Base Area	4 cm x 4 cm
Base Temperature	110 °C
Ambient Temperature	20 °C

The vertical flat plate heat sink was optimized for fin thickness, fin packing fraction and fin height with the heat sink optimization parameters listed in the table below.

Table 6   Optimization parameters of the plate-fin heat sink

Parameter	Value
Fin Thickness	1mm – 10 mm with 0.5 mm increments
Fin Height	1cm – 30 cm with 1 cm increments
Fin Packing Fraction	10% - 50 %

At a fin height of 15 cm, the thermal resistance of the heatsink approaches an asymptotic value as illustrated in Figure 32(a). The diminishing returns in thermal resistance with fin height are explained by the reduction in fin efficiency of an individual fin. A fin height of 15 cm provides considerable heat flow without extruding out significantly. A fin thickness of 1.5 mm provides the smallest thermal resistance of 1.67 K/W at a packing fraction of 25 % as shown in Figure 32(b).
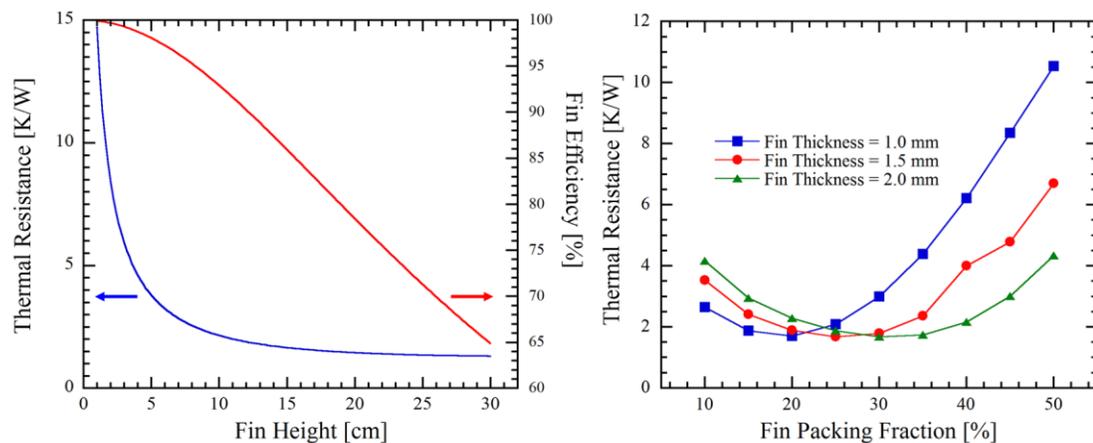
Figure 32: a) **Heat sink thermal resistance and fin efficiency for varied fin height for a fin packing fraction of 26.25% and fin thickness of 1.5 mm. (b) Heat sink thermal resistance for varied fin thicknesses and packing fractions for a fin height of 15 cm.**

The minimum thermal resistance of the optimized heat sink is 1.67 K/W, and the relevant fin parameters are listed in Table 7.

Table 7 **Dimensions of the optimized vertical flat plate heat sink**

Parameter	Value
Heat Exchanger Base Area	4 cm x 4 cm
Fin Height	15 cm
Fin Thickness	1.5 mm
Fin Packing Fraction	26.25%

TEG Optimization

      The optimized heat sink described in Table 7 was combined with a TEG. The

TEG was optimized by increasing the TE leg height from 0.4 mm to 4 mm while holding

the leg fill factor to 19.85 %. The thermoelectric power generated was compared for two

modules, one composed of the Half-Heusler alloy and the other composed of the Bi_2Te_3

material. A peak power density of 101.79 mW/cm^2 is obtained for at leg height of 1.5mm

for the Half-Heusler alloy, and a peak power density of 133 mW/cm^2 is obtained at a leg

height of 0.8mm for the Bi_2Te_3 material as illustrated in Figure 33. The TEG made of

Half-Heusler produces a total power of 1.63 W and the one composed of Bi_2Te_3 produces

2.128 W. The larger power produced by the Bi_2Te_3 material stems from its superior

performance at the device operation temperature range.
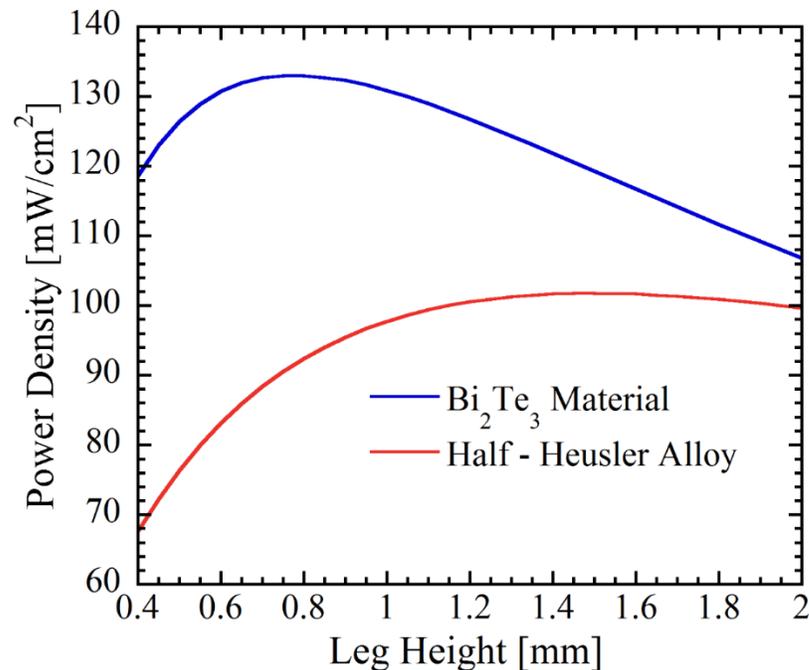
Figure 33:   **Power density vs. varied leg height for a fixed leg packing fraction of 19.85% for a TEG composed of the Half-Heusler alloy and Bi_2Te_3 material.**

Harvesting Body Heat Using a TEG-Natural Convection Heat Sink System

The human body emits significant quantities of waste heat with an average heat flow from the human body found to be 19 mW/cm^2 for data collected from 100 persons [41]. Many wearable electronic devices use much less power than ever before and could be powered by waste heat from the human body. There has been a considerable amount of work done to demonstrate the potential of harvesting body heat using TEGs. The concept of using body heat to power electronic devices was pioneered to power an electronic watch [42] producing 22.5 µW of power. Further applications of TEGs harvesting body heat have been used to power wireless sensor nodes [6] where a pin fin heat sink is used to improve heat transfer from the cold side of the TEG. Further applications examine using TEGs to power autonomous wireless sensors for body area networks. Additional applications include utilizing a TEG to power a pulse oximeter, which measures the oxygen level in the body [7, 43]. Experimental work has been done on a TEG used to harvest body heat, where copper heat spreaders were used to extract body heat [44]. Experimental work done has examined the best location to recover waste heat from the human body, when no airflow is considered the wrist is the best position to extract waste body heat. Interestingly, the work does not use a heat sink but uses copper heat spreaders on both the hot and cold side of the TEG[45]. To obtain a larger temperature difference across the TEG, the thermal resistance of the TEG has to be increased; this has been accomplished by stacking commercially available TEGs on top of each other [46].

TEG- Heat Sink System Model for Harvesting Waste Heat from the Body

The TEG- Heat sink heat transfer model for harvesting body heat is illustrated in Figure 34. The known inputs into the model are the body core temperature, which is assumed to be 37°C and the ambient temperature of 22°C. The body regulates the heat flow from itself by adjusting the thermal resistance between the core and the skin. The thermal resistance of the skin is obtained by the following equation:

$$R_{th} = \frac{1}{U \cdot A_b} \tag{4-24}$$

where A_b is the cross sectional area of the TEG placed on the skin, U is the heat transfer coefficient accounting for heat transfer through the skin, which was found to be equal to 25 W/m²·K [46]. The model also considers the contact resistance between the human skin and the TEG. The contact resistance between the skin and the TEG is given by the following equation [8]:

$$R_{th(contact)} = \frac{1}{h_c \cdot A_b} \tag{4-25}$$

$$h_c = 1.25 \frac{\kappa_s \Delta a}{\sigma} \left(\frac{P}{H_c}\right)^{0.95} \tag{4-26}$$

where κ_s is the harmonic mean thermal conductivity, Δa is the surface roughness, P is the applied pressure, H_c is the micro-hardness of the skin and A_b is as defined above. The smallest contact resistance value is obtained for the forearm, where the h_c value varies from 50 -75 Wm⁻²K⁻¹[8]. The conservative value of 50 Wm⁻²K⁻¹ was used in the model. The two thermal resistances connected in series were combined into one thermal resistance with an overall heat transfer coefficient of 16.67 Wm⁻²K⁻¹.
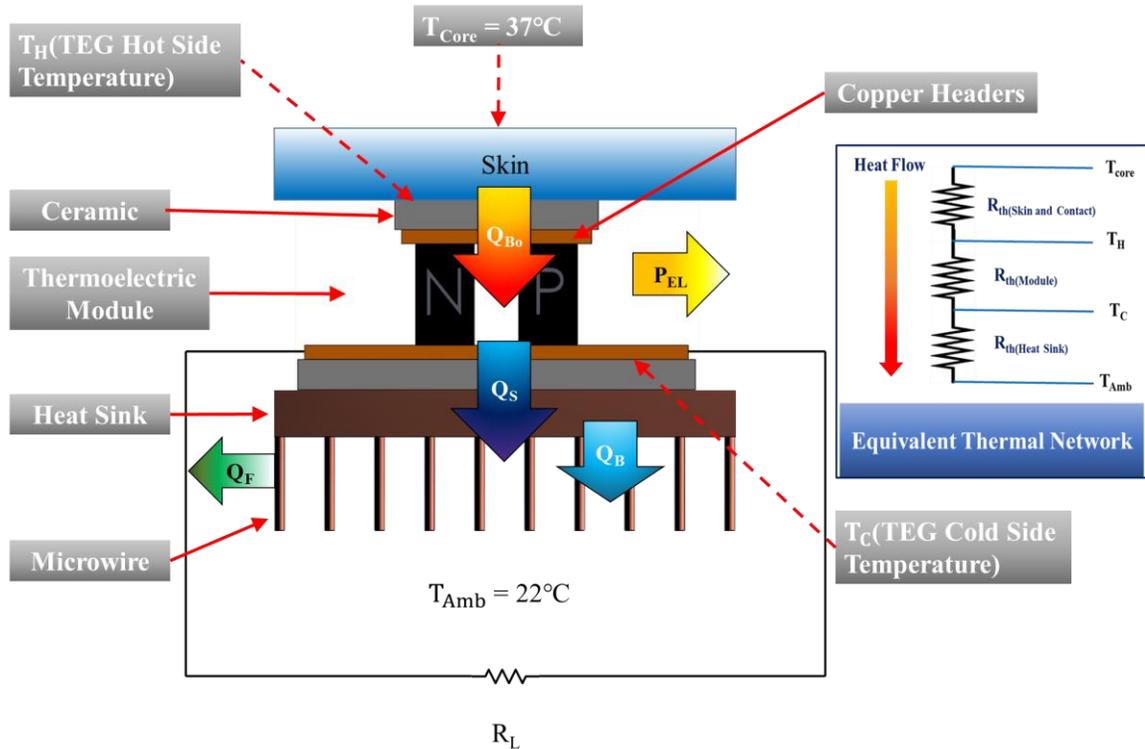
Figure 34: The TEG-Heat Sink heat transfer model, where Q_{Bo} is the heat transferred from the body, which is equal to the heat input to the TEG. Q_s is the heat transfer from the heat sink, which is equal to the heat leaving the cold side of the TEG. P_{EL} is the thermoelectric power generated by the TEG, Q_B is the heat transferred from the heat sink base, and Q_F is the heat transfer from the fins. The TEG is connected to an electrical load resistance R_L. The equivalent thermal network is shown in the figure with T_{core} being the core temperature of the body and T_{amb} being the ambient temperature.

The model is solved in a similar iterative manner to the TEG-Heat Sink model for the wireless sensor node. However, this model requires two iterative conditions to be satisfied. Firstly, the heat flow through the human skin (Q_{Bo}) has to match the heat flow in to the hot side of the TEG, Q_H as explained by the following equation:

$$abs(Q_{BO} - Q_H) < CC \qquad (4\text{-}27)$$

where CC is the convergence criteria and is equal to 10^{-6} W. The second condition is that the heat leaving the cold side of the TEG, Q_c has to match the heat flow through the micro-wire heat sink (Q_S) as explained by the following equation:

$$abs(Q_s - Q_C) < CC \qquad\qquad (4\text{-}28)$$

The hot side temperature of the TEG (T_H) and the cold side temperature of the

TEG (T_C) are unknown and will be solved by satisfying the aforementioned iterative

conditions. Eventually, the model will solve for the heat flow from the body, in the

process obtaining the total power output of the TEG, along with the hot side temperature,

cold side temperature, operational current and voltage.

Heat Sink Optimization

Two types of heat sinks were considered to be implemented with a TEG to

recover waste body heat. A vertical flat plate heat sink and a horizontal base square pin

fin heat sink, it is interesting to note that these two heat sinks are oriented perpendicular

to each other as illustrated in Figure 30. The fin height was capped at 3 cm, as a design

that is bulky is not desirable for waste heat recovery from the body. A base area of 4 cm x

4 cm is selected to match a conventional base area of a TEG. A flat plate heat sink and

square pin fin heat sink were optimized to obtain the smallest thermal resistance. The

thermal resistance of both the plate fin heat sink and the square pin fin heat sink are

illustrated in Figure 35 for varied packing fractions and fin thickness. A minimum

thermal resistance of 19.25 K/W is obtained for the flat plate heat sink for a fin thickness

of 1 mm and packing fraction of 12.5%. For the square pin fin heat sink, diminishing

returns in thermal resistance is observed at a packing fraction of 42.5% for a fin thickness

of 1 mm where a minimum thermal resistance of 17.3 K/W is observed.
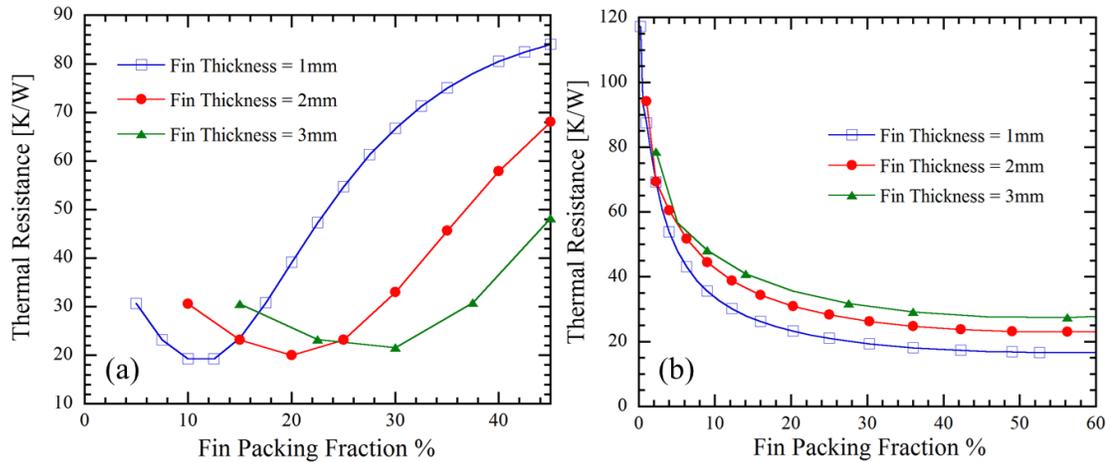
Figure 35: **(a) Thermal resistance of the plate fin heat sink for varied packing fraction and fin thickness for a fixed fin height of 3 cm (b) Thermal resistance of the square pin fin heat sink for varied packing fraction and fin thickness for a fixed fin height of 3 cm.**

TEG Optimization

The principle of thermal impedance matching is used to design the thermoelectric generator. For small temperature differences, the TEG thermal resistance should match the sum of the external thermal resistances. Such a condition is required to obtain the highest possible heat flow through the TEG while having the largest possible temperature difference across the module. If the thermal resistance of the module is much smaller than the external thermal resistance, the temperature drop across the module will be small, resulting in smaller thermoelectric power. On the other hand, if the thermal resistance of the module is much larger than the external thermal resistance the heat flow through the module is restricted. The thermal resistance of the module composed of the Bi_2Te_3 material described in chapter 2, is varied by adjusting the thermoelectric leg height. The leg packing fraction, which is the ratio of the leg area to the base area, was held constant. For the TEG combined with a flat plate heat sink a total power output of 0.717 mW at a power density of 44.82 $\mu W/cm^2$ is obtained for a leg height of 0.65 mm

for a leg packing fraction of 0.63% as shown in Figure 36. Similarly, for the TEG

combined with a horizontal base square pin fin heat sink a total power output of 0.731

mW at a power density of 45.69 μW/cm^2 was obtained for a leg height of 0.6mm.
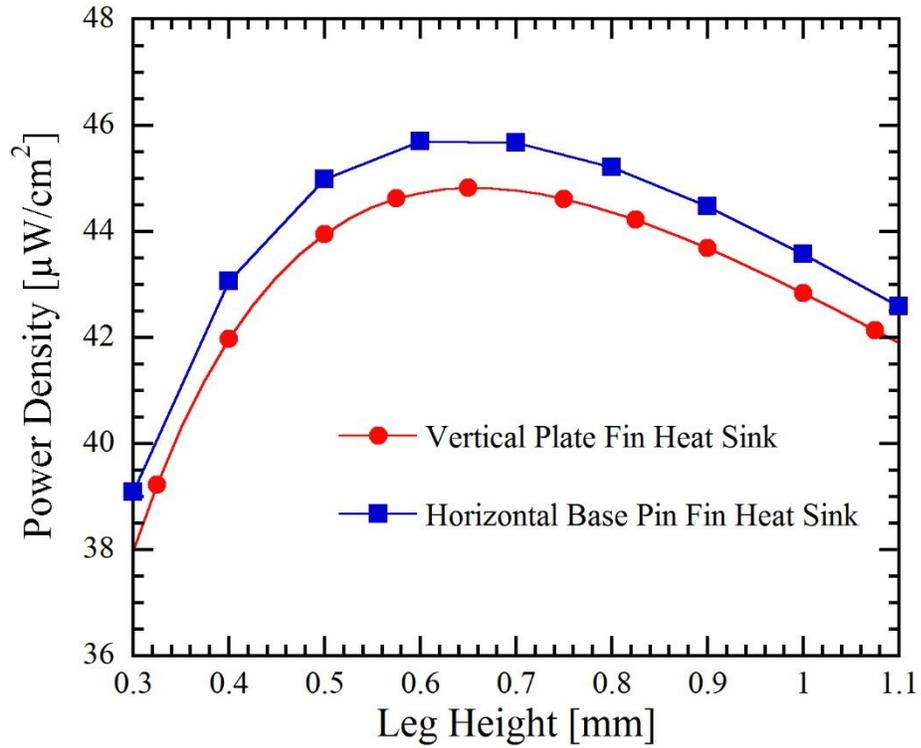
Figure 36:   **The power density vs. leg height for a TEG – Heat Sink system that uses a vertical flat plate heat sink and horizontal base pin fin heat sink. The leg packing fraction was held constant at 0.63%.**

THERMOELECTRIC GENERATORS COMBINED WITH NATURAL

CONVECTION MICROWIRE HEAT SINKS

Introduction

Natural convection heat transfer is driven by buoyancy effects, which require a

large temperature difference for effective heat transfer. Natural convection heat sinks

offer the advantages of not requiring any pumping power, low cost, and high reliability.

As established in Chapter 4, natural convection heat sinks have limited heat flow, and

convection coefficients are largely dependent upon the temperature difference between

the heat sink and the ambient temperature. Heat transfer in microscale structures (sub 100

µm) experience much larger natural convection coefficients when compared with its

macro-scale counterparts. Natural convection heat transfer in micro-structures is

dominated by heat conduction to the ambient air, and buoyancy effects have a limited

effect [47], this conclusion has been reached by the observed phenomenon that

orientation of the microstructure with regard to gravitational fields has no effect on the

heat transfer performance of a microstructure. Further explanations of the enhanced heat

transfer suggest that the increased surface area to volume allow for much larger heat

conduction with the ambient fluid [48]. It should also be noted that the thermal boundary

layer created by heat transfer from micro-structures is thin, which leads to better heat

transfer [49]. This chapter examines the development of a natural convection heat sink,

which uses micro-wires as its extended surface. A proposed heat sink that utilizes micro-

scale extended surfaces can be manufactured by additive manufacturing methods.

Flat plate heat sinks with fin heights of 200µm have been experimentally investigated by Mahmoud et al. [50]. However, the smallest fin thickness is 1mm, which cannot be considered to be of micro-scale. Similarly, the thermal performance of heat sinks with a minimum thickness of 200 µm and a maximum height of 0.8 mm have been examined, while considering the orientation of the heat sink with respect to the gravitational field [51]. Heat transfer of square micro pin fin with the smallest dimension of 0.4 mm under natural convection has been examined [52]. The work mentioned above do not fully exploit the micro-scale effects, which are observed at dimensions smaller than a 100 µm. Additionally, flat plate heat sinks with micro-scale dimensions of 40 µm have been examined by Kim et. al [53]. The heat sink heights are capped at 200 µm that limit their performance as will be explained in the following sections.

Microwire Convection Coefficient

Convection coefficients for micro-wires with diameters in the range from 10.6 µm to 95.6 µm are experimentally obtained [47]. The convection coefficient is obtained for microwires of both horizontal and vertical orientations with respect to the gravitational field. The convection coefficient for natural convection in a micro-wire is given by the following equation [47]:

$$h = \frac{k_a}{1 + K_n} \left(\frac{1}{d}\right) \left[\frac{1}{16} ln^2 \left(\frac{\alpha_a}{d^2}\right) - 0.292 \, ln \left(\frac{\alpha_a}{d^2}\right) + 0.958\right]^{-1/2} \tag{5-1}$$

where d is the pin diameter, k_a is the thermal conductivity of air, α_a is the thermal diffusivity of air and K_n is the Knudsen number which is the ratio of the mean free path of air to the pin diameter. As evidenced by equation 5-1, the convection coefficient is independent of the temperature difference between the surface and the ambient. The

equation suggests an inverse relationship between the convection coefficient and the fin diameter. Furthermore, experimental data indicate that the microwire orientation has no influence on the convection coefficient. The length or the length to diameter ratio has no impact on the convection coefficient as confirmed by the experimental data in the source.

A similar experimental convection coefficient has been obtained for natural convection from copper microwires using both air and water as the ambient fluid [49]. The experimental results have been confirmed by a 3-D numerical model, which also revealed details about the thin boundary layer thickness around the microwire. The convection coefficient follows the form of conventional natural convection Nusselt numbers, and is given by the following equation:

$$Nu = 1.03 \cdot (Gr \cdot Pr)^{0.035} \qquad\qquad \textit{30 μm} < D < \textit{120 μm} \qquad (5\text{-}2)$$

$$\textit{0.0001} < Gr < \textit{2.5}$$

$$Gr = \frac{g \cdot \beta \cdot (T_s - T_\infty)d^3}{v^2} \qquad\qquad (5\text{-}3)$$

where Pr is the Prandtl number, g is the gravitational acceleration, T_s is the surface temperature, T_∞ is the ambient temperature, d is the microwire diameter, and v is the kinematic viscosity. The experimental results were obtained for microwire diameters of 39.9 μm, 65.9 μm, and 119.1 μm. The inclusion of the temperature difference between the microwire surface and the ambient fluid resulting from the inclusion of the Grashof number may suggest the importance of the temperature difference. However, experimental results from the source show a weak relationship between the convection coefficient and the temperature dependence, which is also illustrated in Figure 37(b).
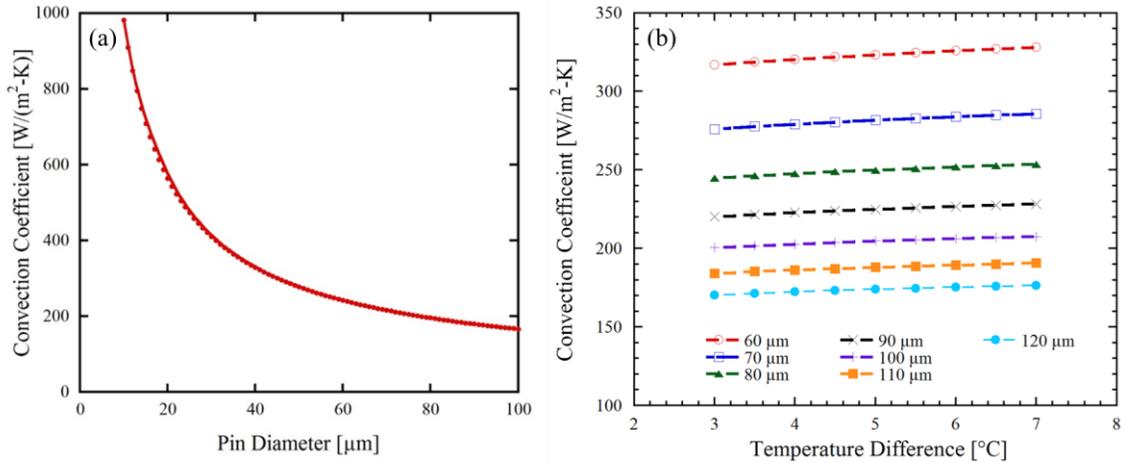
Figure 37: **(a) Microwire Convection Coefficient obtained from equation 5-1 [47]. (b) Nusselt number dependent convection coefficient obtained from equations 5-2 and 5-3 [49].**

Microwire Pin Fin Heat Sink Model

The enhanced heat transfer from the microwires can be exploited in natural convection applications. A steady state numerical model is built in a MATLAB environment utilizing the microwires as extended surfaces on a heat sink. For this model, the ambient temperature of the fluid adjacent to a fin and the ambient temperature of the fluid further away from the heat sink base is treated differently as shown in Figure 38. The ambient temperature away from the heat sink base will be referred to as T_∞ and the ambient temperature adjacent to the fin will be denoted by T_{amb}.
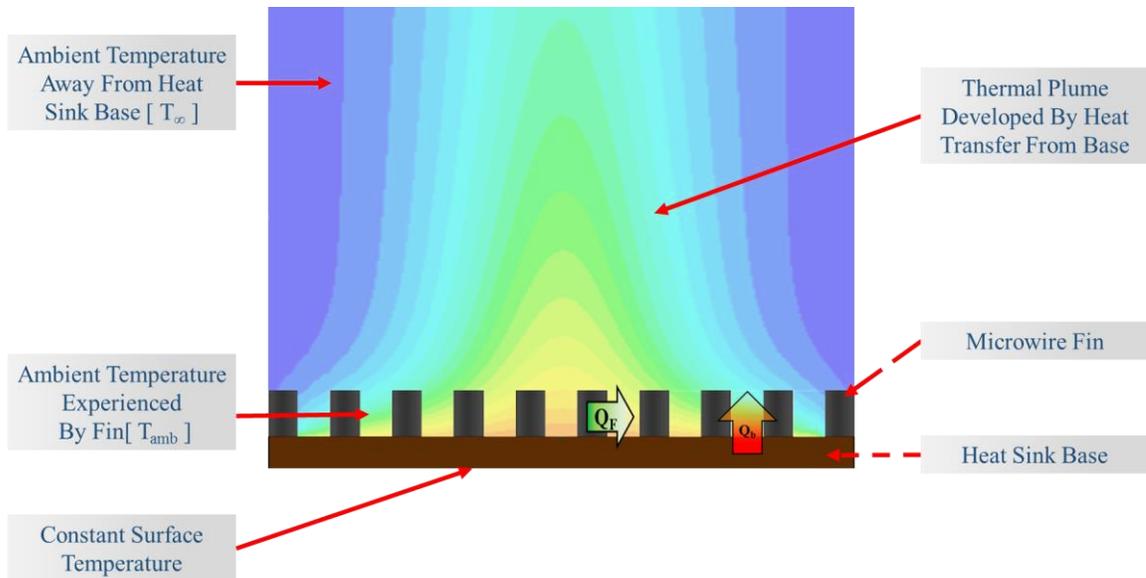
Figure 38: **Microwire pin fin heat sink with the thermal plume created by heat transfer from the base in the background. Q_F is the heat transfer from the microwire fins and Q_b is the heat transfer from the base.**

Each microwire is treated as an individual fin, conventionally fins in a natural convection heat sink can be treated as an individual fin if the boundary layers of the adjacent fins do not mix [31]. A similar principle is applied which limits the packing fraction of the microwire heat sink governed by a minimum spacing requirement between the microwires. The spacing requirement is obtained by using the microwire diameter dependent boundary layer thickness data from Guan et al. [49]. The purpose of incorporating the spacing limit into the model is to be able to treat the microwires as individual fins. Each microwire fin is solved for by a finite element model with a varied ambient temperature adjacent to each fin and each fin finite element. The ambient temperature surrounding the fin will be influenced by heat transfer from the horizontal base as illustrated in Figure 38. The ambient temperature surrounding the fins are obtained in the next section and is used as an input into the fin model. The model assumes an adiabatic tip and a constant base temperature and is solved by a one-

dimensional linear finite element model. The temperature profile along the fin is required to obtain the heat transfer from an individual microwire and is obtained by the following equation [21]:

$$T = K^{-1}F \tag{5-4}$$

where T is the temperature vector, K^{-1} is the inverse global stiffness matrix, and F is the forcing vector. The assembly of the global stiffness matrix requires elemental stiffness matrix similar to that in Chapter 2, which is obtained as follows:

$$K_e = \int_l [B]^T[D][B]A dx + \int_l hP[N]^T[N] dx \tag{5-5}$$

where B is the strain displacement matrix, the D matrix contains the elemental thermal conductivity terms and A is the area of the element, h is the microwire convection coefficient obtained from equation 5-1, P is the circumference of the fin and N is the shape function for the linear element. The model uses one-dimensional linear elements, which simplify to the following elemental stiffness matrix:

$$K_e = \frac{A_e k_e}{l_e}\begin{bmatrix} 1 & -1 \\ -1 & 1 \end{bmatrix} + \frac{hP}{l_e}\begin{bmatrix} 2 & 1 \\ 1 & 2 \end{bmatrix} \tag{5-6}$$

where A_e is the elemental area, k_e is the thermal conductivity, l_e is the elemental length, h and P are as defined above. The elemental loading vector was developed taking into consideration heat transfer from the surface of the fin by the following equation:

$$F_e = \int_S hT_{amb}[N]^T dS \tag{5-7}$$

where T_{amb} is the ambient temperature adjacent to the fluid, once again the forcing vector simplifies to the following equation for a one-dimensional linear element:

$$F_e = \frac{hPT_{amb}l_e}{2}\begin{bmatrix} 1 \\ 1 \end{bmatrix} \tag{5-8}$$

Once the temperature profile T is obtained, it is used to obtain the convection heat transfer from each element and is summed to obtain the total heat transfer from the fin.

$$Q_{T\_Fin} = \sum_{i=1}^{elems} h \cdot A_{e\_s} \cdot (\frac{T_n + T_{n+1}}{2} - T_{amb(n)}) \tag{5-9}$$

where *elems* is the total number of elements, A_{e_s} is the elemental surface area, T_n is the nodal temperature and $T_{amb(n)}$ is the ambient temperature for each element. The total heat transfer from the heat sink sums up the heat transferred by all of the fins as well as heat transferred from the unfinned base area obtained by the following equation:

$$Q_{HS} = \sum_{i=1}^{Fins} Q_{T\_Fin} + h_{hp} \cdot A_{uf} \cdot (T_b - T_\infty) \tag{5-10}$$

where *Fins* is the total number of fins, h_{hp} is the convection coefficient for an upward facing horizontal plate, A_{uf} is the unfinned area, T_b is the base temperature, and T_∞ is the ambient temperature away from the base of the heat sink.

Ambient Fluid Temperature

The fluid temperature adjacent to a fin is used as an input into the model as evidenced by equations 5-8 and 5-9. Heat transfer from the base of the heat sink produces a thermal plume for a horizontal upward facing orientation [54]. The thermal boundary layer produced by the heat transfer from the base results in much warmer ambient temperatures for the microwire fins when compared to temperatures further away from the base (T_∞). This phenomenon is particularly apparent near the base of the heat sink up to a height of around 5 mm. If the model were to use the ambient temperature away from the heat sink base, T_∞ illustrated in Figure 38; it would significantly overestimate the performance of the heatsink. To capture the influence of the thermal boundary layer

developed by the heat sink base, the temperature profile over a horizontal flat plate was

obtained and implemented in the model. The temperature profile over a horizontal flat

plate for laminar natural convection was obtained from Guha et al.[55], where an

analytical solution for a horizontal plate for a varied surface temperature is available. The

available equation was adjusted for a constant surface temperature condition, which

realizes in the following equations:

$$\frac{T_{x,y} - T_\infty}{T_s - T_\infty} = (1 - y/\delta)^2 \tag{5-11}$$

$$\delta = 4.317x \left[\frac{Pr + (16/21)}{Pr \cdot Gr_x} \right]^{1/5} \tag{5-12}$$

$$Gr_x = \frac{g \cdot \beta \cdot (T_s - T_\infty)x^3}{\upsilon^2} \tag{5-13}$$

where $T_{x,y}$ is the temperature along the surface, T_∞ is the ambient temperature away from

the plate, T_s is the plate surface temperature, and y is the vertical distance from the base of

the plate. The thermal boundary layer thickness δ is given by equation 5-12, x is the

horizontal distance from the edge of the base, Pr is the Prandtl number, Gr_x is the local

Grashof number, β is the thermal coefficient of expansion and υ is the kinematic

viscosity. Equation 5-11 only provides the temperature profile for a surface above the

horizontal plate from the edge towards the midpoint of the plate. To obtain the complete

temperature profile above the horizontal plate, equation 5-11 was rotated around the

center of the plate, which sweeps the complete horizontal plate. The temperature profile

obtained from equation 5-11 was compared with a 3D model developed in Ansys Icepak

for laminar natural convection as illustrated in Figure 39. The temperature profile above

the heat sink compares fairly well with the 3-D model temperature profiles up until a

height of approximately 6 mm. The temperature profile obtained using equation 5-11 mostly overestimates the ambient temperature compared to the 3-D model, which serves to make the overall model more conservative. The corresponding temperature above the base was used as the input into the ambient temperature for the fin model, which was established based on the location of the fin. A microwire located at the edge of the base would experience adjacent fluid temperature smaller than that of a microwire located at the center of the base.
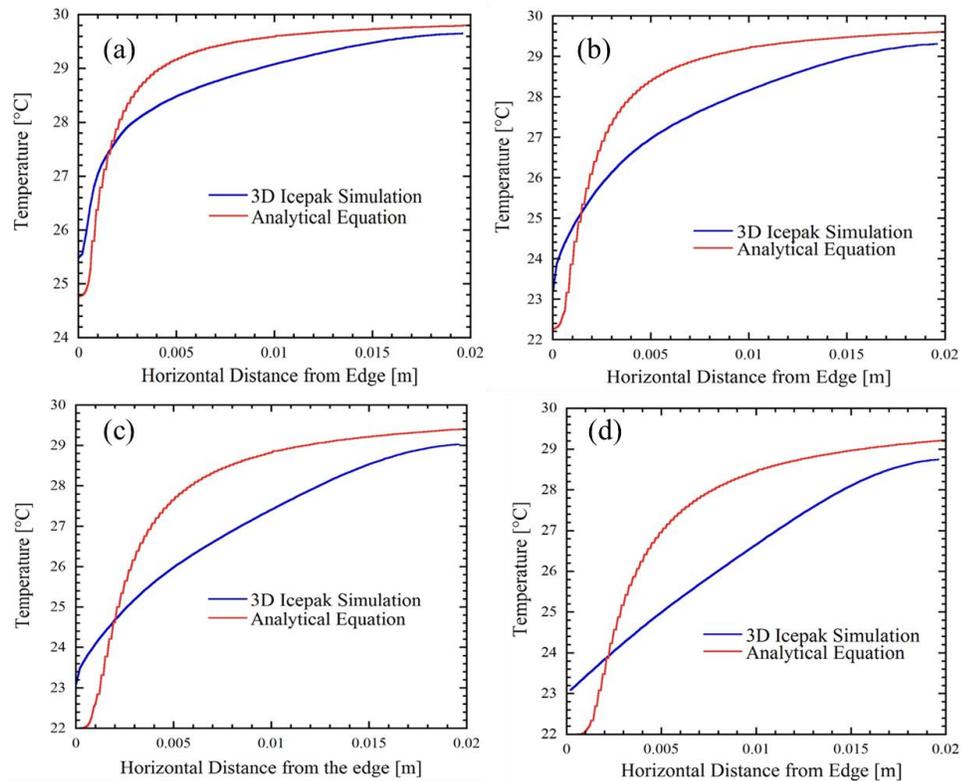
Figure 39: **Temperature comparison along a horizontal line using the analytical equation 5-11 and a 3-D Icepak simulation at heights above the plate of (a) 1mm (b) 2mm (c) 3mm and (d) 4mm.**

Model Assumptions

The model has some simplifying assumptions, which are listed below.

1) The model assumes the heat source is a thermal reservoir, such that the base of the heat sink can be maintained at a constant temperature, this means that there is no lateral heat spreading effects along the base. This assumption is required as more heat is transferred from the corner fins, as they are influenced less by the thermal plume of the base. As the corner fins transfer more heat, lateral heat variations are to be expected if the heat sink is not attached to a thermal reservoir.

2) The boundary layer of the microwire has little influence on the ambient temperature surrounding the fins, which is justified based on the small thicknesses of the boundary layer data available from Guan et al.[49].

3) Each heat sink fin is treated as an individual fin, where the convection coefficient of one fin is not influenced by the heat transfer from the adjacent fin. To make this assumption a minimum fin spacing condition was established allowing each fin to be treated as an individual extended surface.

4) The microwire convection coefficients are used as the convection coefficient for the heat sink fins, which are of microscale order.

5) The heat transfer from the unfinned base area affects the ambient temperature and is captured in the model.

6) The model does not take into account the structural stability of the microwires and only considers the heat transfer process.

TEG- Microwire Heat Sink Model for Harvesting Waste Heat from the Human

Body

The heat sinks designed in Chapter 4 provide limited heat transfer and are quite

bulky. The microwire heat sinks provide better thermal performance while providing a

compact heat sink which can be implemented with a TEG to harvest waste heat from the

body. The following sections detail the design of a microwire heat sink to be placed on

the cold side of the TEG to harvest waste body heat. A theoretical microwire heat sink

design is suggested with a large fin height-to-diameter ratio. A more practical design is

suggested while capping the height-to-diameter ratio to 20. The TEG-Microwire Heat

Sink model is similar to the model described in section 0 and described in Figure 34,

where this model uses microwires as the heat sink fins.

Microwire Heat Sink Optimization

The microwire heat sink was optimized to minimize thermal resistance, for

temperature differences of 1°C and 5°C. Copper was chosen as the heat sink base and

microwire material as it has a thermal conductivity of approximately 401 W/m-K at room

temperature. Similar to the previous section, a heat sink base area of 4 cm x 4 cm was

chosen to match the surface area of a conventional module. The microwire fin height,

diameter and fin packing fraction were optimized to obtain the lowest possible thermal

resistance for the heat sink. The following table lists the optimization parameters.

Table 8   **Heat sink optimization parameters**

Parameter	Value
Fin Diameter	10 µm, 50µm, 100 µm
Fin Height	1 mm , 2 mm, 3 mm, 4 mm, 5 mm
Fin Packing Fraction [10 µm, 50 µm and 100 µm]	0.9 % - 1.9 %, 1.2%, 2.2%

The fin height was optimized for a fixed fin diameter of 10 µm and packing fraction of 1.9%. As shown in Figure 40, the thermal resistance reaches diminishing returns for a fin height of 3 mm. This observation is explained by shrinking fin efficiencies, although the fin material is composed of Copper, the large convection coefficients and small cross-sectional areas result in smaller fin efficiencies. At a fin height of 3 mm, a thermal resistance of 0.821 K/W is obtained for a temperature difference of 1°C compared to thermal resistances of 0.776 K/W at 4 mm and 0.760 K/W at 5 mm. Similarly, for a temperature difference of 5°C a fin height of 3 mm results in a thermal resistance of 0.706 K/W compared to thermal resistances of 0.673 K/W at 4 mm and 0.664 at 5 mm. The proposed fin heights for a fin diameter of 10 µm suggest fin diameter to height ratios of 100 to 500 for the optimized fin heights. These height-to-diameter ratios could be difficult to manufacture and have little structural integrity.
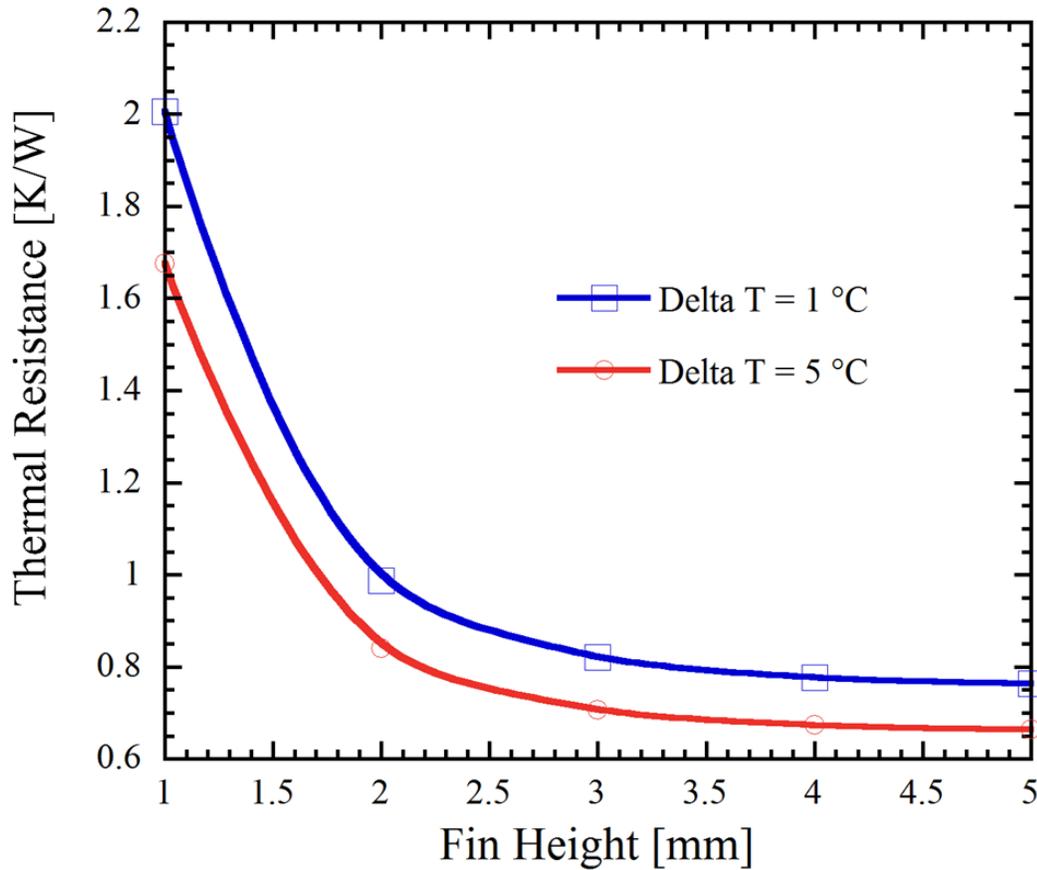
Figure 40: **Heat sink thermal resistance variation with fin height for a fin diameter of 10 μm and packing fraction of 1.9%.**

Similarly, the fin diameter and packing fractions were optimized for a fixed fin height of 3 mm. The fin packing fraction is capped to a maximum of 1.9% for the 10 μm heat sink and 2.2 % for the 50 μm and 100 μm heat sinks. The packing fraction is restricted by the spacing limit requirement between the fins, which was explained previously. The thermal resistances of varied fin diameters and packing fractions are compared for a temperature difference of 1 °C and 5°C. The heat sinks with a pin diameter of 10μm provide smaller thermal resistances compared to the 50 μm and 100 μm heat sink as shown in Figure 41. This is attributable to the much larger convection coefficient for the 10 μm fin diameter of 982.4 W/m^2-K compared to 277.5 W/m^2-K for the 50 μm fin diameter and 166.4 W/m^2-K for the 100 μm fin diameter.
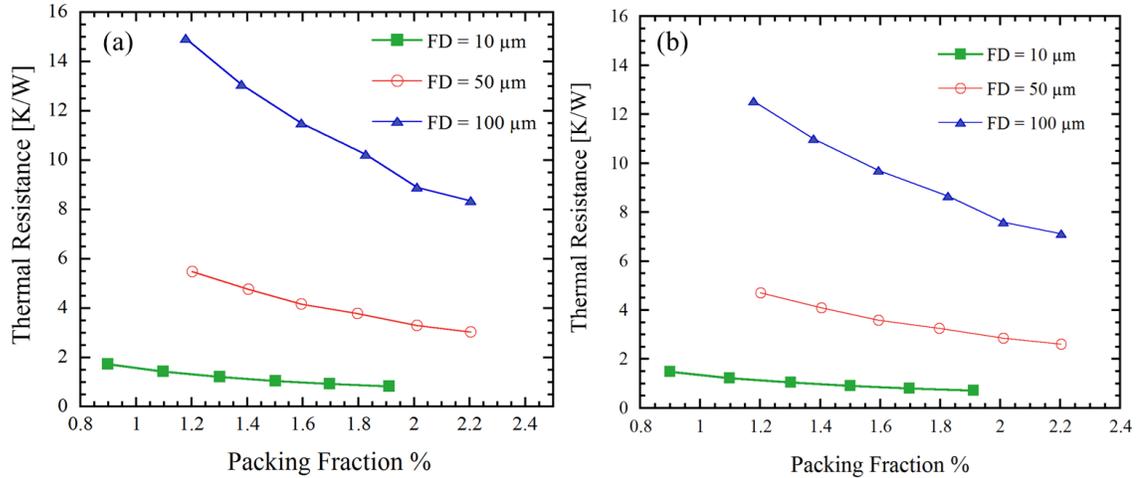
Figure 41: **Thermal resistance variation of the heat sink with fin diameter and packing fraction variation for a fin height of 3mm (a) Base-Ambient temperature difference of 1 °C and (b) Base – Ambient temperature difference of 5 °C.**

A minimum thermal resistance of 0.820 K/W is obtained for a temperature difference of 1°C, and a minimum thermal resistance of 0.706 K/W is obtained for a temperature difference of 5°C for the optimized heat sink design parameters listed in Table 9.

Table 9   **Optimized heat sink parameters of the theoretical heat sink**

Parameter	Value
Heat Exchanger Base Area	40 mm x 40 mm
Heat Exchanger Base Thickness	0.5 mm
Fin Diameter	10 μm
Fin Height	3 mm
Fin Packing Fraction	1.9 %

A comparison of the microwire heat sink to the horizontal base pin fin heat sink can be found in Table 10. It is important to note that the macro-scale heat sink had a pin height of 3 cm compared to the micro-scale pin height of 3mm; therefore, a normalizing

parameter was developed by accounting for the different fin heights. The adjusted

thermal resistance was obtained by multiplying the thermal resistance by the fin height.

Table 10   Thermal resistance comparison for a micro-scale heat sink and horizontal base pin fin heat sink

Heat Sink Type	Thermal Resistance $\Delta T = 1°C$	Adjusted Thermal Resistance $\Delta T = 1°C$	Thermal Resistance $\Delta T = 5°C$	Adjusted Thermal Resistance $\Delta T = 5°C$
Macro-scale	28.68 K/W	77.05 K-cm/W	12.90 K/W	38.70 K-cm/W
Micro-scale	0.820 K/W	0.246 K-cm/W	0.706 K/W	0.212 K-cm/W

The microwire heat sink design suggested in Table 9 has a fin height to diameter

ratio of 300, which could be difficult to manufacture through additive manufacturing. A

practical heat sink design is implemented by restricting the pin height to diameter ratio to

20. The thermal resistances are significantly higher than the theoretical minimum as

displayed by Figure 42. The 10-µm diameter fin heat sinks are now ineffective, as at their

height of 200 µm is fully bathed in the thermal plume created by heat transfer from the

base. The lack of a significant temperature difference limits heat flow from the fins,

regardless of the high convection coefficient. The 100 µm heat sink has the lowest

thermal resistance with a packing fraction of 2.2%, as the pin height is 2mm, where it is

not affected by the thermal plume of the base to the extent the 10µm diameter heatsinks

are.
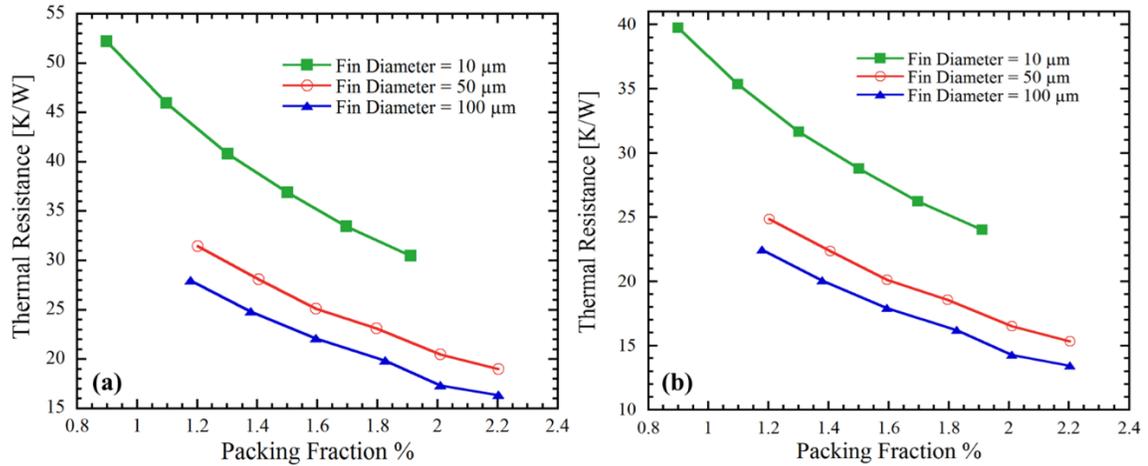
Figure 42: **Thermal resistance variation of the heat sink with fin diameter and packing fraction variation for a fin height to diameter ratio of 20 for (a) Base-Ambient temperature difference of 1 °C and (b) Base – Ambient temperature difference of 5 °C.**

The optimized parameters for the practical heat sink are listed in the table below with a minimum thermal resistance of 16.35 K/W for a temperature difference of 1°C and a minimum thermal resistance of 13.41 K/W for a temperature difference of 5°C.

Table 11   Optimized heat sink parameters of the practical heat sink

Parameter	Value
Heat Exchanger Base Area	40 mm x 40 mm
Heat Exchanger Base Thickness	0.5 mm
Fin Diameter	100 μm
Fin Height	2 mm
Fin Packing Fraction	2.2%

TEG Optimization

The principle of thermal impedance matching is used to design the thermoelectric generator, similar to the TEG designed in Chapter 4. The thermal resistance of the module is varied by adjusting the thermoelectric leg height. The leg packing fraction,

which is the ratio of the leg area to the base area, was held constant. The maximum

power density of 66.13µW/cm^2 was obtained for a leg height of 0.5 mm as illustrated in

Figure 43 for the theoretical design. The heat flow from the body was 11.81 mW/cm$^{2\,-}$

when the maximum power was obtained . For the practical heat sink design a maximum

power density of 49.14 µW/cm^2 for a leg height of 0.65 mm, with a heat flow of 8.91

mW/cm^2 was achieved.
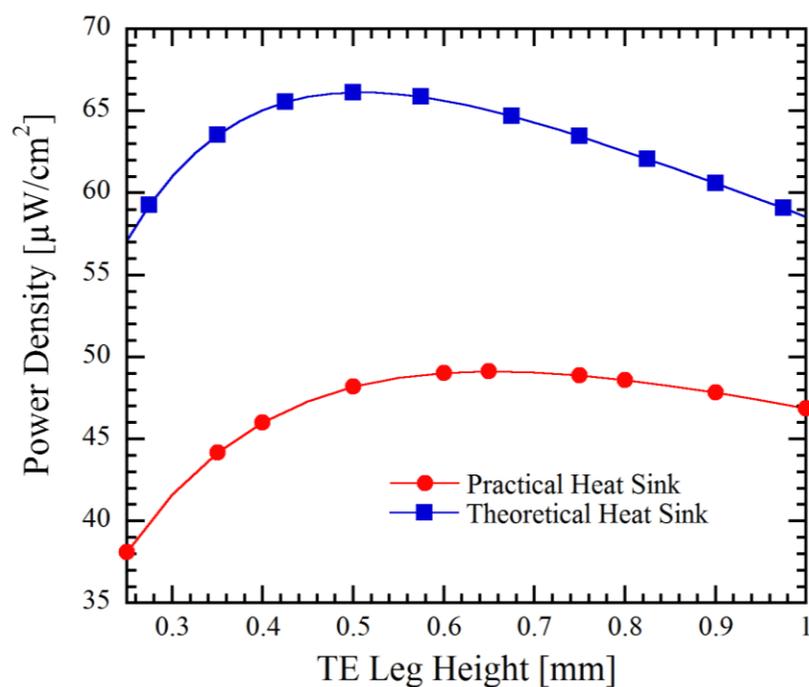
Figure 43:   Power Density using the TEG Heat Sink model using the two different heat sink designs established in Table 9 and Table 11. The thermal resistance of the TEG was varied by changing the leg height while holding the packing fraction constant at 0.63%.

The larger power density for the theoretical design stems from the better thermal

performance of the heat sink, which allows more heat to be transferred from the body and

through the TEG. However, the improvements in thermal resistance of the theoretical

design are not matched by increased power density in the combined TEG system. This

observation is explained by the thermal resistance of the human skin (and the contact resistance between the TEG and skin) limiting heat flow from the human body.

The power density of the practical design is larger than the maximum power density obtained by combining a macro-scale natural convection heat sink to a TEG which was obtained in section 0. Furthermore, the microwire heat sink occupies a smaller volume when compared to the macro-scale heat sink. The results from this work are compared to that of other similar works. Table 12 compares both the base area power density and volumetric power density. The base area power density is the ratio of the thermoelectric power generated to the base area of the TEG-heat sink, while the volumetric power density is the ratio of the thermoelectric power generated to the volume of the complete TEG-heat sink system.

Table 12   **A comparison of the power density by the base area utilized by a complete TEG-Heat Sink device for similar works, along with a comparison of the power density by considering the overall volume of a TEG-Heat Sink device when a fair comparison was viable.**

Ref.	Base Area Power Density [$\mu W/cm^2$]	Volumetric Power Density [$\mu W/cm^3$]
Theoretical HS	66.13	165.33
Practical HS	49.137	156.0
[6]	20.00	22.22
[7]	30.00	20.00
[41]	0.44	0.30
[44]	28.50	57.00
[45]	6.1	50.83
[46]	60.00	10.00

CONCLUSIONS AND FUTURE WORK

Conclusions

<u>Temperature Dependent Finite Element Model for a Thermoelectric Module</u>

The temperature dependent finite element model developed can be used as a starting point for the design of a thermoelectric module. The model was validated using a 3-D model in an ANSYS environment for three popular thermoelectric materials and a number of temperature differences pertaining to the operating temperature of the materials. The thermoelectric power estimation of the model performs reasonably well considering the assumptions made in the model with the largest average percent error of 11.93 % obtained for the Half-Heusler alloy model.

Improvements to the unicouple design are suggested by using a ceramic material composed of a higher thermal conductivity compared to the standard ceramic material used in a unicouple. The power generated was found to be improved by a factor of 1.34 for a unicouple with a ceramic composed of Beryllia compared to a unicouple with a ceramic of Alumina, when a temperature difference of 500°C is applied across the unicouple.

The model developed was used to examine segmented unicouples, which can be used to obtain increased power and efficiency. For a temperature difference of 580 °C a unicouple composed of the Half-Heusler alloy and Bi_2Te_3 material produced 16% more power and was 61% more efficient compared to a unicouple composed of only the Half-Heusler alloy. Similarly, a unicouple made of the PbTe material and Bi_2Te_3 material

produced 49.5 % more power and was 65.5 % more efficient compared to a unicouple made of only the PbTe material.

<u>TEG – Heat Exchanger Model</u>

The heat exchanger model developed is used in combination with the thermoelectric module model to compose a complete thermoelectric system. The heat exchanger model was compared to a 3D model developed in ANSYS Icepak. The work done on the heat exchanger model examines the convection heat transfer coefficient used in heat exchangers by implementing a duct convection coefficient for the model and a compact heat exchanger convection coefficient. The results using the two convection coefficients are compared, where the results indicate that the compact heat exchanger convection coefficient provides more accurate results compared to the model using the duct convection coefficient.

<u>TEG – Natural Convection Heat Sink Model</u>

Natural convection heat sinks to be implemented with TEGs are examined. Three different natural convection heat sinks are examined considering the fin type and orientation with regards to the gravitational field. The heat sinks are then optimized and applied to harvest waste heat from a pipe in a nuclear power plant. The optimized TEG-Heat Sink system produces a power density of 133 mW/cm^2 for a module composed of Bi_2Te_3 which can be used to power a wireless sensor node making the sensor node fully autonomous. Further application of a TEG-Heat Sink system is used to harvest waste body heat. An optimized system produces a power density of 44.82 µW/cm^2 for a TEG attached to a vertical plate fin heat sink and a power density of 45.69 µW/cm^2 for a TEG attached to a horizontal base pin fin heat sink.

Natural Convection Microwire Heat Sink

A numerical model for a heat sink composed of microwires has been developed. The heat sink model was then used to optimize a heat sink to harvest waste heat from the human body by placing the heat sink on the cold side of TEG. Two heat sink designs are suggested, one a theoretical design, and a more practical design whose height is restricted by a fin height to diameter ratio. When the theoretical heat sink design is used with a TEG a maximum power density of 66.13 μW/cm^2 is acquired, while the TEG combined with the practical design suggested acheieves a maximum power density of 49.14 μW/cm^2. The power density from both TEG- Heat sink designs are larger than the power density obtained from a TEG- Macro scale heat sink obtained in Chapter 4. Furthermore, the microwire heat sink provides a more compact design, which is important when harvesting waste heat from the human body.

Future Work

Temperature Dependent Finite Element Model for a Thermoelectric Module

The available model could be improved to account for radiation and convection losses from the surfaces of the unicouple. Furthermore, the model could be improved to incorporate 3-D heat diffusion effects, which diminish the accuracy of the model. Furthermore, the available model could be used to study the thermal stress developed in the unicouple due to the large temperatures experienced.

TEG – Heat Exchanger Model

The pressure drop across the heat exchanger is an important parameter in the heat exchanger design. The model could be improved to perform pressure drop calculations for a given heat exchanger design. Using the pressure drop values the net power

generated from a complete heat exchanger system could be obtained to evaluate the complete TEG – Heat exchanger design.

Natural Convection Microwire Heat Sink

The natural convection microwire heat sink has a number of limiting assumptions. The model developed is only valid when the heat sink base can be maintained at a constant temperature. The model could be improved to account for when this condition cannot be met. Which would require the model to consider lateral heat spreading in the base. Furthermore, the current model considers a heat sink with a horizontal base with vertical pins. Future work could examine the model for a vertical base plate, where the microwire fins are horizontal to the gravitational field. Although it was stated that the convection microwire convection coefficient are not influenced by orientation, the thermal boundary layer developed by the base plate is dependent upon its orientation to the gravitational field. Finally, the model could be used to obtain data for numerous designs with varied fin diameters, packing fractions and fin heights. Using the collected data, convection heat transfer coefficients could be developed for the complete heat sink considering heat flow, base to ambient temperature difference and total heat sink surface area.

REFERENCES

[1]   D. Rowe, *Thermoelectrics handbook*, 1st ed. Boca Raton: CRC/Taylor & Francis, 2006.

[2]   H. S. Kim, W. S. Liu, G. Chen, C. W. Chua, and Z. F. Ren, "Relationship between thermoelectric figure of merit and energy conversion efficiency," *Proceedings of the National Academy of Sciences of the United States of America,* vol. 112, pp. 8205-8210, Jul 7 2015.

[3]   Y. L. Zhang, M. Cleary, X. W. Wang, N. Kempf, L. Schoensee, J. Yang*, et al.*, "High-temperature and high-power-density nanostructured thermoelectric generator for automotive waste heat recovery," *Energy Conversion and Management,* vol. 105, pp. 946-950, Nov 15 2015.

[4]   J. H. Yang and F. R. Stabler, "Automotive Applications of Thermoelectric Materials," *Journal of Electronic Materials,* vol. 38, pp. 1245-1251, Jul 2009.

[5]   V. Lee, "Waste heat reclamation in aircraft engines", M.S. thesis, Massachusetts Institute of Technology, 2014.

[6]   V. Leonov, T. Torfs, P. Fiorini, and C. Van Hoof, "Thermoelectric converters of human warmth for self-powered wireless sensor nodes," *Ieee Sensors Journal,* vol. 7, pp. 650-657, May-Jun 2007.

[7]   T. Torfs, V. Leonov and R. Vullers, "Pulse Oximeter Fully Powered by Human Body Heat", *Sensors & Transducers*, vol. 80, no. 6, pp. 1230-1238, 2007.

[8]   F. Suarez, A. Nozariasbmarz, D. Vashaee, and M. C. Ozturk, "Designing thermoelectric generators for self-powered wearable electronics," *Energy & Environmental Science,* vol. 9, pp. 2099-2113, 2016.

[9]   K. Qiu and A. C. S. Hayden, "Development of a thermoelectric self-powered residential heating system," *Journal of Power Sources,* vol. 180, pp. 884-889, Jun 1 2008.

[10]   Y. L. Zhang, X. W. Wang, M. Cleary, L. Schoensee, N. Kempf, and J. Richardson, "High-performance nanostructured thermoelectric generators for micro combined heat and power systems," *Applied Thermal Engineering,* vol. 96, pp. 83-87, Mar 5 2016.

[11]   G. Snyder, "Small Thermoelectric Generators", *The Electrochemical Society Interface*, pp. 54-56, 2008.

[12]   L. Jiji, *Heat conduction*, 1st ed. [Place of publication not identified]: Springer, 2014.

[13]   S. Chen and Z. F. Ren, "Recent progress of half-Heusler for moderate temperature thermoelectric applications," *Materials Today,* vol. 16, pp. 387-395, Oct 2013.

[14]   E. Antonova and D. Looman, "Finite Elements for Thermoelectric Device Analysis in ANSYS", in *IEEE International Conference on Thermoelectrics*, Clemson, SC, 2005, pp. 215-218.

[15]   X. Hu, A. Yamamoto and K. Nagase, "Characterization of half-Heusler unicouple for thermoelectric conversion", *Journal of Applied Physics*, vol. 117, 2015.

[16]   S. Kumar, S. D. Heister, X. F. Xu, J. R. Salvador, and G. P. Meisner, "Thermoelectric Generators for Automotive Waste Heat Recovery Systems Part I: Numerical Modeling and Baseline Model Analysis," *Journal of Electronic Materials,* vol. 42, pp. 665-674, Apr 2013.

[17]   J. L. Yu and H. Zhao, "A numerical model for thermoelectric generator with the parallel-plate heat exchanger," *Journal of Power Sources,* vol. 172, pp. 428-434, Oct 11 2007.

[18]   M. Chen, H. Lund, L. A. Rosendahl, and T. J. Condra, "Energy efficiency analysis and impact evaluation of the application of thermoelectric power cycle to today's CHP systems," *Applied Energy,* vol. 87, pp. 1231-1238, Apr 2010.

[19]   X. Gao, S. J. Andreasen, M. Chen, and S. K. Kaer, "Numerical model of a thermoelectric generator with compact plate-fin heat exchanger for high temperature PEM fuel cell exhaust heat recovery," *International Journal of Hydrogen Energy,* vol. 37, pp. 8490-8498, May 2012.

[20]   M. F. Zhou, Y. L. He, and Y. M. Chen, "A heat transfer numerical model for thermoelectric generator with cylindrical shell and straight fins under steady-state conditions," *Applied Thermal Engineering,* vol. 68, pp. 80-91, Jul 2014.

[21]   P. Nithiarasu, R. Lewis and K. Seetharamu, *Fundamentals of the finite element method for heat and mass transfer*, 1st ed. Chichester, West Sussex: Wiley, 2016.

[22]   S. R. Annapragada, T. Salamon, P. Kolodner, M. Hodes, and S. V. Garimella, "Determination of Electrical Contact Resistivity in Thermoelectric Modules (TEMs) from Module-Level Measurements," *Ieee Transactions on Components Packaging and Manufacturing Technology,* vol. 2, pp. 668-676, Apr 2012.

[23]   T. Varghese, C. Hollar, J. Richardson, N. Kempf, C. Han, P. Gamarachchi*, et al.*, "High-performance and flexible thermoelectric films by screen printing solution-processed nanoplate crystals," *Scientific Reports,* vol. 6, Sep 12 2016.

[24]   Borland W (1989) In: Electronic materials handbook: packaging, vol 1. ASM International, New York

[25]   D. de Faoite, D. J. Browne, F. R. Chang-Diaz, and K. T. Stanton, "A review of the processing, composition, and temperature-dependent mechanical and thermal properties of dielectric technical ceramics," *Journal of Materials Science,* vol. 47, pp. 4211-4235, May 2012.

[26]   G. Snyder and T. Ursell, "Thermoelectric efficiency and compatability", *Physics Review Letters*, vol. 91, no. 14, 2003.

[27]   B.Y. Moizhes, Y. P. Shishkin, A.V. Petrov, and L. A.Kolomoets, Sov. Phys. Tech. Phys. **7**, 336 (1962).

[28]   T. S. Ursell and G. J. Snyder, in *Proceedings of the 21st International Conference on Thermoelectrics* (IEEE, New York, 2002), p. 412. Figures and tables in [15] calculate *u* a factor of 2 smaller than defined here.

[29]   Z. L. Ouyang and D. W. Li, "Modelling of segmented high-performance thermoelectric generators with effects of thermal radiation, electrical and thermal contact resistances," *Scientific Reports,* vol. 6, Apr 7 2016.

[30]   G. B. Zhang, L. H. Fan, Z. Q. Niu, K. Jiao, H. Diao, Q. Du*, et al.*, "A comprehensive design method for segmented thermoelectric generator," *Energy Conversion and Management,* vol. 106, pp. 510-519, Dec 2015.

[31]   F. Incropera and D. DeWitt, *Fundamentals of heat transfer*, 1st ed. New York: Wiley, 1981.

[32]   R. Shah and D. Sekulic, *Fundamental of Heat Exchanger Design*, 1st ed. Hoboken, NJ: John Wiley & Sons, Inc, 2003.

[33]   A. Kraus, A. Aziz and J. Welty, *Extended Surface Heat Transfer*, 1st ed. New York, NY: John Wiley & Sons, Inc., 2001.

[34]   A. R. Wieting, "Empirical Correlations for Heat-Transfer and Flow Friction Characteristics of Rectangular Offset-Fin Plate-Fin Heat-Exchangers," *Journal of Heat Transfer-Transactions of the Asme,* vol. 97, pp. 488-490, 1975.

[35]   A. Bar-Cohen, M. Iyengar, and A. D. Kraus, "Design of optimum plate-fin natural convective heat sinks," *Journal of Electronic Packaging,* vol. 125, pp. 208-216, Jun 2003.

[36]   A. Bar-Cohen and W. M. Rohsenow, "Thermally Optimum Spacing of Vertical, Natural-Convection Cooled, Parallel Plates," *Journal of Heat Transfer-Transactions of the Asme,* vol. 106, pp. 116-123, 1984.

[37]   Y. Joo and S. Kim, "Comparison of thermal performance between plate-fin and pin-fin heat sinks in natural convection", *International Journal of Heat and Mass Transfer*, vol. 83, pp. 345-356, 2015.

[38]   E. M. Sparrow and S. B. Vemuri, "Orientation Effects on Natural-Convection Radiation Heat-Transfer from Pin-Fin Arrays," *International Journal of Heat and Mass Transfer,* vol. 29, pp. 359-368, Mar 1986.

[39]   D. Sahray, G. Ziskind, and R. Letan, "Scale-Up and Generalization of Horizontal-Base Pin-Fin Heat Sinks in Natural Convection and Radiation," *Journal of Heat Transfer-Transactions of the Asme,* vol. 132, Nov 2010.

[40]   J. Chen, "Design and Analysis of a Thermoelectric Energy Harvesting System for Powering Sensing Nodes in Nuclear Power Plant", M.S. thesis, Viginia Polytechnic Institute and State University, 2015.

[41]   V. Leonov, P. Fiorini, S. Sedky, T. Torfs, and C. Van Hoof, Proceedings of 13th International Conference on Solid-State Sensors, Actuators and Microsystems, Vol. 1 (Seoul, Korea, 2005), pp. 291–294.

[42]   M. Kishi, H. Nemoto, T. Hamao, M. Yamamoto, S. Sudou, M. Mandai, and S. Yamamoto,*Proceedings of International Conference on Thermoelectrics* (Baltimore, USA, 1999), pp. 301–307.

[43]   T. Torfs, V. Leonov, and R. Vullers, *Sensors Transducers J.* 80, 1230 (2007).

[44]   K. T. Settaluri, H. Y. Lo, and R. J. Ram, "Thin Thermoelectric Generator System for Body Energy Harvesting," *Journal of Electronic Materials,* vol. 41, pp. 984-988, Jun 2012.

[45]   M. Hyland, H. Hunter, J. Liu, E. Veety, and D. Vashaee, "Wearable thermoelectric generators for human body heat harvesting," *Applied Energy,* vol. 182, pp. 518-524, Nov 15 2016.

[46]   M. Lossec, B. Multon, and H. Ben Ahmed, "Sizing optimization of a thermoelectric generator set with heatsink for harvesting human body heat," *Energy Conversion and Management,* vol. 68, pp. 260-265, Apr 2013.

[47]   Z. L. Wang and D. W. Tang, "Investigation of heat transfer around microwire in air environment using 3 omega method," *International Journal of Thermal Sciences,* vol. 64, pp. 145-151, Feb 2013.

[48]   X. J. Hu, A. Jain, and K. E. Goodson, "Investigation of the natural convection boundary condition in microfabricated structures," *International Journal of Thermal Sciences,* vol. 47, pp. 820-824, Jul 2008.

[49] N. Guan, Z. G. Liu, C. W. Zhang, and G. L. Jiang, "Natural convection heat transfer on surfaces of copper micro-wires," *Heat and Mass Transfer,* vol. 50, pp. 275-284, Feb 2014.

[50] S. Mahmoud, R. Al-Dadah, D. K. Aspinwall, S. L. Soo, and H. Hemida, "Effect of micro fin geometry on natural convection heat transfer of horizontal microstructures," *Applied Thermal Engineering,* vol. 31, pp. 627-633, Apr 2011.

[51] L. Micheli, K. S. Reddy, and T. K. Mallick, "General correlations among geometry, orientation and thermal performance of natural convective micro-finned heat sinks," *International Journal of Heat and Mass Transfer,* vol. 91, pp. 711-724, Dec 2015.

[52] N. Matsumoto, T. Tomimura and Y. Koito, "Heat Transfer Characteristics of Square Micro Pin Fins under Natural Convection", *Journal of Electronics Cooling and Thermal Control*, vol. 04, no. 03, pp. 59-69, 2014.

[53] J. S. Kim, B. K. Park, and J. S. Lee, "Natural convection heat transfer around microfin arrays," *Experimental Heat Transfer,* vol. 21, pp. 55-72, 2008.

[54] A. Bejan, *Convection heat transfer*, 1st ed.

[55] A. Guha and S. Samanta, "Closed-Form Analytical Solutions for Laminar Natural Convection on Horizontal Plates," *Journal of Heat Transfer-Transactions of the Asme,* vol. 135, Oct 2013.

APPENDIX A

ANSYS Model for Thermoelectric Unicouple

The ANSYS model developed in Chapter 2 is described as follows. The

dimensions of the individual components are the same as that listed in Table 1. A mesh

with 98186 nodes and 19359 elements was used, a refined mesh was used as the

calculations were used to validate the 1-D finite element model. The following figure

illustrates the mesh used.
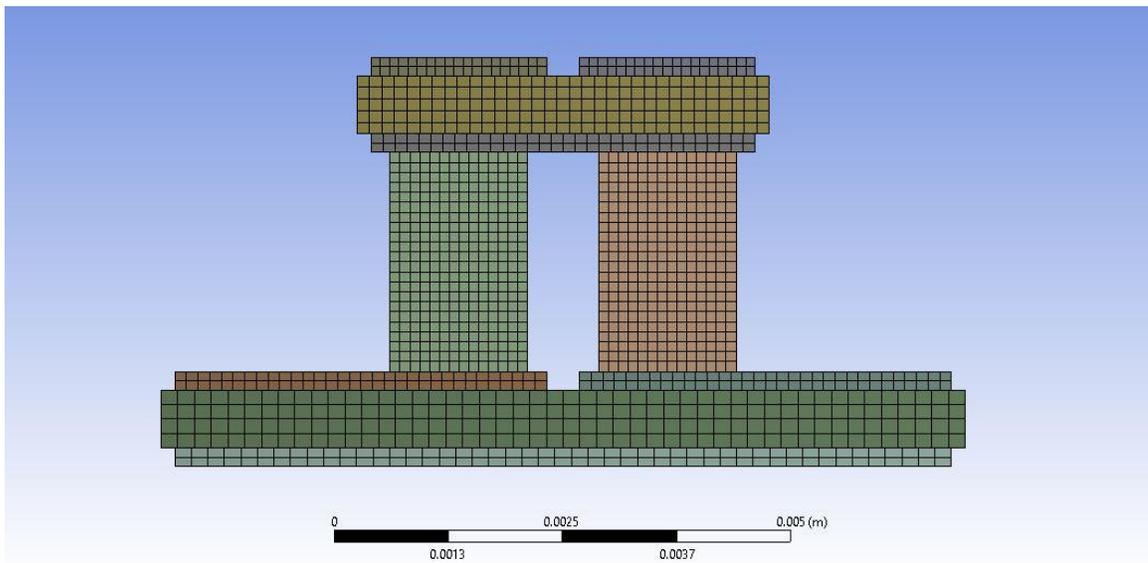
Figure 44:   Mesh used in the 3-D ANSYS model.

The boundary conditions applied to the finite element were applied to the ANSYS

model, where the top of the unicouple is assumed to be at a constant hot side temperature,

and the bottom of the unicouple is assumed to be at a constant cold side temperature as

shown in the following figure. Additionaly, the bottom copper header attached to the n-

leg was assigned a zero voltage boundary condition.
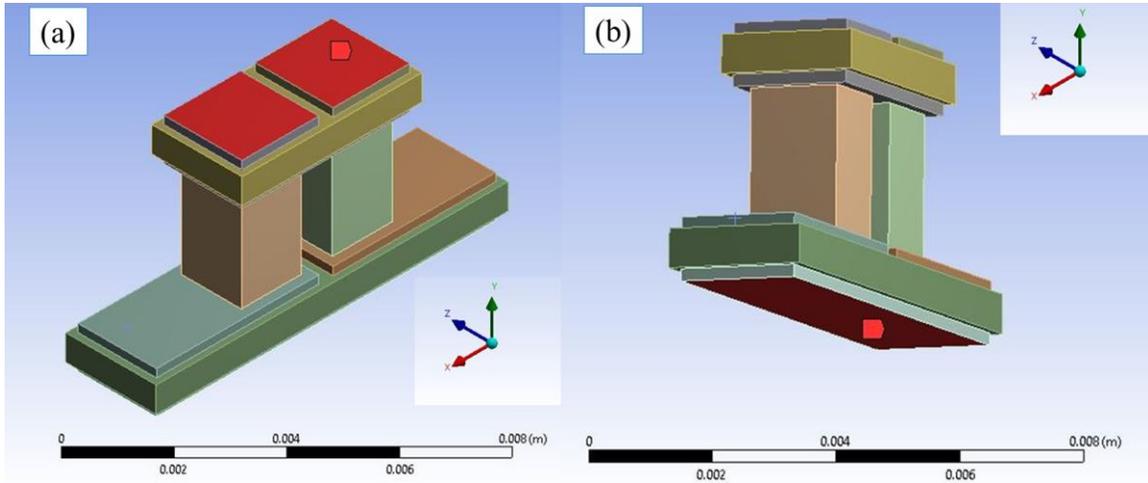
Figure 45: **(a) Top surface boundary condition applied in ANSYS model (b) Bottom surface boundary condition applied in ANSYS model.**

APPENDIX B

Temperature Dependent Finite Element Model for a Thermoelectric Unicouple

Matlab Code

```matlab
%% Finite Element Model for TE Unicouple
% Pasindu Gamarachchi - Email: pgamarachchi@gmail.com

clc
clear all

% Naming Convention
% property/leg/otherconsideration   no slashes

% Nodes and Elements
elems =100; %
numn = 2*elems +1;

% Input Temperatures
Th = 600;
Tc = 100;



% Dimensions

% N - Leg
hn = (1.7*10^-3);
ln = 2.0*10^-3;
tn = 2.0*10^-3;
% P - Leg

hp = (1.7*10^-3);
lp = 2.0*10^-3;
tp = 2.0*10^-3 ;



%  T3 - Copper
t3w = 1.93*10^-3;
t3l = 1.96*10^-3;
t3t = 0.2032*10^-3;

% T2 - Ceramic
t2w = 4.51*10^-3;
t2l = 2.26*10^-3;
t2t = 0.635*10^-3;
% it2t = t2t;

% T1 - Copper
t1w = 4.21*10^-3;
t1l = 1.96*10^-3;
t1t = 0.2032*10^-3;

% B3 - Copper
b3w = 8.50*10^-3;
```

```matlab
b3l = 1.96*10^-3;
b3t = 0.2032*10^-3;


% B2- Ceramic
b2w = 8.81*10^-3;
b2l = 2.26*10^-3;
b2t = 0.635*10^-3;


% B1 - Copper
b1w = 4.07*10^-3;
b1l = 1.96*10^-3;
b1t = 0.2032*10^-3;


ws = warning('off', 'all');


% Temperature Dependent properties
syms T


% Seebeck - N
TNS = [ 20 ,50, 100, 200, 300, 400, 500, 600 ];
SN = [ -0.000135243, -0.000142471, -0.000153643, -0.000171607, -
0.000187049, -0.000202244, -0.000211448, -0.000217053];
CNS = polyfit( TNS, SN, 6);
snf = int ( CNS(1)*T^6 + CNS(2)*T^5 + CNS(3)*T^4 + CNS(4)*T^3 +
CNS(5)*T^2 + CNS(6)*T + CNS(7));


% Electrical - N
TNP = [ 20 ,50, 100, 200, 300, 400, 500, 600 ];
PN = [ 6.56786E-06, 6.7325E-06, 7.03657E-06, 7.60784E-06, 8.0957E-06,
8.4766E-06, 8.6924E-06, 8.77723E-06];
CNP = polyfit( TNS, PN, 6);
pnf = int ( CNP(1)*T^6 + CNP(2)*T^5 + CNP(3)*T^4 + CNP(4)*T^3 +
CNP(5)*T^2 + CNP(6)*T + CNP(7));


% Theramal - N
TNK = [ 20 ,50, 100, 200, 300, 400, 500, 600 ];
KN = [ 5.308966362, 5.001685214, 4.609217214, 4.251736671, 4.069193415,
3.95510388, 3.962709849, 4.175676981];
CNK = polyfit( TNK, KN, 6);
knf = int ( CNK(1)*T^6 + CNK(2)*T^5 + CNK(3)*T^4 + CNK(4)*T^3 +
CNK(5)*T^2 + CNK(6)*T + CNK(7));


% Seebeck - P
TPS = [ 20 ,50, 100, 200, 300, 400, 500, 600 ];
SP = [7.39928E-05, 7.95446E-05, 8.87751E-05, 0.00010694, 0.000125184,
0.000142737, 0.000161509, 0.00017735 ];
CPS = polyfit( TPS, SP, 6);
spf = int ( CPS(1)*T^6 + CPS(2)*T^5 + CPS(3)*T^4 + CPS(4)*T^3 +
CPS(5)*T^2 + CPS(6)*T + CPS(7));


% Electrical - P
TPP = [ 20 ,50, 100, 200, 300, 400, 500, 600 ];
PP = [1.97399E-06, 2.13811E-06, 2.46366E-06, 3.18329E-06, 4.01544E-06,
4.92E-06, 5.85437E-06, 6.7556E-06 ];
CPP = polyfit( TPP, PP, 6);
```

```
ppf = int ( CPP(1)*T^6 + CPP(2)*T^5 + CPP(3)*T^4 + CPP(4)*T^3 +
CPP(5)*T^2 + CPP(6)*T + CPP(7));


% Thermal - P
TPK = [ 20 ,50, 100, 200, 300, 400, 500, 600 ];
KP = [7.533937719, 7.251196645, 6.711129425, 5.980450245, 5.438397484,
5.05121694, 4.773241165, 4.550860545];
CPK = polyfit( TPK, KP, 6);
kpf = int ( CPK(1)*T^6 + CPK(2)*T^5 + CPK(3)*T^4 + CPK(4)*T^3 +
CPK(5)*T^2 + CPK(6)*T + CPK(7));



% Conductivity Copper 102
TCK = [2.85, 27.85, 77.85, 127.85, 177.85, 227.85, 277.85 , 327.85,
377.85, 427.85, 477.85, 527.85, 577.85, 627.85, 677.85, 727.85, 777.85,
827.85, 877.85, 927.85, 977.85, 1027.85, 1077.85, 1084.85 ];
KC = [388.23 ,386.52 ,385.47, 384.59, 383.6, 382.34, 380.69, 378.59,
376.06, 373.12, 369.85, 366.33, 362.67, 358.98, 355.33, 351.8, 348.44,
345.26, 342.2, 339.16, 335.98, 332.39, 328.07,327.39];
CCK = polyfit( TCK, KC, 4);
kcf = int ( CCK(1)*T^4 + CCK(2)*T^3 + CCK(3)*T^2 + CCK(4)*T + CCK(5));

% Resistivity Copper 102
TCP = [0, 19.85, 26.85, 76.85, 126.85, 226.85, 326.85, 426.85, 526.85,
626.85, 726.85, 826.85, 926.85, 1026.85, 1084.45 ];
PC = [1.5430E-08    1.6780E-08  1.7250E-08  2.0630E-08  2.4020E-08
3.0900E-08  3.7920E-08  4.5140E-08  5.2620E-08  6.0410E-08  6.8580E-08
7.7170E-08  8.6260E-08  9.5920E-08  1.0171E-07];
CCP = polyfit( TCP, PC, 4);
pcf = int ( CCP(1)*T^4 + CCP(2)*T^3 + CCP(3)*T^2 + CCP(4)*T + CCP(5));

% Conductivity Al2O3
TAK = [19.85 ,37.8298, 55.8096, 73.78939, 91.76919, 109.749, 127.7288,
145.7086, 163.6884, 181.6682, 199.648, 217.6278, 235.6076, 253.5874,
271.5672, 289.547, 307.5268, 325.5066, 343.4864, 361.4662 ...
    379.446, 397.4258, 415.4056, 433.3854, 451.3652, 469.3449,
487.3247, 505.3045, 523.2843, 541.2641, 559.2439,577.2237, 595.2035,
613.1833, 631.1631, 649.1429, 667.1227, 685.1025, 703.0823, 721.0621
...
    739.0419, 757.0217, 775.0015, 792.9813, 810.9611, 828.9409,
846.9207, 864.9005, 882.8803, 900.8601, 918.8399, 936.8197, 954.7995,
972.7793,  990.7591,  1008.739,  1026.719,  1044.698,  1062.678
...
    1080.658    1098.638    1116.618    1134.597    1152.577
1170.557    1188.537    1206.517    1224.496    1242.476    1260.456
1278.436    1296.416    1314.395    1332.375    1350.355    1368.335
...
    1386.315    1404.294    1422.274    1440.254    1458.234
1476.214    1494.193    1512.173    1530.153    1548.133    1566.113
1584.092    1602.072    1620.052    1638.032    1656.012    1673.991
...
    1691.971    1709.951    1727.931    1745.911    1763.89 1781.87
1799.85];


KA = [35.4396    33.51727    31.9325 30.42353    28.98777    27.6227
26.32582    25.0947 23.92694    22.82018    21.77212    20.78048
```

```
      19.84306     18.95768      18.1222 17.33454      16.59267      15.89457
15.23832 ...
       14.62198      14.04371      13.50169      12.99413      12.51932
12.07557      11.66125      11.27474      10.91452      10.57906      10.26692
9.976668      9.70694 9.456409      9.223791      9.007849      8.80739
8.621267      ...
       8.448375      8.287655      8.138092      7.998718      7.868607
7.746878      7.632696      7.525269      7.42385 7.327738      7.236275
7.148849      7.064891      6.983877      6.90533 6.828814      6.75394
6.680364      6.607784 ...
       6.535945      6.464636      6.393691      6.322987      6.252448      6.18204
6.111777      6.041714      5.971953      5.902639      5.833964      5.766163
5.699515      5.634345      5.571022      5.509959      5.451616      5.396494
...
       5.345142      5.298152      5.25616 5.219848      5.189943      5.167214
5.152478      5.146594      5.150467      5.165047      5.191326      5.230344
5.283184      5.350973      5.434884      5.536134      5.655984      5.795741
...
       5.956756      6.140425      6.348187      6.581527      6.841975
7.131104      7.450535      7.801928 ];
CAK = polyfit( TAK, KA, 4);
kaf = int ( CAK(1)*T^4 + CAK(2)*T^3 + CAK(3)*T^2 + CAK(4)*T + CAK(5));


syms kn kp sn sp pp pn T % k: Conductivity, s: Seebeck, p: resistivity,
p: p-leg, n:n-leg


kn = symfun( knf, T); % Temperature dependent k for n-leg
kp = symfun (kpf, T); % Temperature dependent k for p-leg
sn = symfun (snf, T); % Temperature dependent s for n-leg
sp = symfun (spf, T); % Temperature dependent k for p-leg
pp = symfun (ppf, T); % Temperature dependent k for p-leg
pn = symfun (pnf, T); % Temperature dependent k for p-leg
kc = symfun (kcf, T); % Temperature dependent k for Copper 102
pc = symfun (pcf, T); % Temperature dependent p for Copper 102
ka = symfun (kaf, T); % Temperature dependent k for Al2O3


% Integral Averages for initial Temperature profile

knm = (kn(Th) - kn (Tc))/(Th-Tc);
knm = double(knm);
kpm = (kp(Th) - kp (Tc))/(Th-Tc);
kpm = double(kpm);
snm =  (sn(Th) - sn(Tc))/(Th-Tc);
snm = double(snm);
spm =  (sp(Th) - sp(Tc))/(Th-Tc);
spm = double(spm);
ppm =  (pp(Th) - pp(Tc))/(Th-Tc);
ppm = double(ppm);
pnm =  (pn(Th) - pn(Tc))/(Th-Tc);
pnm = double(pnm);


kcm =  (kc(Th) - kc(Tc))/(Th-Tc);
```

```
kcm = double(kcm);
pcm =  (pc(Th) - pc(Tc))/(Th-Tc);
pcm = double(pcm);


kam =  (ka(Th) - ka(Tc))/(Th-Tc);
kam = double(kam);




% Thermal Circuit for initial temperature profile
rc1 = (t3t/(kcm*t3l*t3w/2));
ra1 = (t2t/(kam*t2l*t2w/2));
rc2 = (t1t/(kcm*t1l*t1w/2));
cp =  (kpm* lp*tp)/hp;
rthp = 1/cp;
cn =  (knm* ln*tn)/hn;
rthn = 1/cn;
RLegs = 1/(cp +cn);


ra2 = (b2t/(kam.*b2l*b2w/2));
rc3 = (b1t/(kcm*b1l*b1w/2));
rc4 = (b3t/(kcm*b3l*b3w/2));

Rtot = rc1 + ra1 + rc2 + RLegs + rc3 + ra2 + rc4;

P1 = rc1/Rtot;
P2 = ra1/Rtot;
P3 = rc2/Rtot;
P4 = rLegs/Rtot;
P5 = rc3/Rtot;
P6 = ra2/Rtot;
P7 = rc4/Rtot;

DelTP1 =  (P1*(Th-Tc));
DelTP2 = (P2*(Th-Tc));
DelTP3 = (P3*(Th-Tc));
DelTP4 = (P4*(Th-Tc));
DelTP5 = (P5*(Th-Tc));
DelTP6 = (P6*(Th-Tc));
DelTP7 = (P7*(Th-Tc));


DeltT = DelTP1+ DelTP2 + DelTP3+ DelTP4+ DelTP5+ DelTP6 + DelTP7;

Tcu1 = Th - DelTP1;
Ta1 = Tcu1 - DelTP2;
Tcu2 = Ta1 - DelTP3;
Tpleg = Tcu2 - DelTP4;
Tcu3 = Tpleg - DelTP5;
Ta2 = Tcu3 - DelTP6;
Tcu4 = Ta2 - DelTP7;


Tp = [ Th Tcu1 Ta1 Tcu2 Tpleg Tcu3 Ta2  Tc];
```

```matlab
TotalHeight = t3t + hp + t2t + t1t + b3t + b2t + b1t;

t3telems = round((t3t/TotalHeight)*elems);
t2telems = round((t2t/TotalHeight)*elems);
t1telems = round((t1t/TotalHeight)*elems);
hpelems = round((hp/TotalHeight)*elems);
b3telems = round((b3t/TotalHeight)*elems);
b2telems = round((b2t/TotalHeight)*elems);
b1telems = round((b1t/TotalHeight)*elems);
summedelems = sum([t3telems , t2telems, t1telems, hpelems, b3telems,
b2telems ,b1telems]);

while ( summedelems ~= elems)

    if (summedelems > elems & t3telems > b3telems)
        t3telems = t3telems -1;
        summedelems = sum([t3telems , t2telems, t1telems, hpelems,
b3telems, b2telems ,b1telems]);
    elseif (summedelems > elems)
        b3telems = b3telems -1;
        summedelems = sum([t3telems , t2telems, t1telems, hpelems,
b3telems, b2telems ,b1telems]);
    elseif (summedelems < elems & t3telems > b3telems)
        b3telems = b3telems +1;
        summedelems = sum([t3telems , t2telems, t1telems, hpelems,
b3telems, b2telems ,b1telems]);
    else
        t3telems = t3telems +1;
        summedelems = sum([t3telems , t2telems, t1telems, hpelems,
b3telems, b2telems ,b1telems]);

    end
end


for i = 1: t3telems

    dt = (Th - Tcu1)/t3telems;
    T_t3t(i+1) = Th - dt*(i);

end
T_t3t(1) = Th;

for i = 1: t2telems

    dt = (Tcu1 - Ta1)/t2telems;
    T_t2t(i+1) = Tcu1 - dt*(i);

end
T_t2t(1) = Tcu1;

for i = 1: t1telems
```

```
    dt = (Ta1 - Tcu2)/t1telems;
    T_t1t(i+1) = Tcu2 - dt*(i);

end
T_t1t(1) = Ta1;

for i = 1: hpelems

    dt = (Tcu2 - Tpleg)/hpelems;
    T_hp(i+1) = Tcu2 - dt*(i);

end
T_hp(1) = Tcu2;

for i = 1: b1telems

    dt = (Tpleg - Tcu3)/b1telems;
    T_b1t(i+1) = Tpleg - dt*(i);

end
T_b1t(1) = Tpleg;


for i = 1: b2telems

    dt = (Tcu3 - Ta2)/b2telems;
    T_b2t(i+1) = Tcu3 - dt*(i);

end
T_b2t(1) = Tcu3;

for i = 1: b3telems

    dt = (Ta2 - Tc)/b3telems;
    T_b3t(i+1) = Ta2 - dt*(i);

End
T_b3t(1) = Ta2;
T_b3t(end) = Tc;


Tp = [ T_t3t T_t2t T_t1t T_hp T_b1t T_b2t T_b3t ];


ppm =  (pp(T_hp(1)) - pp(T_hp(end)))/(T_hp(1)-T_hp(end));
ppm = double(ppm);
pnm =  (pn(T_hp(1)) - pn(T_hp(end)))/(T_hp(1)-T_hp(end));
pnm = double(pnm);

rp = (ppm * hp )/(lp*tp);
rn = (pnm * hn )/(ln*tn);
```

```matlab
pt1tm =  (pc(T_t1t(1)) - pc(T_t1t(end)))/(T_t1t(1) - T_t1t(end) );
pt1tm = double(pt1tm);


pb1tpm =  (pc(T_b1t(1)) - pc(T_b1t(end)))/(T_b1t(1) - T_b1t(end) );
pb1tpm = double(pb1tpm);


pb1tnm =  (pc(T_b1t(1)) - pc(T_b1t(end)))/(T_b1t(1) - T_b1t(end) );
pb1tnm = double(pb1tnm);




snm =  (sn(T_hp(1)) - sn(T_hp(end)))/(T_hp(1)-T_hp(end));
snm = double(snm);
spm =  (sp(T_hp(1)) - sp(T_hp(end)))/(T_hp(1)-T_hp(end));
spm = double(spm);

% Contact Resistance
C_pho = 10*(10^-6);
CR_n = C_pho/(tp*100)*(lp*100);
CR_p = C_pho/(tp*100)*(lp*100);
CR = 2*(CR_n + CR_p);



Rt1t = (pt1tm* t1w)/(t1l*t1t);
Rb1tp = (pb1tpm* b1w)/(b1l*b1t);
Rb1tn =  (pb1tnm* b1w)/(b1l*b1t) ;
Rt = rp +rn + Rt1t + Rb1tp +Rb1tn + CR;
RL = Rt ;
R = RL + Rt ;
S =  spm -snm ;
I = (S*(T_hp(1) -T_hp(end)))/(R);



t1te_h = t1t/t1telems;


Jh_t1t = (I^2)* Rt1t;
Jh_b1tp = (I^2)*Rb1tp;
Jh_b1tn = (I^2)*Rb1tn;


Jh_t1t_e = Jh_t1t/(t1telems*2);
Jh_b1tp_e = Jh_t1t/(b1telems);
Jh_b1tn_e = Jh_t1t/(b1telems);


shp = hp/hpelems;
shn = hn/hpelems;

%% Thermoelectric Energy Generation calculations using initial
temperature profile  guess
%% to be input into FE calculations
for j = 1:hpelems

    knm(j) = (kn(T_hp(j)) - kn(T_hp(j+1)))/(T_hp(j)-T_hp(j+1));
    kpm(j) = (kp(T_hp(j)) - kp(T_hp(j+1)))/(T_hp(j)-T_hp(j+1));
```

```matlab
    snm(j) =  (sn(T_hp(j)) - sn(T_hp(j+1)))/(T_hp(j)-T_hp(j+1));
    spm(j) =  (sp(T_hp(j)) - sp(T_hp(j+1)))/(T_hp(j)-T_hp(j+1));
    ppm(j) =  (pp(T_hp(j)) - pp(T_hp(j+1)))/(T_hp(j)-T_hp(j+1));
    pnm(j) =  (pn(T_hp(j)) - pn(T_hp(j+1)))/(T_hp(j)-T_hp(j+1));


    rp1(j) = (ppm(j)* shp )/(lp*tp);
    rn1(j) = (pnm(j)* shn )/(ln*tn);
    cp(j) =  (kpm(j)* lp*tp)/shp;
    cn(j) = (knm(j)* ln*tn)/shn;

    Qhp(j) = spm(j)*T_hp(j)*I + cp(j)*(T_hp(j)-T_hp(j+1))-
(0.5)*(I^2)*rp1(j);
    Qcp(j) = spm(j)*T_hp(j+1)*I + cp(j)*(T_hp(j)-T_hp(j+1))+
0.5*(I^2)*rp1(j);
    Pp(j) = double((Qhp(j)- Qcp(j))) ;

    Qhn(j) = abs(snm(j))*T_hp(j)*I + cn(j)*(T_hp(j)-T_hp(j+1)) -
(0.5)*(I^2)*rn1(j) ;
    Qcn(j) = abs(snm(j))*T_hp(j+1)*I + cn(j)*(T_hp(j)-T_hp(j+1)) +
0.5*(I^2)*rn1(j) ;
    Pn(j) = double(Qhn(j)- Qcn(j));


end


% Temperature Dependent elemental k - matrix
for i = 1:t3telems

    k_t3tp_e(i) = double((kc(T_t3t(i)) - kc(T_t3t(i+1)))/(T_t3t(i) -
T_t3t(i+1)));
    k_t3tn_e(i) = double((kc(T_t3t(i)) - kc(T_t3t(i+1)))/(T_t3t(i) -
T_t3t(i+1)));
    A_t3t(i) = t3w*t3l;

end

for i = 1:t2telems

    k_t2tp_e(i) = double((ka(T_t2t(i)) - ka(T_t2t(i+1)))/(T_t2t(i) -
T_t2t(i+1)));
    k_t2tn_e(i) = double((ka(T_t2t(i)) - ka(T_t2t(i+1)))/(T_t2t(i) -
T_t2t(i+1)));
    A_t2tp(i) = 0.5*(t2w*t2l);
    A_t2tn(i) = 0.5*(t2w*t2l);

end

for i = 1:t1telems

    k_t1tp_e(i) = double((kc(T_t1t(i)) - kc(T_t1t(i+1)))/(T_t1t(i) -
T_t1t(i+1)));
```

```matlab
        k_t1tn_e(i) = double((kc(T_t1t(i)) - kc(T_t1t(i+1)))/(T_t1t(i) -
T_t1t(i+1)));
        A_t1tp(i) = 0.5*(t1w*t1l);
        A_t1tn(i) = 0.5*(t1w*t1l);
end

for i = 1:hpelems

    k_hp_e(i) = double((kp(T_hp(i)) - kp(T_hp(i+1)))/(T_hp(i) -
T_hp(i+1)));
    k_hn_e(i) = double((kn(T_hp(i)) - kn(T_hp(i+1)))/(T_hp(i) -
T_hp(i+1)));
    A_p(i) = lp*tp;
    A_n(i) = ln*tn;


end

for i = 1:b1telems

    k_b1tp_e(i) = double((kc(T_b1t(i)) - kc(T_b1t(i+1)))/(T_b1t(i) -
T_b1t(i+1)));
    k_b1tn_e(i) = double((kc(T_b1t(i)) - kc(T_b1t(i+1)))/(T_b1t(i) -
T_b1t(i+1)));
    A_b1t(i) = b1w*b1l;
end

for i = 1:b2telems

    k_b2tp_e(i) = double((ka(T_b2t(i)) - ka(T_b2t(i+1)))/(T_b2t(i) -
T_b2t(i+1)));
    k_b2tn_e(i) = double((ka(T_b2t(i)) - ka(T_b2t(i+1)))/(T_b2t(i) -
T_b2t(i+1)));
    A_b2tp(i) = 0.5*(b2w*b2l);
    A_b2tn(i) = 0.5*(b2w*b2l);
end


for i = 1:b3telems

    k_b3tp_e(i) = double((kc(T_b3t(i)) - kc(T_b3t(i+1)))/(T_b3t(i) -
T_b3t(i+1)));
    k_b3tn_e(i) = double((kc(T_b3t(i)) - kc(T_b3t(i+1)))/(T_b3t(i) -
T_b3t(i+1)));
    A_b3tp(i) = 0.5*(b3w*b3l);
    A_b3tn(i) = 0.5*(b3w*b3l);

end

kp_elems = [ k_t3tp_e, k_t2tp_e, k_t1tp_e, k_hp_e, k_b1tp_e, k_b2tp_e,
k_b3tp_e];
kn_elems = [ k_t3tn_e, k_t2tn_e, k_t1tn_e, k_hn_e, k_b1tn_e, k_b2tn_e,
k_b3tn_e];
```

```matlab
Ap_elems = [ A_t3t, A_t2tp, A_t1tp, A_p, A_b1t, A_b2tp, A_b3tp];
An_elems = [ A_t3t, A_t2tn, A_t1tn, A_n, A_b1t, A_b2tn, A_b3tn];


Kp = sparse(numn, numn);
Kn = sparse(numn, numn);


el_l = TotalHeight/elems;

%% Global K- Matrix Assembly
for i=1:2:numn-2

    if (i == 1)
        j = i ;
    else
        j =i-(prvj);
    end
    prvj = j;

    ke_p = (kp_elems(j))*(Ap_elems(j))/(6*el_l)*[14, -16, 2; -16, 32, -
16; 2, -16, 14];
    ke_n = (kn_elems(j))*(An_elems(j))/(6*el_l)*[14, -16, 2; -16, 32, -
16; 2, -16, 14];

    dof = [ i, i+1, i+2];
    Kp(dof, dof) = ke_p +  Kp(dof, dof);
    Kn(dof, dof) = ke_n +  Kn(dof, dof);

end

% F - Vector assembly using TE energy generation and joule heating
C0 = t3telems;
C1 = t3telems + t2telems;
C2 = C1 + t1telems;
C3 = C2 + hpelems;
C4 = C3 + b1telems;
C5 = C4 + b2telems;

for i = C1+1: C2

    E_gen_t1t(i) = Jh_t1t_e/(Ap_elems(i) * el_l);

end

for i = 1:hpelems

    E_genp(i) = -Pp(i)/(Ap_elems(i+C2)*el_l);
    E_genn(i) = -Pn(i)/(Ap_elems(i+C2)*el_l);

end

for i = C3+1: C4

    j= i -C3;
    E_gen_b1tp(j) = Jh_b1tp_e/(Ap_elems(i)* el_l);
```

```matlab
        E_gen_b1tn(j) = Jh_b1tn_e/(Ap_elems(i)* el_l);

    end
E_gen_b2t = zeros(b2telems,1)';
E_gen_b3t = zeros(b3telems,1)';


E_Gen_pL = [ E_gen_t1t, E_genp, E_gen_b1tp, E_gen_b2t, E_gen_b3t];
E_Gen_nL = [ E_gen_t1t, E_genn, E_gen_b1tn, E_gen_b2t, E_gen_b3t];


prvj =1;
for i = 3:2: numn-2

    j = i - prvj;
    prvj =j;
    fe_p = (E_Gen_pL(j)*Ap_elems(j)*el_l/6)*[1, 4, 1]';
    fe_n = (E_Gen_nL(j)*An_elems(j)*el_l/6)*[1, 4, 1]';

    dof = [i, i+1, i+2];
    F_p(dof) =fe_p;
    F_p(i) = fe_p(1) + fe_p(3);


    F_n(dof) =fe_n;
    F_n(i) = fe_n(1) + fe_n(3);
end


%% Adjusing for Boundary Conditions
F_p(1) = Th;
F_n(1) = Th;
F_p(2) = F_p(2) - Kp(2,1)*Th;
F_n(2) = F_n(2) - Kn(2,1)*Th;
F_p(3) = F_p(3) - Kp(3,1)*Th;
F_n(3) = F_n(3) - Kn(3,1)*Th;


F_p(end-2) = F_p(end -2) - Kp(end-2,end)*Tc;
F_p(end -1) = F_p(end -1) - Kp(end-1,end)*Tc;
F_p(end) = Tc;


F_n(end-2) = F_n(end -2) - Kn(end-2,end)*Tc;
F_n(end -1) = F_n(end -1) - Kn(end-1,end)*Tc;
F_n(end) = Tc;


for i = 1: numn
    Kp(numn,i) = 0;
    Kp(i,numn) = 0;
    Kp(numn,numn) =1;
    Kp(1,i) = 0;
    Kp(i,1) = 0;

    Kn(numn,i) = 0;
    Kn(i,numn) = 0;
    Kn(numn,numn) =1;
    Kn(1,i) = 0;
    Kn(i,1) = 0;
```

```matlab
end
Kp(1,1) =1;
Kn(1,1) =1;



Tempr_p = Kp\F_p';
Tempr_n = Kn\F_n';


F_nold = F_n;
F_pold = F_p;



ppm =  (pp(Tempr_p(C2*2 +1)) - pp(Tempr_p(C3*2 +1)))/(Tempr_p(C2*2 +1)-
Tempr_p(C3*2 +1));
ppm = double(ppm);
pnm =  (pn(Tempr_p(C2*2 +1)) - pn(Tempr_p(C3*2 +1)))/(Tempr_p(C2*2 +1)-
Tempr_p(C3*2 +1));
pnm = double(pnm);


pt1tm =  (pc(Tempr_p(C1*2 +1 )) - pc(Tempr_p(C2*2 +1)))/(Tempr_p(C1*2
+1) - Tempr_p(C2*2 +1) );
pt1tm = double(pt1tm);


pb1tpm =  (pc(Tempr_p(C3*2 +1)) - pc(Tempr_p(C4*2 +1)))/(Tempr_p(C3*2
+1) - Tempr_p(C4*2 +1) );
pb1tpm = double(pb1tpm);


pb1tnm =  (pc(Tempr_n(C3*2 +1)) - pc(Tempr_n(C4*2 +1)))/(Tempr_n(C3*2
+1) - Tempr_n(C4*2 +1) );
pb1tnm = double(pb1tnm);


snm =  (sn(Tempr_n(C2*2 +1)) - sn(Tempr_n(C3*2 +1)))/(Tempr_n(C2*2 +1)-
Tempr_n(C3*2 +1));
snm = double(snm);
spm =  (sp(Tempr_p(C2*2 +1)) - sp(Tempr_p(C3*2 +1)))/(Tempr_p(C2*2 +1)-
Tempr_p(C3*2 +1));
spm = double(spm);


Rt1t = (pt1tm* t1w)/(t1l*t1t);
Rb1tp = (pb1tpm* b1w)/(b1l*b1t);
Rb1tn =  (pb1tnm* b1w)/(b1l*b1t) ;
Rt = rp +rn + Rt1t + Rb1tp +Rb1tn + CR ;
RL = Rt ;
R = RL + Rt ;


S =  spm -snm ;
Voc_av = S*(Tempr_p(C2*2 +1) -Tempr_p(C3*2 +1));
I = S*(Tempr_p(C2*2 +1) -Tempr_p(C3*2 +1))./(R);



for k = 1:hpelems

    if ( k ==1)
        j = C2*2 + 1;
```

```matlab
        else
            j = C2*2 +1 + (k-1)*2;
        end




    knm(k) = (kn(Tempr_p(j)) - kn(Tempr_p(j+2)))/(Tempr_p(j)-
Tempr_p(j+2));
    kpm(k) = (kp(Tempr_p(j)) - kp(Tempr_p(j+2)))/(Tempr_p(j)-
Tempr_p(j+2));

    snm(k) =  (sn(Tempr_n(j)) - sn(Tempr_n(j+2)))/(Tempr_n(j)-
Tempr_n(j+2));
    spm(k) =  (sp(Tempr_p(j)) - sp(Tempr_p(j+2)))/(Tempr_p(j)-
Tempr_p(j+2));
    ppm(k) =  (pp(Tempr_p(j)) - pp(Tempr_p(j+2)))/(Tempr_p(j)-
Tempr_p(j+2));
    pnm(k) =  (pn(Tempr_n(j)) - pn(Tempr_n(j+2)))/(Tempr_n(j)-
Tempr_n(j+2));

    rp1(k) = (ppm(k)* shp )/(lp*tp);
    rn1(k) = (pnm(k)* shn )/(ln*tn);
    cp(k) =  (kpm(k)* lp*tp)/shp;
    cn(k) = (knm(k)* ln*tn)/shn;

    V_oc_e(k) = (spm(k)-snm(k))*(Tempr_p(j) -Tempr_p(j+2));

    Qhp(k) = spm(k)*Tempr_p(j)*I  + cp(k)*(Tempr_p(j)-Tempr_p(j+2))-
(0.5)*(I^2)*rp1(k)  ;
    Qcp(k) = spm(k)*Tempr_p(j+2)*I + cp(k)*(Tempr_p(j)-Tempr_p(j+2))+
0.5*(I^2)*rp1(k)  ;
    Pp(k) = double((Qhp(k)- Qcp(k)))  ;

    Qhn(k) = abs(snm(k))*Tempr_p(j)*I + cn(k)*(Tempr_p(j)-Tempr_p(j+2))
- (0.5)*(I^2)*rn1(k);
    Qcn(k) = abs(snm(k))*Tempr_p(j+2)*I + cn(k)*(Tempr_p(j)-
Tempr_p(j+2)) + 0.5*(I^2)*rn1(k);
    Pn(k) = double(Qhn(k)- Qcn(k));

end

%% Iterative Process for Temperature profiles to converge
it =1;
cc = 1;
err = cc*3; % Initalize Error value
while err > cc

    if it ==1
        Tempr_p = Tempr_p;
        Tempr_n = Tempr_n;
    else
        Tempr_p = Tempr_p2;
        Tempr_n = Tempr_n2;
    end
```

```matlab
%% Temperature Dependent elemental k - matrix using new Temperature
profile
for i = 1:t3telems %  t3t (Very Top Cu Layer) Copper Conductivity and
Area

    if ( i ==1)
        j =  1;
    else
        j = (i-1)*2 +1;
    end

    k_t3tp_e(i) = double((kc(Tempr_p(j)) -
kc(Tempr_p(j+2)))/(Tempr_p(j) - Tempr_p(j+1)));
    k_t3tn_e(i) = double((kc(Tempr_n(j)) -
kc(Tempr_n(j+2)))/(Tempr_n(j) - Tempr_n(j+2)));


end

for i = 1:t2telems % t22 Top Alumina Conductivity and Area

     if ( i ==1)
        j = C0 + 1;
    else
        j = C0 +(i-1)*2 +1;
    end


    k_t2tp_e(i) = double((ka(Tempr_p(i)) -
ka(Tempr_p(i+1)))/(Tempr_p(i) - Tempr_p(i+1)));
    k_t2tn_e(i) = double((ka(Tempr_n(i)) -
ka(Tempr_n(i+1)))/(Tempr_n(i) - Tempr_n(i+1)));


end

for i = 1:t1telems % t1t ( Copper Layer Connecting Legs ) Conductivity
and Area

     if ( i ==1)
        j = C1 + 1;
    else
        j = C1 +(i-1)*2 +1;
    end

    k_t1tp_e(i) = double((kc(Tempr_p(i)) -
kc(Tempr_p(i+1)))/(Tempr_p(i) - Tempr_p(i+1)));
    k_t1tn_e(i) = double((kc(Tempr_n(i)) -
kc(Tempr_n(i+1)))/(Tempr_n(i) - Tempr_n(i+1)));

end

for i = 1:hpelems % Leg conductivity and area

    if ( i ==1)
```

```matlab
            j = C2 + 1;
        else
            j = C2 +(i-1)*2 +1;
        end


    k_hp_e(i) = double((kp(Tempr_p(i)) - kp(Tempr_p(i+1)))/(Tempr_p(i)
- Tempr_p(i+1)));
        k_hn_e(i) = double((kn(Tempr_n(i)) - kn(Tempr_n(i+1)))/(Tempr_n(i)
- Tempr_n(i+1)));


end

for i = 1:b1telems % Bottom Copper Conductivity and Area

    if ( i ==1)
        j = C3 + 1;
    else
        j = C3 +(i-1)*2 +1;
    end

    k_b1tp_e(i) = double((kc(Tempr_p(i)) -
kc(Tempr_p(i+1)))/(Tempr_p(i) - Tempr_p(i+1)));
    k_b1tn_e(i) = double((kc(Tempr_n(i)) -
kc(Tempr_n(i+1)))/(Tempr_n(i) - Tempr_n(i+1)));

end

for i = 1:b2telems % Bottom Alumina Conductivity and Area

    if ( i ==1)
        j = C3 + 1;
    else
        j = C3 +(i-1)*2 +1;
    end


    k_b2tp_e(i) = double((ka(Tempr_p(i)) -
ka(Tempr_p(i+1)))/(Tempr_p(i) - Tempr_p(i+1)));
    k_b2tn_e(i) = double((ka(Tempr_n(i)) -
ka(Tempr_n(i+1)))/(Tempr_n(i) - Tempr_n(i+1)));

end


for i = 1:b3telems % Bottommost Copper Conductivity and Area

    if ( i ==1)
        j = C4 + 1;
    else
        j = C4 +(i-1)*2 +1;
    end
```

```
       k_b3tp_e(i) = double((kc(Tempr_p(i)) -
kc(Tempr_p(i+1)))/(Tempr_p(i) - Tempr_p(i+1)));
       k_b3tn_e(i) = double((kc(Tempr_n(i)) -
kc(Tempr_n(i+1)))/(Tempr_n(i) - Tempr_n(i+1)));

end


kp_elems = [ k_t3tp_e, k_t2tp_e, k_t1tp_e, k_hp_e, k_b1tp_e, k_b2tp_e,
k_b3tp_e];
kn_elems = [ k_t3tn_e, k_t2tn_e, k_t1tn_e, k_hn_e, k_b1tn_e, k_b2tn_e,
k_b3tn_e];


Ap_elems = [ A_t3t, A_t2tp, A_t1tp, A_p, A_b1t, A_b2tp, A_b3tp];
An_elems = [ A_t3t, A_t2tn, A_t1tn, A_n, A_b1t, A_b2tn, A_b3tn];


Kp = sparse(numn, numn);
Kn = sparse(numn, numn);


el_l = TotalHeight/elems;

%% Global K- Matrix Assembly
for i=1:2:numn-2

    if (i == 1)
        j = i ;
    else
        j =i-(prvj);
    end
    prvj = j;

    ke_p = (kp_elems(j))*(Ap_elems(j))/(6*el_l)*[14, -16, 2; -16, 32, -
16; 2, -16, 14];
    ke_n = (kn_elems(j))*(An_elems(j))/(6*el_l)*[14, -16, 2; -16, 32, -
16; 2, -16, 14];

    dof = [ i, i+1, i+2];
    Kp(dof, dof) = ke_p +  Kp(dof, dof);
    Kn(dof, dof) = ke_n +  Kn(dof, dof);

end
F_p = sparse(1,numn);
F_n = sparse(1,numn);

% F - Vector assembly using TE energy generation and joule heating
C0 = t3telems;
C1 = t3telems + t2telems;
C2 = C1 + t1telems;
C3 = C2 + hpelems;
C4 = C3 + b1telems;
C5 = C4 + b2telems;

for i = C1+1: C2

  E_gen_t1t(i) = Jh_t1t_e/(Ap_elems(i) * el_l);
```

```matlab
    end

    for i = 1:hpelems

        E_genp(i) = -Pp(i)/(Ap_elems(i+C2)*el_l);
        E_genn(i) = -Pn(i)/(Ap_elems(i+C2)*el_l);

    end

    for i = C3+1: C4

        j= i -C3;
        E_gen_b1tp(j) = Jh_b1tp_e/(Ap_elems(i)* el_l);
        E_gen_b1tn(j) = Jh_b1tn_e/(Ap_elems(i)* el_l);

    end
    E_gen_b2t = zeros(b2telems,1)';
    E_gen_b3t = zeros(b3telems,1)';

    E_Gen_pL = [ E_gen_t1t, E_genp, E_gen_b1tp, E_gen_b2t, E_gen_b3t];
    E_Gen_nL = [ E_gen_t1t, E_genn, E_gen_b1tn, E_gen_b2t, E_gen_b3t];

    prvj =1;
    for i = 3:2: numn-2

        j = i - prvj;
        prvj =j;
        fe_p = (E_Gen_pL(j)*Ap_elems(j)*el_l/6)*[1, 4, 1]';
        fe_n = (E_Gen_nL(j)*An_elems(j)*el_l/6)*[1, 4, 1]';

        dof = [i, i+1, i+2];
        F_p(dof) =fe_p;
        F_p(i) = fe_p(1) + fe_p(3);

        F_n(dof) =fe_n;
        F_n(i) = fe_n(1) + fe_n(3);
    end

    %% Adjusing for Boundary Conditions
    F_p(1) = Th;
    F_n(1) = Th;
    F_p(2) = F_p(2) - Kp(2,1)*Th;
    F_n(2) = F_n(2) - Kn(2,1)*Th;
    F_p(3) = F_p(3) - Kp(3,1)*Th;
    F_n(3) = F_n(3) - Kn(3,1)*Th;

    F_p(end-2) = F_p(end -2) - Kp(end-2,end)*Tc;
    F_p(end -1) = F_p(end -1) - Kp(end-1,end)*Tc;
    F_p(end) = Tc;

    F_n(end-2) = F_n(end -2) - Kn(end-2,end)*Tc;
    F_n(end -1) = F_n(end -1) - Kn(end-1,end)*Tc;
    F_n(end) = Tc;
```

```matlab
for i = 1: numn
    Kp(numn,i) = 0;
    Kp(i,numn) = 0;
    Kp(numn,numn) =1;
    Kp(1,i) = 0;
    Kp(i,1) = 0;

    Kn(numn,i) = 0;
    Kn(i,numn) = 0;
    Kn(numn,numn) =1;
    Kn(1,i) = 0;
    Kn(i,1) = 0;

end
Kp(1,1) =1;
Kn(1,1) =1;


Tempr_p2 = Kp\F_p';
Tempr_n2 = Kn\F_n';

diffp = abs(Tempr_p -Tempr_p2) ;
diffn =  abs(Tempr_n -Tempr_n2);

err = sum(diffp + diffn)
it = it +1


end


%% Thermoelectric Calculations using Final Temperature Profile
ppm =  (pp(Tempr_p2(C2*2 +1)) - pp(Tempr_p2(C3*2 +1)))/(Tempr_p2(C2*2
+1)-Tempr_p2(C3*2 +1));
ppm = double(ppm);
pnm =  (pn(Tempr_p2(C2*2 +1)) - pn(Tempr_p2(C3*2 +1)))/(Tempr_p2(C2*2
+1)-Tempr_p2(C3*2 +1));
pnm = double(pnm);

pt1tm =  (pc(Tempr_p2(C1*2 +1 )) - pc(Tempr_p2(C2*2
+1)))/(Tempr_p2(C1*2 +1) - Tempr_p2(C2*2 +1) );
pt1tm = double(pt1tm);

pb1tpm =  (pc(Tempr_p2(C3*2 +1)) - pc(Tempr_p2(C4*2
+1)))/(Tempr_p2(C3*2 +1) - Tempr_p2(C4*2 +1) );
pb1tpm = double(pb1tpm);

pb1tnm =  (pc(Tempr_n2(C3*2 +1)) - pc(Tempr_n2(C4*2
+1)))/(Tempr_n2(C3*2 +1) - Tempr_n2(C4*2 +1) );
pb1tnm = double(pb1tnm);

snm =  (sn(Tempr_n2(C2*2 +1)) - sn(Tempr_n2(C3*2 +1)))/(Tempr_n2(C2*2
+1)-Tempr_n2(C3*2 +1));
snm = double(snm);
```

```matlab
spm =  (sp(Tempr_p2(C2*2 +1)) - sp(Tempr_p2(C3*2 +1)))/(Tempr_p2(C2*2
+1)-Tempr_p2(C3*2 +1));
spm = double(spm);


Rt1t = (pt1tm* t1w)/(t1l*t1t);
Rb1tp = (pb1tpm* b1w)/(b1l*b1t);
Rb1tn =  (pb1tnm* b1w)/(b1l*b1t) ;
Rt = rp +rn + Rt1t + Rb1tp +Rb1tn + CR ;
RL = Rt ;
R = RL + Rt ;


S =  spm -snm ;
Voc_av = S*(Tempr_p2(C2*2 +1) -Tempr_p2(C3*2 +1));
I = S*(Tempr_p2(C2*2 +1) -Tempr_p2(C3*2 +1))./(R);



for k = 1:hpelems

    if ( k ==1)
        j = C2*2 + 1;
    else
        j = C2*2 +1 + (k-1)*2;
    end




    knm(k) = (kn(Tempr_p2(j)) - kn(Tempr_p2(j+2)))/(Tempr_p2(j)-
Tempr_p2(j+2));
    kpm(k) = (kp(Tempr_p2(j)) - kp(Tempr_p2(j+2)))/(Tempr_p2(j)-
Tempr_p2(j+2));

    snm(k) =  (sn(Tempr_n2(j)) - sn(Tempr_n2(j+2)))/(Tempr_n2(j)-
Tempr_n2(j+2));
    spm(k) =  (sp(Tempr_p2(j)) - sp(Tempr_p2(j+2)))/(Tempr_p2(j)-
Tempr_p2(j+2));
    ppm(k) =  (pp(Tempr_p2(j)) - pp(Tempr_p2(j+2)))/(Tempr_p2(j)-
Tempr_p2(j+2));
    pnm(k) =  (pn(Tempr_n2(j)) - pn(Tempr_n2(j+2)))/(Tempr_n2(j)-
Tempr_n2(j+2));

    rp1(k) = (ppm(k)* shp )/(lp*tp);
    rn1(k) = (pnm(k)* shn )/(ln*tn);
    cp(k) =  (kpm(k)* lp*tp)/shp;
    cn(k) = (knm(k)* ln*tn)/shn;

    V_oc_e(k) = (spm(k)-snm(k))*(Tempr_p(j) -Tempr_p(j+2));

    Qhp(k) = spm(k)*Tempr_p2(j)*I  + cp(k)*(Tempr_p2(j)-Tempr_p2(j+2))-
(0.5)*(I^2)*rp1(k) ;
    Qcp(k) = spm(k)*Tempr_p2(j+2)*I + cp(k)*(Tempr_p2(j)-
Tempr_p2(j+2))+ 0.5*(I^2)*rp1(k) ;
    Pp(k) = double((Qhp(k)- Qcp(k))) ;
```

```
    Qhn(k) = abs(snm(k))*Tempr_p2(j)*I + cn(k)*(Tempr_p2(j)-
Tempr_p2(j+2)) - (0.5)*(I^2)*rn1(k);
    Qcn(k) = abs(snm(k))*Tempr_p2(j+2)*I + cn(k)*(Tempr_p2(j)-
Tempr_p2(j+2)) + 0.5*(I^2)*rn1(k);
    Pn(k) = double(Qhn(k)- Qcn(k));


end

Qhin = max(Qhp) + max(Qhn);
TotalP = sum(Pp);
TotalN = sum(Pn);
Power = TotalP + TotalN - (Rt1t + Rb1tn + Rb1tp + CR)*I^2
V_oc = sum(V_oc_e);
Eff = Power*100/Qhin;
```

APPENDIX C

TEG – Heat Exchanger Model Matlab Code

```matlab
% Hot Side Heat Exchanger and TE Unicouple model combined
% Pasindu Gamarachchi - Email: pgamarachchi@gmail.com
clc
clear all


global hxl hxh hxw N Tin tf TEMW TEML TempC cvl Thg  Tbg mf

% HX Dimensions & Input
hxl = 0.16;
hxh = 0.02;
hxw = 0.04;
N = 30;
mf = 0.5*9.7*10^-3;
Tin = 558;
tf = 0.1*10^-3;
s = (hxw - (N.*tf))./(N+1); % Fin Spacing

% TEM Dimensions

TEMW = 40*10^-3; % [m]
TEML = 40*10^-3; % [m]

TempC = 94; % [C]

cvl = 40*(10^-3);
cv  = round(hxl./(cvl)); % Number of control volumes

% Guesses and Error
Err = 0.005; % Convergence Error
Thg = 5; % Temperature Outlet Guess
Tbg = 180;  % Base/TEM Hot Side Temperature
Tdg = 10;
TempCh = Err*0.9;
ErrMult = 5;
DiffLim = 1;

% Fin Material and Fluid Properties
syms x
caf = int( 3.134242E-10*x^4 - 8.519344E-07*x^3 + 7.480582E-04*x^2 -
3.006360E-02*x + 1.007301E+03); % specific Heat of air
ca =  symfun(caf,x);
%
knif = int( -9.32400932E-11*x^4 + 1.13247863E-07*x^3 + 6.33449883E-
05*x^2 -9.47163947E-02*x + 8.13811189E+01); % Thermal Conductivity of
Nickel
kni =  symfun(knif,x);

%%
T = zeros(cv,1);
```

```matlab
T(1) = Tin;

% Calculations for each control volume
for j = 1:length(T)


    Tin = T(j);
    Th = Tin;
    Thi = Tin -Thg;
    Ti =Tin;

    cam = (ca(Th) - ca(Thi))./(Th-Thi);
    cam = double(cam);

    cp = cam;

    Tog = Ti - Tdg;

    if j==1;
        Tb = Ti-Tbg;
    else
    end

    [Q,P,Eff] = TEModule(Tb,TempC, Un);% Function with finite element
% unicouple function and number of unicouples

    To = Ti - (Q/(mf*cp));
    Pf = 2*(cvl);
    Af = cvl*tf;

    Tfl = (Ti + To)/2;

    kNim = (kni(Tb) -kni(Tb-10))./(10);
    kNim = double(kNim);

    % Fin Heat Transfer Calcs
    [h, v, Re] = convcoeff(Tfl,mf); % Function with Duct Convection
% Coefficient

    M = (sqrt(h*Pf*kNim*Af))*(Ti - Tb);
    Un_ar = (hxw- tf*N)*cvl;

    m = sqrt((h*Pf)/(kNim*Af));
    Qf = M*tanh(m*hxh/2)*((N-1)) + Un_ar*h*(Tb - Tfl) ;

    [QTET, P, Eff] = TEModule(Tb,TempC, Un);

    i=0;

    % Convergence Requirement
    while abs(Qf-QTET)>Err

        Tb = Tb+(Err);
```

```
        [h, v, Re]= convcoeffv3(T(j),mf);
        M = (sqrt(h*Pf*kNim*Af))*((Ti- Tb));
        m = sqrt((h*Pf)/(kNim*Af));
        Qf = M*tanh(m*hxh/2)*((N-1)) + Un_ar*h*(Tb - Tfl) ;
        [QTET, P, Eff] = TEModule(Tb,TempC, Un);

        if Qf - QTET> Err & Qf -QTET< (Err*DiffLim)
            Tb = Tb +(TempCh);
        elseif Qf - QTET> (Err*DiffLim)
            Tb  = Tb  + (ErrMult*TempCh);
        elseif (Qf -QTET ) < (Err*-1) & Qf -QTET > (Err*- DiffLim)
            Tb = Tb -(TempCh);
        elseif (Qf - QTET) < (Err*- DiffLim)
            Tb = Tb -(ErrMult*TempCh);
        end
        diff = Qf-QTET;

    end

    progress = j/length(T)
    QTETv(j) = QTET;
    Pv (j) = P;
    Effv(j) = Eff;

    hv(j) = h;
    vv(j) = v;
    Rev(j) = Re;

    To = Ti - (Qf./(mf*cp));
    Tbv(j) = Tb;
    Qhv(j) = Qf;
    T(j+1) = To;

end
```

APPENDIX D

Compact Heat Exchanger Convection Coefficient Matlab Code

```matlab
% Function calculates the convection coefficient along with Velocity and
% Reynolds Number for the hot side of the heat exchanger
% Pasindu Gamarachchi - Email : pgamarachchi@gmail.com
 function [h, v, Re] = convcoeff(Th, mf)

 global hxl hxh hxw N tf Thg

Thi = Th - Thg;

%%  Temperature dependent properties

% Density of steam/ Hot side fluid
 syms x % ps cs ms ks ps
daf = int(2.876602E-12*x^4 - 7.350893E-09*x^3 + 7.284062E-06*x^2 -
3.760334E-03*x + 1.251051E+00);
% Specific Heat Capacity of steam
caf = int( 3.134242E-10*x^4 - 8.519344E-07*x^3 + 7.480582E-04*x^2 -
3.006360E-02*x + 1.007301E+03);
% Dynamic viscocity of Steam
maf = int(-1.17230617E-17*x^4 +3.14251436E-14*x^3 -3.87294440E-11*x^2
+4.96283182E-08*x + 1.71301016E-05);
% Thermal Cond of Steam
kaf = int(1.146049E-14*x^4 + 5.825050E-12*x^3 - 4.412201E-08*x^2 +
8.330657E-05*x + 2.396400E-02);
% Prandtl Number of Steam
paf = int( 1.946038E-13*x^4 - 8.530084E-10*x^3 + 9.958116E-07*x^2 -
3.351574E-04*x + 7.176453E-01);
% Thermal Conductivity of Fin Material
knf = int(-9.32400932E-11*x^4 + 1.13247863E-07*x^3 +6.33449883E-05*x^2
+ -9.47163947E-02*x + 8.13811189E+01);

da =  symfun(daf,x);
ca =  symfun(caf,x);
ma =  symfun(maf,x);
ka =  symfun(kaf,x);
pa =  symfun(paf,x);

kb = symfun(knf,x);
% Integral averages


cam = (ca(Th) - ca (Thi))/(Th-Thi);
cam = double(cam);

mam = (ma(Th) - ma (Thi))/(Th-Thi);
mam = double(mam);

kam = (ka(Th) - ka (Thi))/(Th-Thi);
kam = double(kam);

pam = (pa(Th) - pa (Thi))/(Th-Thi);
```

```matlab
pam = double(pam);

% Intermediate Calculations
s = (hxw - (N*tf))/(N+1); % Fin Spacing
dh = (4*s*(hxh/2))/(s + hxh );  % Hydraulic Diameter, hxh is divided by
2, because of adiabatic tip
v = mf/(dam*s*(hxh/2)*(N-1));
Re = v*dam*dh/(mam);
Pr = (cam*mam)/(kam);


% Colburn and pressure factors
al = s/(hxh/2);
if Re<=1000
    j_f = 0.483*(hxl/dh)^(-0.162)*al^(-0.184)*Re^(-0.536);
else
    j_f =0.242*(hxl/dh)^(-0.322)*(tf/dh)^0.089*Re^(-0.368);
end

h = j_f*Re*(Pr^(1/3))*kam/(dh);

 end
```

APPENDIX E

Duct Convection Coefficient Matlab Code

```matlab
% Function calculates the convection coefficient along with Velocity and
% Reynolds Number for the hot side of the heat exchanger
% Pasindu Gamarachchi - Email : pgamarachchi@gmail.com
 function [h, v, Re] = convcoeffv_Duct(Th, mf)

 global  hxh hxw N tf Thg

Thi = Th - Thg;

%%  Temperature dependent properties

% Density of steam/ Hot side fluid
 syms x % ps cs ms ks ps
daf = int(2.876602E-12*x^4 - 7.350893E-09*x^3 + 7.284062E-06*x^2 -
3.760334E-03*x + 1.251051E+00);
% Specific Heat Capacity of steam
caf = int( 3.134242E-10*x^4 - 8.519344E-07*x^3 + 7.480582E-04*x^2 -
3.006360E-02*x + 1.007301E+03);
% Dynamic viscocity of Steam
maf = int(-1.17230617E-17*x^4 +3.14251436E-14*x^3 -3.87294440E-11*x^2
+4.96283182E-08*x + 1.71301016E-05);
% Thermal Cond of Steam
kaf = int(1.146049E-14*x^4 + 5.825050E-12*x^3 - 4.412201E-08*x^2 +
8.330657E-05*x + 2.396400E-02);
% Prandtl Number of Steam
paf = int( 1.946038E-13*x^4 - 8.530084E-10*x^3 + 9.958116E-07*x^2 -
3.351574E-04*x + 7.176453E-01);

% Thermal Conductivity of Fin Material
knf = int(-9.32400932E-11*x^4 + 1.13247863E-07*x^3 +6.33449883E-05*x^2
+ -9.47163947E-02*x + 8.13811189E+01);

da =  symfun(daf,x);
ca =  symfun(caf,x);
ma =  symfun(maf,x);
ka =  symfun(kaf,x);
pa =  symfun(paf,x);

kb = symfun(knf,x);
% Integral averages

dam = (da(Th) - da (Thi))/(Th-Thi);
dam = double(dam);



cam = (ca(Th) - ca (Thi))/(Th-Thi);
cam = double(cam);

mam = (ma(Th) - ma (Thi))/(Th-Thi);
mam = double(mam);
```

```matlab
kam = (ka(Th) - ka (Thi))/(Th-Thi);
kam = double(kam);


pam = (pa(Th) - pa (Thi))/(Th-Thi);
pam = double(pam);




% Intermediate Calculations
s = (hxw - (N*tf))/(N+1);
dh = (4*s*(hxh/2))/(s + hxh );
v = mf/(dam*s*(hxh)*(N-1));


Re = v*dam*dh/(mam);
Pr = (cam*mam)/(kam);

% Colburn and pressure factors
al = s/(hxh/2);

if Re < 2500
    Nu = 7.541*(1- 2.61*al +4.97*al^2 -5.199*al^3 + 2.702*al^4 -
0.548*al^5);
else
    Nu = 0.026*Re^(0.8)*Pr^(0.3);
end

h = Nu*kam/dh;

end
```

APPENDIX F

TEG-Combined with Flat Plate Heat Sink Matlab Code

```matlab
% TEG Combined with Vertical Flat Plate Heat Sink
% Pasindu Gamarachchi - Email : pgamarachchi@gmail.com
clc
clear all

global hxl cvl NC tf_C Tcg Tcbg hxhC hxwC hxlC Cb  hn ln tn hp lp tp

Th =200; % Hot Side Temperature
Tamb= 120;


hnv =  0.2*(10^-3): (0.1*(10^-3)): 2.0*(10^-3);
leng = length(hnv)
%%



%%Heat Sink Dimensions
NC = 7;
tf_C = 1.50*(10^-3);
hxhC = 0.15;
hxwC = 0.04;
hxl  = 0.04;
hxlC = hxl;
Cb = 1*10^-2;
cvl = hxl;
PackFracColdSide = (tf_C*NC/hxwC)
sC = (hxwC - (NC.*tf_C))./(NC-1)



% TC Dimensions
ln = 1.8*(10^-3);
tn = 1.8*(10^-3);
lp = 1.8*(10^-3);
tp = 1.8*(10^-3);
F =7;
G =7;
C = F*G;
FillFactor = (tn*ln*2*C)/(hxwC*hxlC)

% Guesses and Error
Err = 10^-6;
Tcg = 1;
Tcbg =35;
ErrMult = 3.5;
DiffLim = 800;
ErrMult = 500;
TempCh = 0.5*Err;

if TempCh > Err
    fprintf('Unlikely to converge\n')
    return
end
```

```matlab
% For each unicouple height
for i = 1:length(hnv)

    hn = hnv(i);
    hp = hn;

    if i ==1
        Tb = Tamb + Tcbg;
        TempC = Tb + Tcg;
    else
    end

    [QHT, QCT, P, n, Volt, I, Qm] = TEModuleDOE_Bi2Te3(Th,TempC,C);
    QTE = QCT;
    [Qc, Q_b, h_f, h_b ,TEMC ,TTip ,et_f, Qr] = HXFreeConvFlat(Tb,
Tamb);


%% Iterative Condition
    while ( abs(Qc -QTE)> Err  )

        [QHT, QCT, P, n, Volt, I, Qm] = TEModuleDOE_Bi2Te3(Th,TempC,C);
        QTE = QCT;
        [Qc, Q_b, h_f, h_b ,TEMC ,TTip ,et_f, Qr] = HXFreeConvFlat(Tb,
Tamb);

        TempC = TEMC;
        if Qc -QTE> Err & Qc -QTE< (Err*DiffLim)
          Tb = Tb -(TempCh);
        elseif Qc - QTE> (Err*DiffLim)
            Tb = Tb -(ErrMult*TempCh);
        elseif (Qc -QTE) < (Err*-1) & Qc -QTE > (Err*-DiffLim)
            Tb = Tb +(TempCh);
        elseif (Qc -QTE) < (Err*-ErrMult)
            Tb = Tb +(ErrMult*TempCh);
        end

        diffcs  = Qc-QTE
        Tb;

    end

    progress = i/length(hnv)

    TotalP = P;
    Eff = (TotalP*100)/QTE;
    TotalPv(i) = P;
    QHTv(i) = QHT;
    QCTv(i) = QCT;
    nv(i) =n;
    Voltv(i) = Volt;
    Iv(i) = I;
    Tbv(i) =Tb;
    TEMCv(i) = TEMC;
```

end

APPENDIX G

Microwire Heat Sink Matlab Code

```matlab
% Micro-wire Heat Sink to calculate heat transferred from Heat Sink for
% varied ambient temperature using finite elements for fins
% Pasindu Gamarachchi - Email : pgamarachchi@gmail.com


 function QTot = HXMicroFinsFiniteElement(Tb, Tamb)

global  hxlC   hxwC    NCx NCz fd fh


temprfile = ['Base', num2str(Tb),'Amb', num2str(Tamb),
'FluidTempDat.mat']; % Load Temperature File based on base and ambient
temperature

load(temprfile);

Nx = floor(NCx/2);
Nz = floor(NCz/2);

elemsize = y(2)-y(1);
elems = ceil(fh/elemsize) -1;
numn =elems+1;
len = size(Tempr);


Nx_norm = round((1:1:Nx).*(len(1))./(Nx));
Nz_norm = round((1:1:Nz).*(len(2))./(Nz));


%%
TambM = zeros(Nx,Nz,length(y));

% for j = 1:Nz
for i = 1:Nx
    for j = 1:Nz

    p = Nx_norm(i);
    q = Nz_norm(j);
    TambM(i,j,:) = Tempr(p,q,:);

    end
end


for i = 1:Nx
    for j = 1:Nz

        [Qf_fe, TTip, Tempr] = FEFinV(TambM(i,j,:),Tb, Tamb, elemsize
); % Function for heat transfer from fins
        Qf_feM(i,j) = Qf_fe;
        TtipM(i,j) = TTip;
```

```matlab
    end
end

% Heat Transfer from Base

h_b = convec_hotplate(Tb, Tamb); % Function to obtain convection coeff
for Heat Transfer from Base
Fin_Ar = 0.25*pi*(fd^2)*(NCx*NCz);
Un_Ar =  (hxwC*hxlC) - Fin_Ar;


Q_b = Un_Ar*(h_b)*(Tb-Tamb); % Heat transfer from Base Area

Qf_Tot = sum(sum((Qf_feM)));
QTot = Qf_Tot*4 + Q_b;


 end


% Finite Element Model for heat transfer from microwire fins
% Pasindu Gamarachchi - Email : pgamarachchi@gmail.com


 function [Qf_fe, Ttip, Tempr] =  FEFinVFTemp(AmbTemp, Tb, Tamb,
elemsize)

global fd fh



elems = ceil(fh/elemsize) -1; % Number of Elements

numn =elems+1;


h = convectionmicro(Tb,Tamb);
kCupf = (5.25E-15*x^6 - 1.34E-11*x^5 + 1.26E-08*x^4 - 5.19E-06*x^3 +
8.71E-04*x^2 - 9.61E-02*x + 3.99E+02);
kCup = symfun(kCupf,x);

kCupm = kCup(Tb) ;
kCupm = double(kCupm);



k = kCupm;


l = fh/elems; % Element length
Tambv = AmbTemp(1:numn);

% Element K Matrix
```

```matlab
A = pi*(fd^2)*0.25;
P = pi*fd;


C1 = k*A/l;
C2 = h*P*l/6;



ke = C1*[1, -1; -1,1] + C2*[2,1; 1,2];



K = sparse(numn, numn);
F = sparse(numn,1);

for i = 1:elems

    dof = [ i, i+1];
    K(dof, dof) = ke +  K(dof, dof);



end

% Calculates Thermal Load for each node
for i = 1:numn
    fe(i) = h*P*l*Tambv(i)/2;

end



% Combines the Thermal Loads from previous element
for i = 2:numn-1
    F(i) = fe(i)+ fe(i-1);

end

F(end) = fe(end); % Last node only has thermal load from itself
F(2) = F(2) - Tb*(ke(2,1));

for i=1:numn
    K(i,1) =0;
    K(1,i) =0;
    F(1) = Tb;
end

K(1,1) =1;

Tempr = K\F;


for i = 1:elems
    Tavg(i) = (Tempr(i) +Tempr(i+1))*0.5;
    Q_elem(i) = h*P*l*(Tavg(i) - Tambv(i));
end
```

```matlab
Qf_fe = sum(Q_elem);
Ttip = Tempr(end);



 end


% Microfins convection coefficient

function h = convectionmicro(Tcb, Tamb)

global  fd


g = 9.81;
lam = 68*10^-9;


% Fin Material
syms x

knif = ( -9.32400932E-11*x^4 + 1.13247863E-07*x^3 + 6.33449883E-05*x^2
-9.47163947E-02*x + 8.13811189E+01); % Thermal Conductivity of Nickel
kni =  symfun(knif,x);

kAlpf = ( 7.00000000E-09*x^4 - 6.18933333E-06*x^3 + 1.25071800E-03*x^2
+ 1.47795093E-02*x + 2.28807284E+02);
kAlp = symfun(kAlpf,x);

kCupf = (5.25E-15*x^6 - 1.34E-11*x^5 + 1.26E-08*x^4 - 5.19E-06*x^3 +
8.71E-04*x^2 - 9.61E-02*x + 3.99E+02);
kCup = symfun(kCupf,x);

kAlpm = kAlp(Tcb);
kAlpm = double(kAlpm);

kCupm = kCup(Tcb) ;
kCupm = double(kCupm);


k = kCupm;



Tcold = Tamb;

%%  Temperature dependent properties

 syms x
```

```
 daf = (2.876602E-12*x^4 - 7.350893E-09*x^3 + 7.284062E-06*x^2 -
3.760334E-03*x + 1.251051E+00);


 caf = ( 3.134242E-10*x^4 - 8.519344E-07*x^3 + 7.480582E-04*x^2 -
3.006360E-02*x + 1.007301E+03);


 maf = (-1.17230617E-17*x^4 +3.14251436E-14*x^3 -3.87294440E-11*x^2
+4.96283182E-08*x + 1.71301016E-05);


kaf =  ( 1.146049E-14*x^4 + 5.825050E-12*x^3 - 4.412201E-08*x^2 +
8.330657E-05*x + 2.396400E-02);


 paf = ( 1.946038E-13*x^4 - 8.530084E-10*x^3 + 9.958116E-07*x^2 -
3.351574E-04*x + 7.176453E-01);


faf = ( 1.093417E-16*x^4 - 1.924826E-13*x^3 + 1.754598E-10*x^2 +
1.375914E-07*x + 1.847226E-05);

% Kinematic Viscocity of Air
vaf = ( 9.471589E-18*x^4 - 3.915231E-14*x^3 + 1.054041E-10*x^2 +
8.961175E-08*x + 1.340998E-05);


da =  symfun(daf,x);
ca =  symfun(caf,x);
ma =  symfun(maf,x);
ka =  symfun(kaf,x);
pa =  symfun(paf,x);
fa =  symfun(faf,x);
va =  symfun(vaf,x);



Tfilm = (Tamb + Tcb)/2;

% Air
dam = da(Tfilm) ;
dam = double(dam);

cam = ca(Tfilm);
cam = double(cam);

mam = ma(Tfilm) ;
mam = double(mam);

kam = ka(Tfilm) ;
kam = double(kam);

pam = pa(Tfilm) ;
pam = double(pam);

fam = fa(Tfilm) ;
fam = double(fam);

vam = va(Tfilm);
vam = double(vam);
```

```matlab
TfilmK = Tfilm +273.15;
Be = 1/TfilmK;



% Intermediate Calculations
Kn = lam/fd;
C = fam/(fd^2);
C1 = (log(C))^2;
C2 = log(C);



h = (kam/(1+Kn))*(1/fd)*((1/16)*C1 -0.292*C2 +0.958)^(-0.5);

    end
```